

This document is confidential and is proprietary to the American Chemical Society and its authors. Do not copy or disclose without written permission. If you have received this item in error, notify the sender and delete all copies.

Colloidal Quantum Dot Photovoltaics: Current Progress and Path to GW-Scale Enabled by Smart Manufacturing

Journal:	<i>ACS Energy Letters</i>
Manuscript ID	nz-2020-01453k.R1
Manuscript Type:	Review
Date Submitted by the Author:	21-Aug-2020
Complete List of Authors:	Kirmani, Ahmad; National Renewable Energy Laboratory, Chemistry and Nanoscience Center Luther, Joseph; National Renewable Energy Laboratory, Abolhasani, Milad; North Carolina State University, Chemical and Biomolecular Engineering Amassian, Aram; North Carolina State University, Materials Sciences and Engineering

SCHOLARONE™
Manuscripts

1
2
3 **Colloidal Quantum Dot Photovoltaics: Current Progress and Path to GW-Scale Enabled by**
4
5 **Smart Manufacturing**
6
7

8 *Ahmad R. Kirmani^{1*}, Joseph M. Luther¹, Milad Abolhasani³, and Aram Amassian^{2*}*
9
10
11
12
13

14 ¹ Chemical and Nanoscience Center, National Renewable Energy Laboratory (NREL), CO 80215
15
16

17 ² Materials Science and Engineering, Organic and Carbon Electronic Laboratories (ORaCEL),
18
19 North Carolina State University (NCSU), Raleigh, NC 27695
20

21 ³ Chemical and Biomolecular Engineering, North Carolina State University (NCSU), Raleigh, NC
22
23 27695
24
25
26
27
28
29
30
31
32
33
34
35
36
37
38
39
40

41 **AUTHOR INFORMATION**
42

43 **Corresponding Authors**
44

45 *E-mails: ahmad.kirmani@nrel.gov, aamassi@ncsu.edu
46
47
48
49
50
51
52
53
54
55
56
57
58
59
60

1
2
3 ABSTRACT: Colloidal quantum dots (QDs) have lately been pursued with intense vigor for
4 optoelectronic applications such as photovoltaics (PV), flexible electronics, displays, mid-infrared
5 photodetectors, lasers, and single photon emitters. These nanometer-sized semiconducting crystals
6 can be suitably mass-produced and size-tuned via cost-effective solution-based chemistry routes,
7 to operate in the quantum size confinement regime endowing them with a wide array of exotic
8 optical and electronic properties. While the first potential market entry could be in displays and in
9 niche applications such as ‘internet-of-things’, ultimately, the technology has the potential to
10 influence large scale terrestrial power generation, as it is amenable to high-throughput synthesis
11 from Earth-abundant materials, large-area solution-based coating, and can be air-stable. In this
12 Review, we chronicle the recent advances that have propelled QD PV to the cusp of
13 commercialization and highlight potential areas for further progress. We present an account of the
14 material compositions being explored as QDs and their various benefits, major chemical
15 passivation and doping strategies that have been developed to allay QD surface traps, and advanced
16 device designs deployed to maximize charge extraction. We also discuss pathways to >20%
17 efficient QD PV and describe recent advances in high precision and autonomous synthesis of such
18 materials. With recent demonstrations of industry-compatible scalable synthesis of high-quality
19 QDs, smart manufacturing of QDs and QD solids, and fabrication of stable solar cells under
20 ambient conditions, we suggest that the technology is beginning to achieve maturity, is on the road
21 to technological relevance and that gigawatt per year distributed panel production sites may be
22 within reach.

23
24
25
26
27
28
29
30
31
32
33
34
35
36
37
38
39
40
41
42
43
44
45
46
47
48
49
50
51
52
53
54
55
56
57
58
59
60

1

2

3 **TOC GRAPHICS:**

4

5

6

7

8

9

10

11

12

13

14

15

16

17

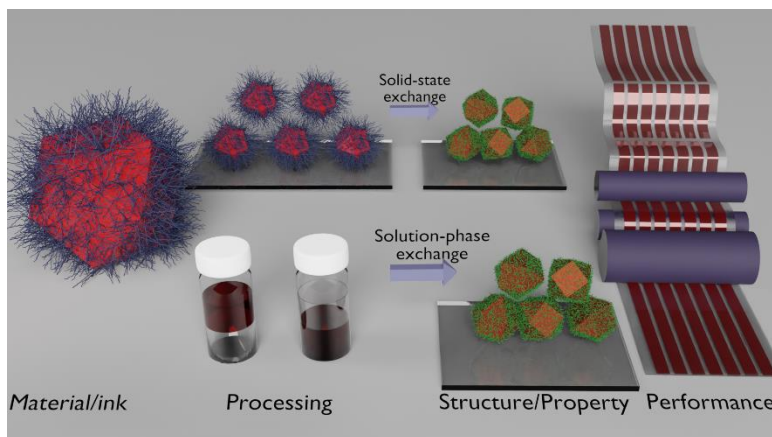
18

19

20

21

22



Colloidal quantum dots (QDs) are solution-synthesized and solution-processed nanocrystals of almost any semiconductor compound, with the added benefit of size, shape and surface chemistry-tunable optical and electronic properties. Conventionally, QDs are synthesized as colloids in organic solvents using the hot-injection method stabilized with long hydrocarbon surface ligands (surfactants). Synthesizing QDs with diameter smaller than the Bohr exciton radius leads to confinement of the photo-generated exciton which allows the QD bandgap to be precisely tuned by controlling the size of the nanocrystals.¹ Some modern semiconductor nanocrystals, such as metal halide perovskites, have many of the benefits of QDs, including tunability, but achieve this through composition tuning rather than size.

Interest in optoelectronics based on QDs has been spurred primarily by i) the promise of multi-exciton generation (MEG) and utilization of hot-carriers that can potentially enable power conversion efficiencies (PCEs) beyond the present-day Si single junction solar cell technology, ii) low-cost manufactured single- and multi-junction architectures, iii) tunable optical bandgaps, iv) tunable charge transport properties by manipulation of their surfaces and packing, v) high defect

tolerance leading to appreciable photoluminescence quantum yields (PLQYs) despite their large surface area, and vi) confinement-induced phase and chemical stabilization.

Since ~50% of the solar spectrum falls in the infrared (IR) which silicon (Si) solar cells, the mainstay of the commercial photovoltaic (PV) technology, cannot efficiently absorb, engineered QDs that harvest further into the IR than currently demonstrated, can be used as bottom cells in tandem device architectures augmenting silicon PV and leading to enhancement of overall PCEs. Demonstrations of QDs tailored to absorb in the long-wavelength spectral region of 1100 – 2500 nm are promising recent developments toward this goal.²⁻⁸ QDs also offer the unique prospect of MEG per absorbed high-energy photon.⁹⁻¹¹ MEG makes QDs exceptional amongst all the other PV materials and, in theory, allows exceeding the single-junction Shockley-Queisser (SQ) limit of *ca.* 33% PCE for a single junction device by relaxing the constraint that each photon only results in a single photogenerated electron-hole pair.¹²⁻¹³ These virtues have put QD solar cells on the roadmap of third generation PV and have fueled intense research activity over the past two decades, though MEG itself has not led to substantial increase in overall efficiency.

Initial demonstrations of solar cells based on inorganic nanocrystals involved a bulk heterojunction of CdSe nanorods with the conjugated polymer poly (3-hexylthiophene) (P3HT) as the absorber layer.¹⁴ This era of initial exploration also produced solar cell architectures where QDs were used to sensitize mesoporous metal oxides in both liquid- and solid-states. CdS, CdSe, PbS and InP QDs were used to sensitize mesoporous metal oxide layers, similar to the concept and design of dye-sensitized solar cells.¹⁵⁻¹⁷ Lead chalcogenide (PbS, PbSe) QDs were the first class of solution-processed semiconductor nanocrystals to be utilized as standalone QD solid absorbers and semiconductor layers in thin film PV cells without a polymer heterojunction or metal oxide scaffold. The success of these materials was ascribed to their large dielectric constants, which

1
2
3 allow efficient delocalization of the photo-generated excitons resulting in high carrier mobilities
4 and large diffusion lengths within the QD solid.¹⁸⁻¹⁹ However, since QDs employ a large surface-
5 to-volume ratio, many surface-related defect/trap states can form due to dangling bonds,
6 atmosphere-induced surface species, and unsatisfied vacancies resulting in charge trapping.
7
8 Therefore, a great deal of research effort has focused on developing strategies to properly address
9 the surface ligand removal/replacement, all the while keeping QD solids as close-packed as
10 possible to maximize charge carrier mobility and diffusion. Despite the large density of surface
11 defects, the recent achievement of ~14% PCEs and remarkable ambient stability and operational
12 stability demonstrates that PbS-based QD solids can be highly tolerant to many of these issues.²⁰
13
14
15
16
17
18
19
20
21
22
23
24
25
26
27 Recently, colloidal metal halide perovskite QDs have emerged as another, perhaps more defect-
28 tolerant material candidate for cost-effective and solution-processed solar cells, LEDs, and
29 displays. In particular, inorganic perovskite QDs, the primary examples of which are cesium lead
30 halides (CsPbX_3 , X=I, Br, Cl), exhibit narrow emission linewidths, strong optical absorption,
31 excellent carrier mobility, and near unity PLQYs, and due to QD processing protocols have lately
32 been used to achieve 16-17% PCE solar cells with graded architectures that cannot easily be
33 formed using bulk lead halide perovskite thin films.²⁴⁻²⁵ The efficiency of these emerging materials
34 is expected to increase well past 20% with more progress in chemistry, processing and device
35 optimization, and will need to leverage chemistry, structure and size confinement to achieve
36 thermodynamic and/or kinetic stability that puts it past the stability of bulk lead halide perovskites.
37
38
39
40
41
42
43
44
45
46
47
48
49
50
51
52
53
54
55
56
57
58
59
50

Besides the obvious virtue of quantum size-confinement in the form of size-tunability of the
optical absorption/emission spectrum, crystallographic phase stability/defect tolerance and
environmental stability have been largely ignored or underappreciated in most discussions on QDs.

This can be best acknowledged in the context of lead halide perovskite QDs. At room temperature, bulk CsPbI_3 has a non-perovskite orthorhombic (δ) preferential crystallographic phase which is optoelectronically incompatible as a solar cell active layer due to its large bandgap (>2.8 eV). However, with expanded lattice, *i.e.* after 300°C post-annealing, the structure undergoes transition into the optoelectronically-compatible cubic (α) phase (bandgap ~ 1.7 eV). The thermal budget involved, however, threatens to make the process unsuitable for low-cost and flexible PV applications. On the other hand, the surface termination of CsPbI_3 QDs causes tensile strain which stabilizes the perovskite phase at room-temperature, solving a crucial challenge. Importantly, CsPbI_3 QD solar cells have outperformed their bulk counterparts in terms of device performance (PCEs), further expanding the benefits portfolio of nanocrystal size effects. $\text{CsPbBr}_x\text{I}_{3-x}$ QD solids have also been employed very recently as interlayers to significantly boost the ambient stability of perovskite solar cells.²⁶

Improved stability under ambient environment for nanometer-sized perovskites has been demonstrated through reduced dimensionality in the context of layered perovskites. For example, Ruddlesden-Popper and Dion-Jacobson perovskites have been shown to exhibit improved resilience against thermal stress, oxygen and moisture compared to bulk phase perovskites.²⁷⁻³⁰ Likewise, oxidation of bulk galena (PbS) in the presence of water has been well-known.³¹ However, due to their size-dependent surface energy, PbS QDs can be made highly air-stable by controlling their crystallographic facets, resulting in highly stable QD solids. Smaller PbS QDs (diameter <4 nm) are mostly covered with Pb-rich (111) facets that bind strongly with surface ligands, increasing air stability of the QDs.³² This improved stability of PbS QDs has allowed fabrication of highly stable and reliable QD solar cells, including a recent report where the PbS

1
2
3 QD solar cells illustrated long-term (>1-year) shelf-life in ambient conditions of high relative
4 humidity (RH >60%) and operational stability over 250 hours of continuous illumination.²²
5
6

7 In most discussions related to QDs to date, surface traps and related phenomena have taken
8 center stage. Despite the well-acknowledged importance of surface traps, the not well-understood
9 and managed surface traps have negatively impacted the performance of QDs optoelectronic
10 devices. However, the above-mentioned discussions clearly highlight the unexpectedly improved
11 stability aspect related to dimensionality reduction of PV absorbers in general, and QDs in
12 particular, despite their inherently large surface-to-volume ratio. We believe that better
13 understanding of this key virtue will increasingly engage researchers in this community to pursue
14 QDs as a viable path to stable, thin-film optoelectronics and photovoltaics.
15
16

17 Surface traps in QDs are a direct consequence of the crystal surface termination and a better
18 understanding of surfaces can potentially lead to efficient trap management strategies. An ideal
19 chemical passivation strategy for QD surfaces will result in suppressed surface traps, reduced
20 interdot spacing, improved charge transport, improved environmental stability, as well as facile
21 and high-speed device processability.
22
23

24 This review is focused on covering recent developments and challenges of visible and NIR-
25 harvesting QD solids including surface traps and successful attempts at alleviating them. Scalable
26 fabrication of long-term stable QD solar cells forms another important focus of this review. Key
27 developments are highlighted where attempts to achieve trap-passivated QD inks and films have
28 directly resulted into devices that can be scalably fabricated. Recent major advancements including
29 solution-phase ligand exchange and the state-of-the-art *n-i-p* device architecture are discussed in
30 detail, and the issue of moisture vulnerability of the *p*-layer is explored. The review also highlights
31 how a comprehensive understanding of the QD surface has paved the way to scalable fabrication
32
33

1
2
3 of robust QD solar cells in realistic ambient environments of high humidity, solving a hurdle to
4 commercialization. The emerging role that data science, machine learning and artificial
5 intelligence are beginning to play in accelerating the development of QD PV technologies and
6 improving their manufacturing will also be discussed. The review will finally discuss the prospects
7 for end-to-end manufacturing of QD solar cells by combining smart in-flow synthesis with smart
8 solution-phase solar cell manufacturing to enable low-cost distributed manufacturing of PV with
9 grid-scale potential.
10
11
12
13
14
15
16
17
18
19

QD Synthesis

20 QDs offer the benefit of low-cost and facile solution-processability. Historically, hot-injection
21 method in batch (flask-based) reactors has been the gold standard technique to synthesize colloidal
22 QDs with high PLQY and high size monodispersity. However, batch synthesis techniques typically
23 suffer from low manufacturing throughputs with difficulties in scale-up while preserving size
24 dispersity, particularly for colloidal QDs with fast formation kinetics (*e.g.*, organic/inorganic lead
25 halide perovskite QDs). To address this issue and accelerate adoption of QDs in energy
26 technologies, microfluidic synthesis techniques have recently been demonstrated with great
27 success. These advances have enabled continuous production of high-quality QDs with
28 significantly higher manufacturing throughputs without sacrificing their quality and size
29 dispersity.
30
31
32
33
34
35
36
37
38
39
40
41
42
43
44
45
46
47
48
49
50
51
52
53
54
55
56
57
58
59
60

Hot-injection synthesis

The most commonly used synthesis method for lead chalcogenide and metal halide perovskite QDs is the so-called ‘hot-injection’ method, which relies on a rapid injection of organometallic precursors into a high boiling point non-coordinating solvent (*e.g.*, octadecene) in the presence of long-chain hydrocarbon surfactants maintained at an elevated temperature (**Figure 1a, b**). Hot-

1
2
3 injection approach was first demonstrated by Murray and Bawendi for the synthesis of CdE (E =
4 S, Se, Te) QDs from organometallic precursors.³³ Hot-injection leads to a rapid nucleation
5 followed by a slow growth of the QDs, effectively decoupling the nucleation and growth stages of
6 nanocrystals in order to avoid Ostwald ripening that is known to cause defocusing/polydispersity
7 of the QD size.³⁴ Hot-injection method results in high size-monodispersity (5-10%) of the final
8 product.^{33, 35-36} This was effectively implemented for PbS QD synthesis in 2003 by Hines and
9 Scholes.³⁷ Oleic acid (OA) capped PbS QDs were precipitated by addition of a non-solvent and
10 finally redispersed in an organic solvent such as chloroform or toluene.
11
12
13
14
15
16
17
18
19
20
21
22
23
24
25
26
27
28
29
30
31
32
33
34
35
36
37
38
39
40
41
42
43
44
45
46
47
48
49
50
51
52
53
54
55
56
57
58
59
60

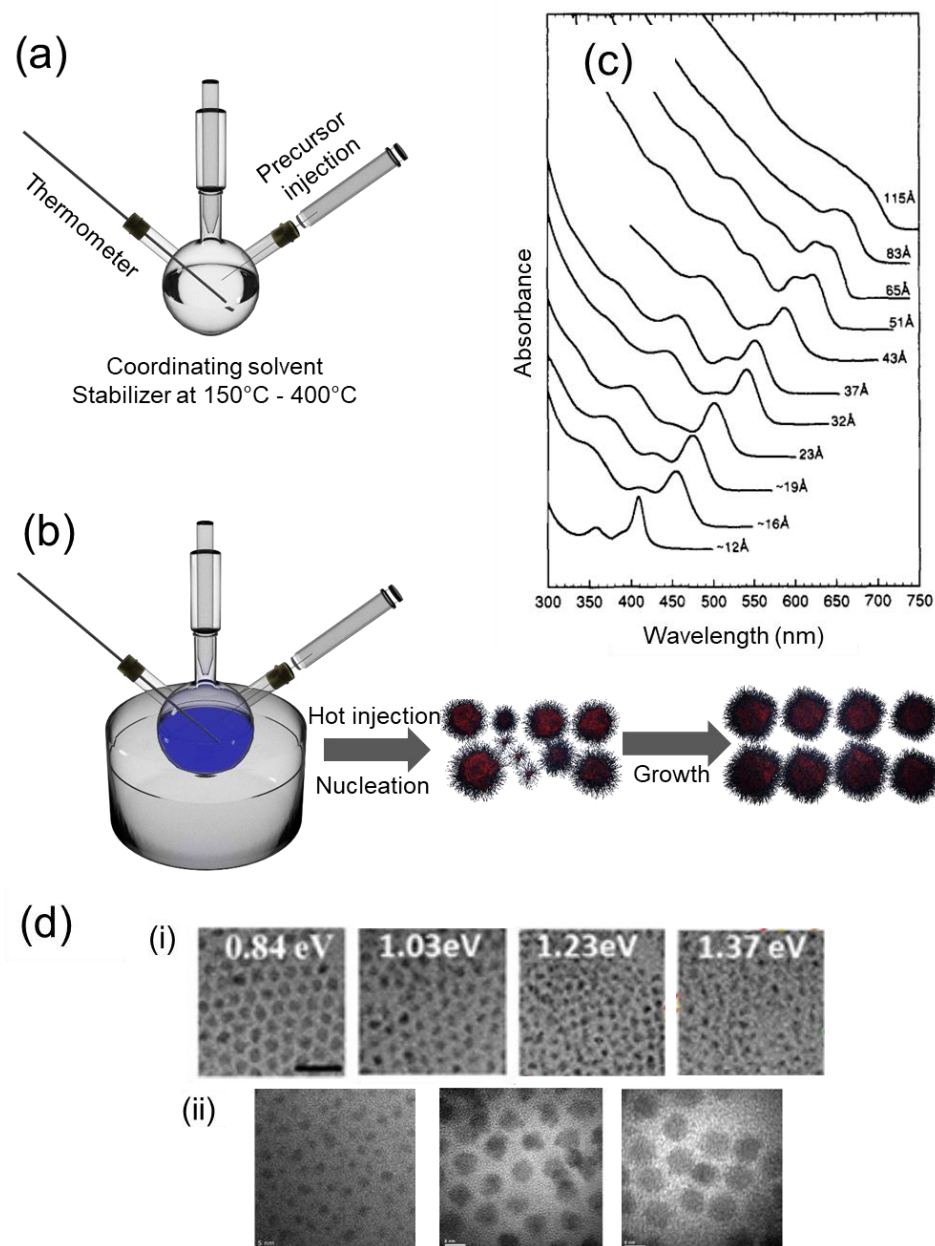


Figure 1. (a) Schematic representation of the hot-injection method. (b) The reaction proceeds with a nucleation burst followed by a slow growth. Reprinted with permission from ref. ³⁸. Copyright 2007 Wiley (c) Optical absorption spectra obtained at room temperature for CdSe QDs in hexane with diameters ranging from 1.2 to 11.5 nm synthesized by the hot-injection method. Adapted with permission from ref. ³³. Copyright 1993 American Chemical Society (d) TEM images of PbS and PbSe QDs synthesized in various sizes relevant for optoelectronic applications (i) PbS QDs (scale bar = 20 nm), reprinted with permission from ref. ³⁹, Copyright 2016 American Chemical Society, and, (ii) PbSe QDs (scale bar = 5 nm). Reprinted with permission from ref. ⁴⁰. Copyright 2015 The Royal Society of Chemistry.

1
2
3 The reliance of hot-injection method, in some cases, on hazardous precursors such as
4 bis(trimethylsilyl) sulfide has motivated research toward utilizing alternative, less-toxic metal
5 precursors.⁴¹⁻⁴² A simplified, alternative non-hot-injection method allows for lower temperature
6 synthesis of QDs without compromising on the physical and chemical properties of the final
7 product.⁴³ Furthermore, large-scale microfluidic synthesis of colloidal QDs has been demonstrated
8 with minimum size dispersity using a numbered-up (parallel microchannels) strategy.⁴⁴⁻⁴⁵
9
10
11
12
13
14
15

16
17 A study by Jean *et al.* concluded that hot-injection is a highly capital-intensive method owing to
18 low yields and, therefore, incompatible with industrial scale-up (**Figure 2a**).⁴⁶ A significant
19 fraction of this high cost is the labor cost which can be attributed to the trial and error-based
20 approach toward discovery, screening, and optimization of QDs, and the lack of a continuous
21 manufacturing technology for cost-efficient production of high-quality QDs. According to this
22 Monte-Carlo cost model, flow-based synthesis and heat-up synthesis can bring down the PbS QD
23 PV module fabrication cost.⁴⁶ Further, the authors find that CsPbI₃ QD PV modules will cost
24 significantly more than PbS QD PV modules, due to the isolation step involved in the synthesis of
25 those QDs. Scale-up of CsPbI₃ QD synthesis is further compounded due to the fast reaction
26 kinetics, which can lead to high size polydispersity.
27
28
29
30
31
32
33
34
35
36
37
38
39
40

41 *Microfluidic synthesis*

42

43 The concept of microfluidic synthesis of colloidal QDs was first introduced in early 2000 by
44 Mathies and Alivisatos,⁴⁷⁻⁴⁸ as well as Jensen and Bawendi.⁴⁹⁻⁵⁰ deMello was the first to
45 demonstrate the potential of rapid synthesis optimization (black-box optimization) of QDs using a
46 glass-based microfluidic reactor integrated with *in situ* spectroscopy.⁵¹ Recently, microfluidic
47 synthesis of QDs,⁵²⁻⁵⁵ particularly lead halide perovskites,⁵⁶⁻⁵⁹ has received significant attention,
48 mainly due to the enhanced heat and mass transfer rates as well as precise process control offered
49
50
51
52
53
54
55
56
57
58
59
60

1
2
3 by microscale fluidic handling technologies.⁶⁰ Microfluidic synthesis of QDs offers the prospect
4 of accelerated formulation screening, fundamental studies, and continuous manufacturing. In
5 2014, Lignos *et al.* reported a droplet-based microfluidic synthesis of PbS and PbSe QDs with
6 narrow size distributions over a wide range of bandgaps with *in situ* PL monitoring. The QDs were
7 found to have a noticeably higher PLQY compared to batch synthesis.⁵² Lignos *et al.* recently
8 demonstrated high-throughput screening of fully inorganic lead halide perovskite QDs using a
9 heat-up synthesis approach in a droplet microfluidic platform.⁵⁶ The developed automated
10 microfluidic platform enabled rapid parameter space mapping as well as kinetic studies of lead
11 halide perovskite QDs. A recent report by Abdel-Latif *et al.* utilized a modular microfluidic
12 platform to demonstrate computer-controlled bandgap tuning of CsPbX₃ QDs (X: Cl, Br, I), shown
13 in Figure 2b.⁵⁸ Using the developed modular microfluidic synthesis technique, called ‘quantum
14 dot exchanger’ (or, QDExer), the QD size distribution, bandgap, and PLQY were simultaneously
15 monitored in real-time using *in situ* UV-Vis absorption and PL spectroscopy, during the automated
16 synthesis/halide exchange of CsPbX₃ QDs.
17
18
19
20
21
22
23
24
25
26
27
28
29
30
31
32
33
34
35
36
37
38
39
40
41
42
43
44
45
46
47
48
49
50
51
52
53
54
55
56
57
58
59
60

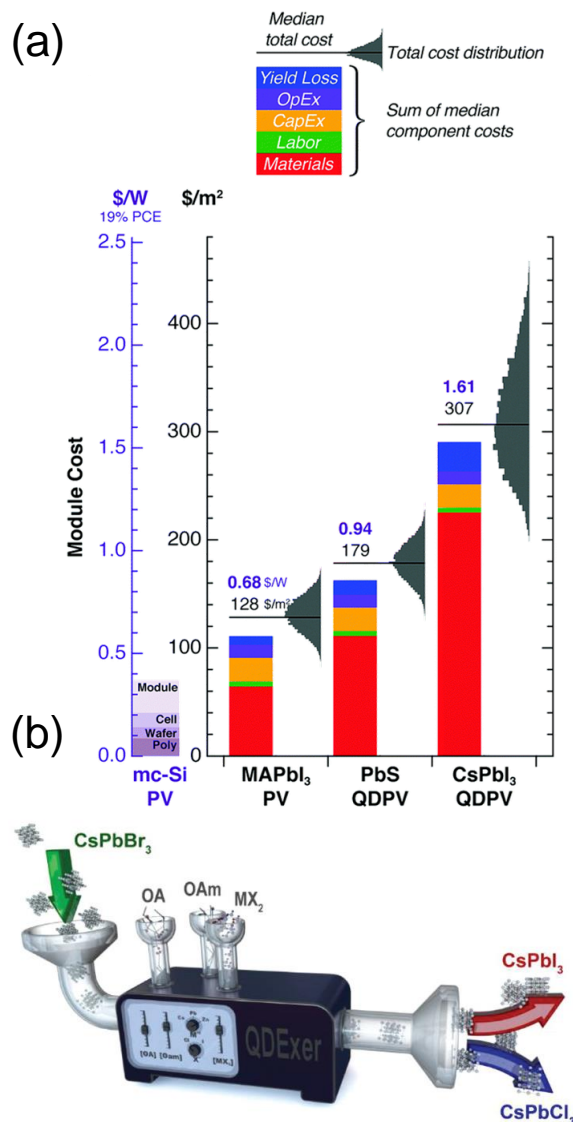


Figure 2. (a) Comparison of the module costs of CsPbI₃ and PbS QD PV as predicted by the Monte Carlo cost model. Reprinted with permission from ref. ⁴⁶, published by The Royal Society of Chemistry. (b) Schematic representation of the QDExer technology for automating the synthesis and exchange of QDs. Reprinted with permission from ref. ⁵⁸. Copyright 2019 Wiley

It was asserted that a scaled-up continuous flow synthesis of QDs using computer-controlled microfluidic reactors would halve the predicted high labor costs involved in the current QD synthesis. To that end, the authors precisely mixed QD synthesis reagents using a train of monodispersed microdroplets flowing through a microreactor, achieving superior mass transfer control compared to batch synthesis.⁵⁸ The technique can synthesize highly size-monodisperse, precisely bandgap engineered QDs at a production rate as high as 1 kg/day with minimal waste

1
2
3 generation. Such modular, computer-controlled QD synthesis platforms integrated with *in situ*
4 diagnostic probes provide an exciting opportunity to combine the wealth of real-time accessible
5 material informatics with rapidly emerging machine learning tools toward achieving autonomous
6
7 QD development and manufacturing, as was recently demonstrated by Epps *et al.*⁶¹
8
9

10
11
12
13 **Optical and Electronic Properties of QDs**
14

15
16 Size-tunability of the optical bandgap can perhaps be singled out as the distinguishing property
17 of QDs that has been the motivating force behind research interest in the field. Lead chalcogenide
18 QDs have high dielectric constants which allow efficient screening of charge carriers resulting in
19 effective delocalization of carrier wavefunctions and hence high mobilities in QD solids. High
20 dielectric constants also result in large Bohr radii of photo-generated excitons in these materials
21 (18 nm for PbS).⁶²⁻⁶⁴ QDs with diameters significantly smaller than the exciton radius harbor
22 unique optical and electronic properties owing to quantum size confinement effects. **Figure 3a**
23 shows the effect of size reduction on the first exciton energy of PbSe QDs. The bandgap of these
24 QDs, and hence the absorption can be tuned simply by changing their size (Figure 3b, c). Thus,
25 whereas bulk PbS exhibits a bandgap of 0.37 eV, PbS QDs of ~3.2 nm size show a bandgap of
26 ~1.3 eV. Coupled with strong absorption, bandgap tunability makes QDs attractive for solar cell
27 applications, allowing for more efficient harvest of the solar spectrum compared to conventional
28 solar modules which are limited by single bandgap absorption (1.1 eV for Si).
29
30
31
32
33
34
35
36
37
38
39
40
41
42
43
44
45
46
47
48
49
50
51
52
53
54
55
56
57
58
59
60

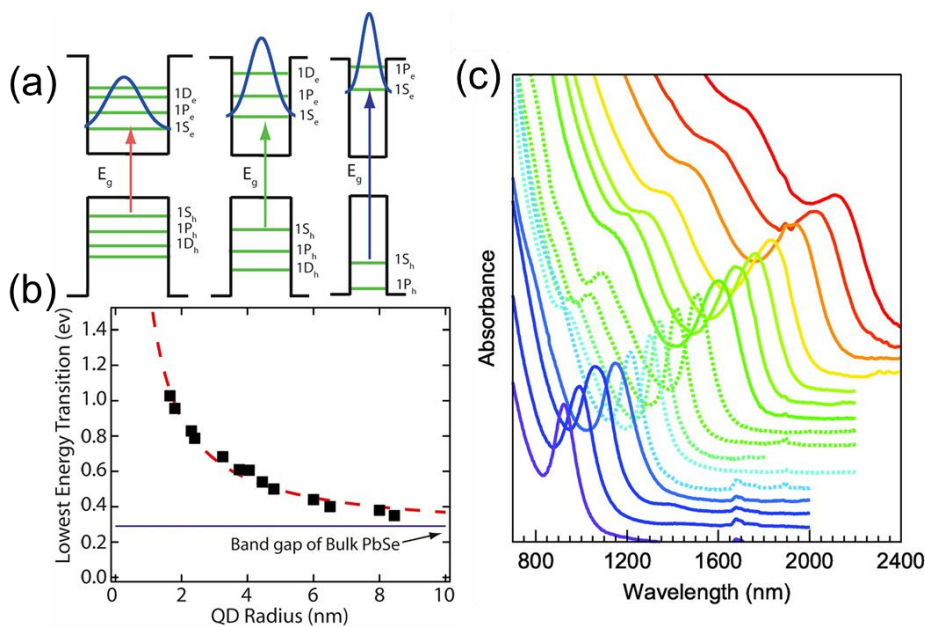


Figure 3. Quantum size effect. (a) Schematic demonstrating increase in quantum confinement with decreasing size of PbSe QDs. Reprinted with permission from ref. ⁶⁵. Copyright 2012 Elsevier (b) Variation of the bandgap of PbSe QDs as a function of their size. Reprinted with permission from ref. ⁶⁵. Copyright 2012 Elsevier (c) Absorbance spectra showing excitonic maxima of PbS QDs with sizes ranging from 3 to 10 nm. Spectra are found to red-shift with increasing size. Reprinted with permission from ref. ⁶⁶. Copyright 2011 American Chemical Society.

From Colloidal Inks to QD Solids

Surface ligands serve *three* crucial purposes during solution-phase synthesis: (i) controlling the growth, leading to enhanced crystallinity, (ii) sterically stabilizing the cores effectively avoiding aggregation, and (iii), electronically passivating the surface of the QDs.⁶⁷ The initial organic ligands used to impart colloidal stability to QDs in organic solvents are long-chain, insulating fatty acids (usually, oleic acid, OA) resulting in poor charge transport through solids made from these QDs, making them the target of substitution with shorter ligands via solid-state (Section 4.1) or solution-phase (Section 4.2) ligand exchange.

The long-chain OA ligands, however, have been shown to impart significant order to the QD assembly, which can form long-range ordered superlattices. The transition of OA-PbS QDs from liquid phase to a solid state and appearance of mesoscale order has been studied in detail using

grazing-incidence small angle X-ray scattering (GISAXS).⁶⁸⁻⁷¹ Drying kinetics, QD size and surface ligand type have been shown to impact the final superlattice configuration. In general, visible-NIR PV-relevant ~1.3 eV bandgap OA-PbS QDs undergo an *fcc-bct-bcc* superlattice transition (Bain transition) during drying.^{68, 72} The potential optoelectronic benefits of QD superlattices have been discussed,⁷³⁻⁷⁶ but have not been directly translated to ligand-exchanged QD solids in PV applications.

Solid-state ligand exchange

The insulating OA-QD solids can be made electrically conductive via a ligand exchange process – wherein the insulating ligands are replaced by shorter, conducting ligands (thiols, halides). Removing the initial OA ligands exposes the QD surfaces to the neighboring environment and creates potentially nefarious surface trap states, which then need to be passivated by the shorter ligand shell. The *solid-state ligand exchange* (SSE) proceeds by briefly dipping the OA-QD solid in a solution of the shorter ligands, as shown in **Figure 4**.

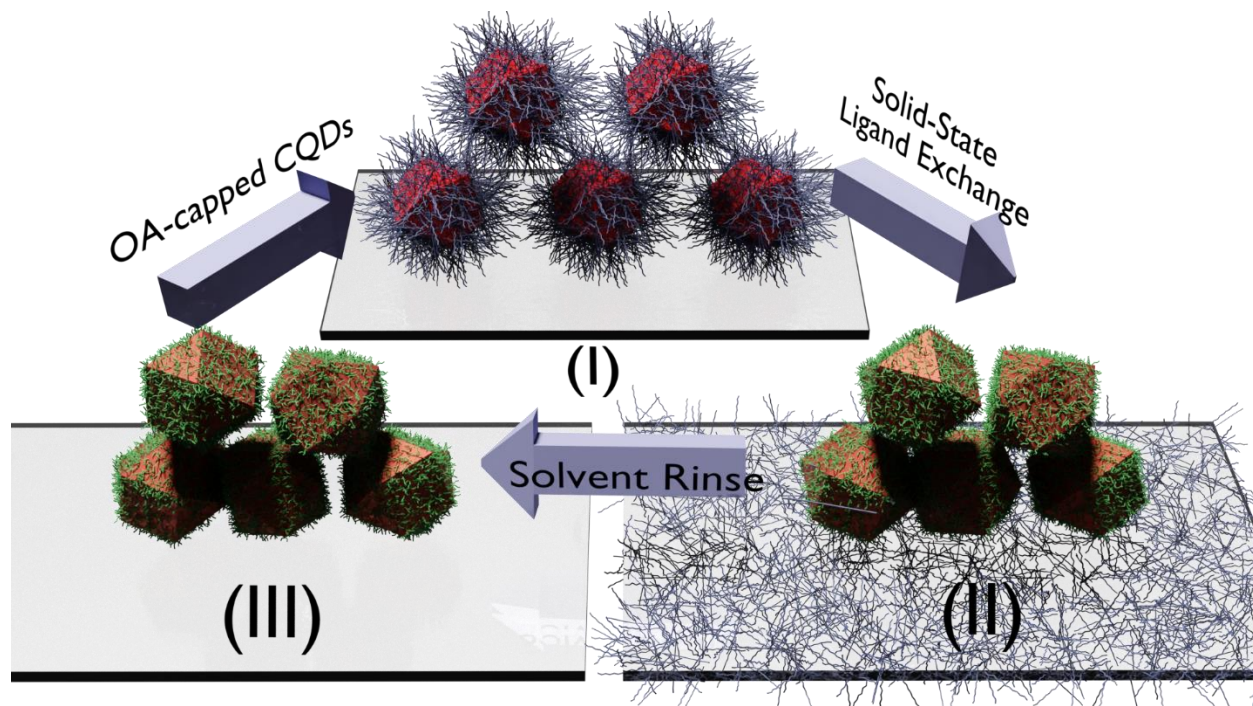


Figure 4. Solid-state ligand exchange. Schematic demonstrates the various steps involved in this exchange process. (I) QDs capped with the longer surfactant (in this case, OA) are cast into a thin solid film. (II) The film is then dipped for a short duration in the solution of a shorter ligand (thiol, halide, amine, etc.). The treatment leads to replacement of the longer ligands with the shorter ones (shown here with green chains capping the QD surfaces). (III) The exchanged thin film is rinsed with a process solvent to remove any traces of the clipped ligands. This process can be repeated several times to build the thickness of an electronically coupled QD active layer for solar cell applications.

It is crucial to supply an optimum number of shorter ligands to the OA-QD surface to enable efficient SSE. As the ligand concentration is tuned, the OA-QDs undergo a steep order-disorder transition, as the authors of this review have recently found.⁷⁷ Below this optimized concentration, solvent effects dominate and the solid remains unexchanged. A sudden transition is then observed near the optimum, above which the various physical and chemical properties of the QD solid (inter-dot spacing, optical absorption, physical density, carrier lifetimes, PCEs) saturate in the case of PbS QDs, signaling completion of exchange (**Figure 5**). This likely happens because the interaction of shorter ligands with the OA ligand coronas is kinetically/sterically hindered, and an optimum concentration is required to initiate exchange due to ligand-ligand cooperativity.⁷⁷

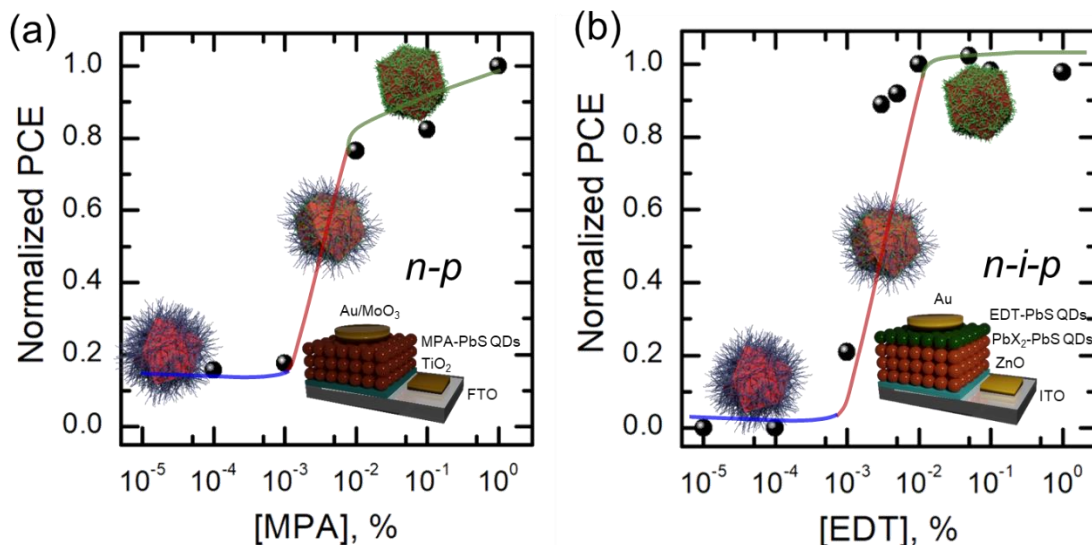


Figure 5. Optimizing solid-state ligand exchange. A sharp phase transition-like behavior in PCEs is observed when shorter ligand concentration (v:v %) during SSE is tuned. Reprinted with permission from ref. ⁷⁷. Copyright 2020 American Chemical Society. This is accompanied by a similar behavior observed for various physico-chemical properties (inter-dot spacing, physical density, optical absorption, carrier lifetimes) and happens due to an increased ligand-ligand

cooperativity once a critical number of short ligands is supplied to the OA-QDs. The study explains why certain solid-state ligand concentrations, often optimized by trial-and-error, have traditionally resulted in the most efficient QD optoelectronics. Insets show the a). *n-p*, and b). *n-i-p* device architectures and will be discussed in detail under Section 5. Also shown in the insets are QD cartoons highlighting the ligand shells getting tuned under the solvent- (blue), transition- (red) and shorter ligand- (green) dominated regimes. Lines are shown as a guide to the eye.

The exchange brings the QDs closer enhancing charge hopping rates besides ensuring that the QD surfaces remain efficiently passivated. The kinetics of the overall process is, however, fast destroying the initial long-range order (Figure 6), and all the reports, to date, have shown the exchanged QD solid to be disordered as the film exhibits only a weak nearest-neighbor coherence peak in GISAXS. The exchanged QD solid is then washed a few times with a process solvent to remove any loosely bound, unexchanged OA and excess shorter ligands. This cycle is repeated around 10-12 times, in a layer-by-layer (LbL) process, to yield a *ca.* 300 nm thick film that can be used as the active layer in a solar cell.⁷⁸⁻⁸⁰

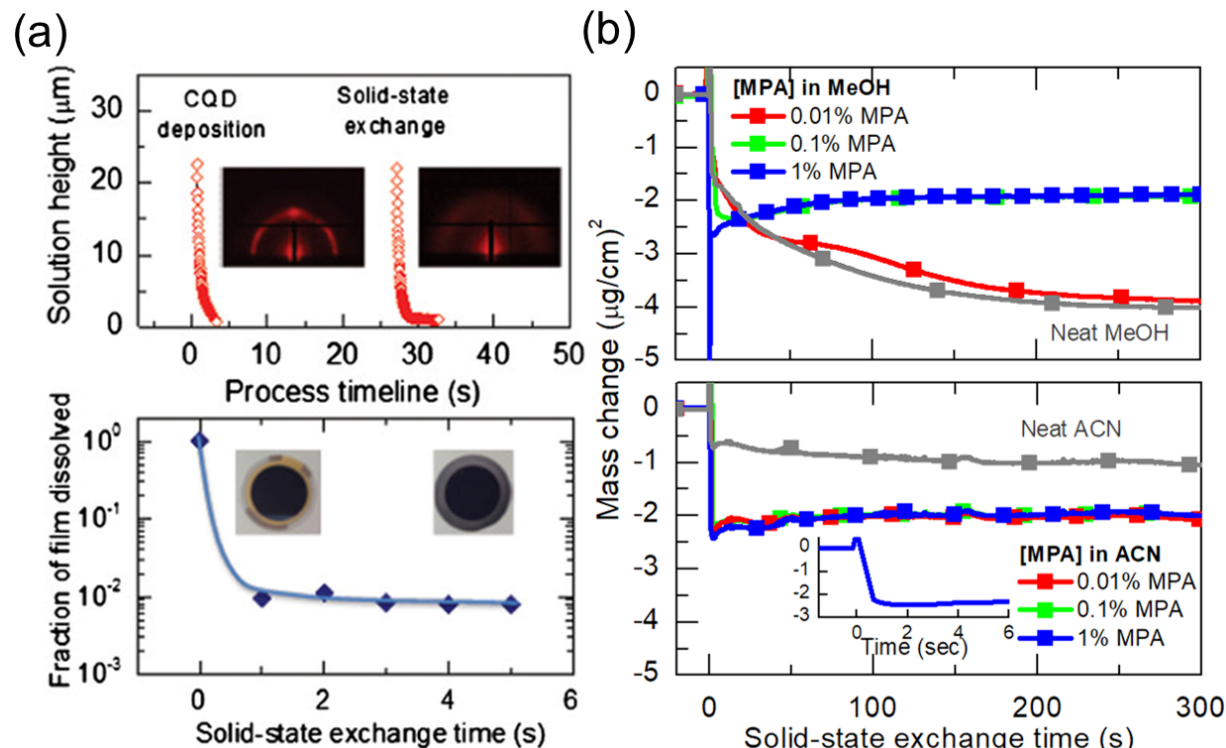


Figure 6. (a) Optical reflectometry and quartz crystal microbalance data demonstrating the rapid volume loss and fast kinetics of SSE. Reprinted with permission from ref. ⁷⁹. Copyright 2013 Cambridge University Press. Insets in top panel of a) are GISAXS patterns highlighting loss of

1
2
3 long-range order in the QD solid upon completion of exchange. b). Mass change of the QD solid
4 during exchange is tracked as a function of exchange time using quartz crystal microbalance, and
5 suggests that exchange is complete within the first ~1-3 s. Insights into exchange kinetics explain
6 the loss of long-range order intrinsic to SSE. Reprinted with permission from ref. ⁸¹. Copyright
7 2014 Wiley.
8

9 The first demonstration of SSE dates back to 2003 by Guyot-Sionnest and involved CdSe QDs
10 capped with trioctylphosphine oxide (TOPO). The bulky organic ligands were replaced by dithiols
11 and diamines enhancing charge transport.⁸²⁻⁸³ The successful demonstration of a solution-
12 processed PbS QD based solar cell by Sargent in 2005 spurred interest in using these quantum
13 materials for optoelectronic applications.¹⁸ Replacing bulky, organic ligands with shorter ones,
14 however, involves significant volume loss and leads to unwanted cracks and pinholes in the film
15 (Figure 7a, b)⁸⁰
16
17
18
19
20
21
22
23
24
25
26
27
28
29
30
31
32
33
34
35
36
37
38
39
40
41
42
43
44
45
46
47
48
49
50
51
52
53
54
55
56
57
58
59
60

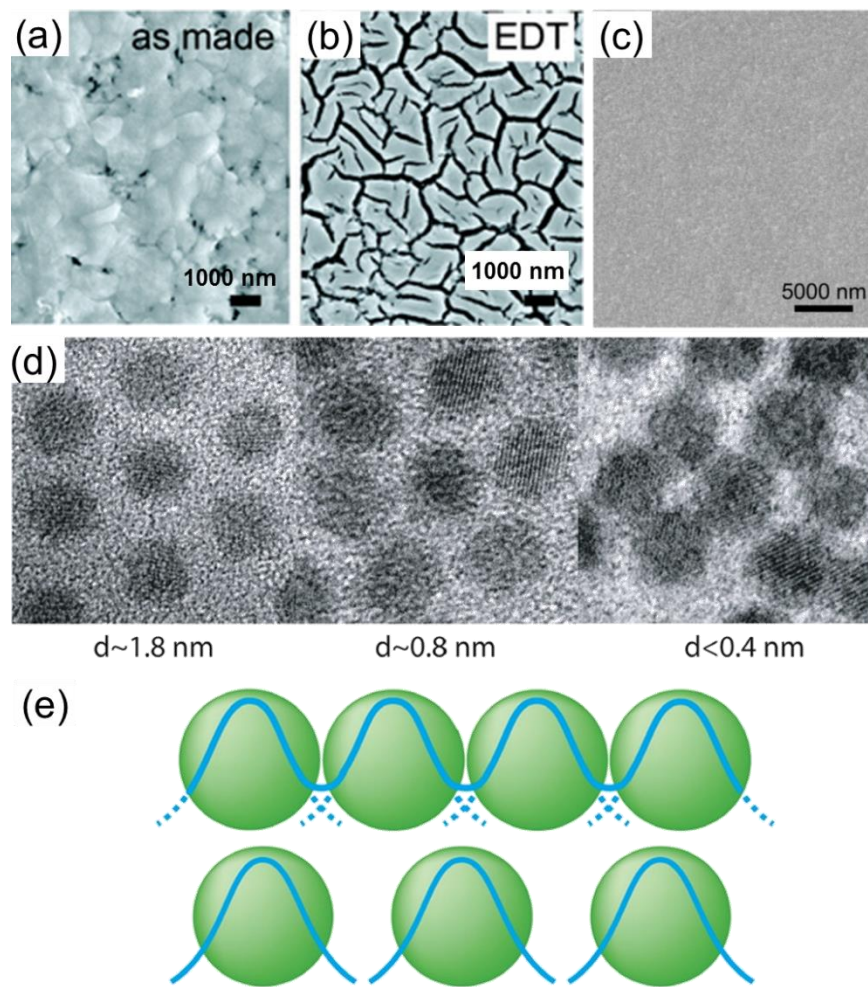


Figure 7. Optical images of spin-coated (a) OA-PbSe QD film and (b) the same film after EDT ligand exchange. Crack formation can be seen owing to the volume contraction upon exchange. (c) SEM image of an LbL film formed via dip-coating shows a smooth surface. Reprinted with permission from ref. ⁸⁰. Copyright 2008 American Chemical Society. (d) TEM images showing reduction in inter-dot distance when OA-PbSe QD solids are dipped in solutions of shorter ligands (aniline and ethylenediamine). Reprinted with permission from ref. ⁸⁴. Copyright 2006 American Chemical Society. (e) Reduced inter-dot distance is suggestive of QDs coming closer leading to enhanced coupling and therefore, a conductive solid. Reprinted with permission from ref. ⁶⁵. Copyright 2012 Elsevier.

A way around was suggested by Luther *et al.* in the form of LbL SSE, in which several layers of exchanged QDs were deposited, in a repetitive process, leading to a crack-free, thick conductive solid (Figure 7c).⁸⁰ Conductive PbSe nanocrystal thin films made by LbL dip-coating and subsequent SSE were obtained using 1,2-ethanedithiol (EDT) as the surface passivant, effectively

1
2
3 reducing the inter-dot distance and enhancing carrier transport.⁸⁰ This important work
4 demonstrated LbL as a general method for fabricating QD solids for solar cell applications.
5
6

7
8 Figure 7d shows a series of TEM images wherein SSE was performed on an OA-PbSe QD
9 solid.⁸⁴ The inter-dot distance decreased from 1.8 nm for OA ligands to 0.8 nm for aniline-capping.
10 This further reduced to < 0.4 nm for the case of ethylenediamine ligands. Reduced inter-dot
11 distance leads to enhanced electronic coupling between adjacent QDs resulting in better
12 wavefunction overlap and charge transport, as illustrated in Figure 7e. The importance of ligand
13 exchange to transforming an ensemble of QDs into a semiconductor solid cannot be overstated
14 and requires simultaneous passivation of surface trap states together with significant reduction of
15 the interdot spacing whilst preserving QD integrity, i.e., quantum confinement.
16
17

18 The LbL process involving SSE is currently the standard protocol for transforming
19 OA/oleylamine-capped CsPbX_3 QDs into coupled, conductive solids for optoelectronic
20 applications.^{24, 85-86} While surface ligand exchange on perovskite QDs is far behind in terms of
21 sophistication and diversity of ligands and protocols, some key concepts transfer over to the
22 perovskite system showing generality. In CsPbI_3 , the strong ionic nature of the compound makes
23 this system incompatible with many polar solvents. It is critical to find a solvent to disperse the
24 new ligands and which does not disperse the QDs with non-polar organic ligands. Methyl acetate
25 was found to accomplish this task well, promoting a moisture-sensitive displacement of native
26 oleate ligands with short acetate molecules.⁸⁶⁻⁸⁷ This process alone creates semiconducting films
27 but it was later found that oleyl ammonium ligands were not fully removed in the process.
28 Perovskite QDs made this way are distinct in that there are both anionic (oleate) and cationic
29 (oleyl ammonium) ligands which can be handled in separate steps. Sanehira *et al.* found that
30 cationic ligands can be replaced with small, typical A-site perovskite cations such as
31
32

1
2
3 formamidinium or methylammonium.⁸⁵ This more complete ligand exchange has two steps but
4 greatly enhances the short circuit photocurrent of perovskite QD devices and leads to tunability of
5 the transport properties. Surface ligand engineering on CsPbBr_3 for efficient LEDs is
6 understandably an important current topic.⁸⁸ The general use of shorter ammonium-based ligands
7 such as quaternary ammonium bromides has been demonstrated.⁸⁹⁻⁹¹ Imran *et al.* reported
8 simultaneous and complete cationic and anionic ligand exchange leading to a variety of
9 advantageous features such as enhanced colloidal stability, thermal stability, and PLQY.⁹² Lu *et*
10 *al.* developed oleate-only ligated perovskite QDs and demonstrated X-type exchange with
11 cinnamate ligands enabling enhanced tunability for photoredox reactions where the nanocrystals
12 can be suspended in semi-polar solvents.⁹³

13
14
15
16
17
18
19 It is important to note that while solid-state ligand exchange has traditionally disrupted
20 mesoscale order of the QD solid's superlattice, carrying out a very slow exchange on a long time
21 scale has been shown to preserve the initial long-range *bcc* superlattice of the OA-QDs, resulting
22 in significantly improved charge transport in the QD solid and highlighted the impact that
23 preservation of long-range order can have on electrical properties of device-relevant QD films.⁷³
24
25 This result highlights the need for more in-depth understanding of the complex ligand exchange
26 process, and a fundamental understanding of ligand exchange kinetics and thermodynamics, their
27 relationship to the mesoscale ordering of the QD solid, and the development of structure-property
28 relationships that govern QD self-assembly, ligand exchange and transformation of electronically
29 uncoupled OA-capped QD solid into a solid-state semiconductor film. Translation of this scientific
30 knowledge into successful engineering and manufacturing practices is therefore crucial.

31
32
33
34
35
36
37
38
39
40
41
42
43
44
45
46
47
48
49
50
51
52
53 **Solution-phase ligand exchange**

1
2
3 Although the SSE process enhances charge transport tremendously, it requires repetitive layer
4 deposition and processing, which are generally reliant on spin-coating, an easy-to-use but highly-
5 wasteful laboratory technique, making the processing incompatible with industrial scale-up. Dip-
6 coating is more scalable to large areas and can be easily automated to meet industrial demands,
7 however, the QD inks and solutions are likely to get contaminated during ligand exchange and
8 may therefore require sophisticated and costly solvent recovery and purification. This expectation
9 is based on an earlier demonstration of large-area scalable spray-coated PbS QD solar cells that
10 required LbL build-up using SSE and consumed 155 g.m⁻² PbS QDs compared to 58 g.m⁻² for
11 laboratory-based spin-coating.⁹⁴⁻⁹⁵
12
13

14 More recently, an alternate route to realizing exchange has been developed that employs a
15 solution phase to carry out the exchange process. The *solution-phase ligand exchange* or SolEx
16 yields an exchanged, *ready-to-coat* QD ink that helps realize single-step deposited active layers,
17 moving away from the time- and materials-wasting LbL process.⁹⁶⁻⁹⁸ SolEx, therefore, presents
18 itself as a more economic and industrially viable route to high-performing QD PV scale-up.
19 Indeed, this can be acknowledged from the fact that recent demonstrations of PbS QD solar cells
20 using SolEx inks have utilized 25 g.m⁻² (spin-coating), 6 g.m⁻² (spray-coating) and 1 g.m⁻² (blade-
21 coating) PbS QDs, which are significantly smaller consumptions than SSE with spin-coating.^{22, 96,}
22
23
24
25
26
27
28
29
30
31
32
33
34
35
36
37
38
39
40
41
42
43
44
45
46
47
48
49
50
51
52
53
54
55
56
57
58
59
60

An efficient SolEx process was demonstrated by Talapin and co-workers that involved replacing
the long-chain, organic insulating ligands on CdSe QDs with inorganic molecular metal
chalcogenides (MCC) in solution-phase yielding field-effect electron mobilities (FET) as high as
38 cm² V⁻¹ s⁻¹.¹⁰⁰⁻¹⁰² These demonstrations illustrate the remarkable ability of SolEx to passivate
surface traps and electronically couple QDs to form a QD solid. The electronic coupling has been
23

1
2
3 shown to result in coherent excitons which can exist over multiple nanocrystals before
4
5 dephasing.¹⁰³
6
7

8 The first attempts at employing SolEx for PV applications goes back to 2005 when Gur *et al.*
9 used pyridine molecules to replace the initial, insulating ligands on rod-shaped CdSe and CdTe
10 nanocrystals. These exchanged nanorods were used as absorber layers in a bilayer structure for
11 solar cells reaching 3.0% PCEs.¹⁰⁴ In the context of PbS QDs, one of the first demonstrations of
12 the SolEx came in the form of a 1.8% PCE Schottky solar cell that employed n-butylamine (BTA)
13 ligand to replace the OA capping layer in solution phase.¹⁰⁵
14
15

16 The previous attempts (noted above) employed more than one layer to achieve the desired
17 absorber thickness. However, the promise of SolEx lies in the possibility of a single-step deposited
18 absorber layer that can do away with the menial LbL protocol. The first such attempt involved
19 replacing the initial OA ligands with shorter, conducting thioglycerol (TG) molecules in solution
20 phase (**Figure 8a**).¹⁰⁶ The exchanged QDs were re-dispersed in a polar solvent, dimethyl sulfoxide
21 (DMSO) and were drop-cast to make the absorber layer. Drop-casting was necessary since DMSO
22 is a high boiling point solvent (189 °C) and therefore film formation requires a longer time (~5
23 hours). The QDs, however, suffered from poor surface coverage leading to low PCEs (~2%). Also,
24 charge transport was found to be limited by the morphological inhomogeneity of the film,
25 including pinhole formation in the drop-cast film, which was reflected by the low fill factor (FF)
26 of 35% in PV devices. The procedure nonetheless opened routes toward achieving directly-
27 deposited conductive active layers of PbS QDs in a single-step, avoiding the rigor and materials
28 wastage involved in the standard SSE process.^{79, 106}
29
30
31
32
33
34
35
36
37
38
39
40
41
42
43
44
45
46
47
48
49
50
51
52
53
54
55
56
57
58
59
60

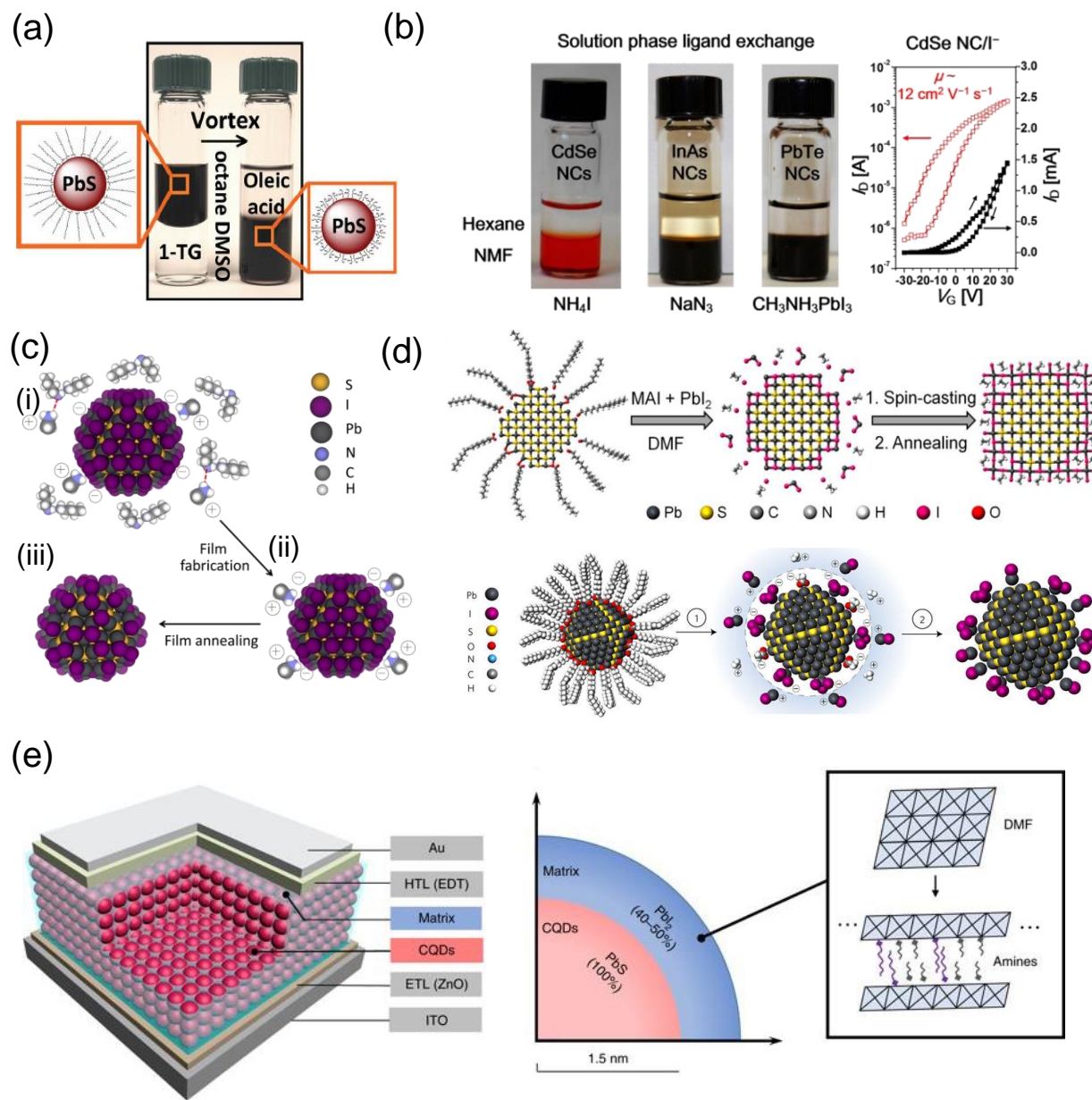


Figure 8. Solution-phase ligand exchange. (a) OA-PbS QDs in octane (left) are mixed in solution-phase with TG. The QDs become soluble in a polar solvent such as DMSO following the exchange (right). Reprinted with permission from ref. ¹⁰⁶, Copyright 2013 Wiley. (b) Halide-, pseudohalide- and halometallate-capped QDs obtained via solution-exchange exhibiting excellent charge transport properties. The exchanged QDs are soluble in N-methylformamide (NMF). Reprinted with permission from ref. ¹⁰⁷, Copyright 2014 American Chemical Society. (c) Iodide-capped QDs obtained using MAI as the precursor, Reprinted with permission from ref ¹⁰⁸, Copyright 2014 American Chemical Society. (d) Perovskite-shelling of QDs (upper panel), reprinted with permission from ref. ⁹⁷, copyright 2015 American Chemical Society, and, PbX_2 -QDs employing ammonium acetate as a colloidal stabilizer (lower panel). Reprinted with permission from ref. ⁹⁶ (e) Two-dimensionally confined PbI_2 matrix shells on QDs for improved carrier diffusion lengths. Reprinted with permission from ref. ¹⁰⁹

Recently, metal halides and hybrid perovskites have been explored as the shorter ligands in the latest brand of solution-exchanged QD inks.^{6, 96-98, 107-108, 110-111} Halide-, pseudohalide- and halometallate-capped QD inks with excellent optical and electronic properties were obtained ushering in a new class of robust inks that could be deposited, in a single-step, as active layers for solar cells.^{98, 107, 110} In one such report, iodide-capped CdSe QD films were found to have field-effect mobilities as high as $12 \text{ cm}^2 \text{ V}^{-1} \text{ s}^{-1}$ (Figure 8b).¹⁰⁷

One of the first demonstrations of high-efficiency solar cells based on these robust, solution-exchanged QD inks came in 2014 when Ning *et al.* demonstrated a solar cell featuring a single-step deposited QD active layer.¹⁰⁸ The QDs were capped with iodide ligands obtained via solution-exchange. The solar cell exhibited a PCE of ~6%, an encouraging device performance given that no solid-state LbL treatment was needed. The steps involved in the exchange process and film fabrication are shown in Figure 8c. A solution of methylammonium iodide (MAI) precursor in dimethylformamide (DMF) was mixed with an octane-based colloid of OA-PbS QDs. Vigorous mixing of the two phases led to ligand exchange in the solution phase observed as a phase separation. These exchanged QDs were then separated, centrifuged and re-dispersed in BTA. The advantage of using the lower boiling point solvent BTA (77-79 °C), as compared to the previous attempt which employed DMSO, was that it enabled a faster solution drying and solidification of the QD film, allowing to move away from drop-casting to spin-coating to achieve sufficiently thick photoactive layers in a single step. The BTA-based QD ink was spin-coated to form a single-step deposited, uniform and continuous active layer. The final film was mildly annealed to remove the organic methylammonium counterions, leaving behind a completely inorganic QD solid.

This demonstration was followed by a report where the authors employed a mixture of MAI and lead iodide (PbI_2) as precursors in the solution-exchange step.⁹⁷ This resulted in replacement of

1
2
3 the OA ligands and formation of methylammonium lead triiodide (MAPbI_3), a hybrid perovskite,
4 on the surface of the QDs, upon mild annealing (Figure 8d, upper panel). These $\text{MAPbI}_3\text{-PbS}$ QD
5 solar cells exhibited high PCEs approaching 9%, which was remarkable for a single-step deposited
6 device.
7
8

9
10 A novel precursor mixture was recently reported wherein the authors aimed to maximize the
11 halide ligand coverage of the QD surfaces (Figure 8d, lower panel).⁹⁶ A mixture of PbX_2 (X = I
12 and Br) and ammonium acetate (AA) dissolved in DMF was used as the precursor solution. AA
13 was found to facilitate the exchange process and was removed from the final QD solid during
14 precipitation. The exchanged QDs were re-dispersed in BTA and spin-coated to form the absorbing
15 layer. As a result of the high halide surface coverage, these QD solids featured significantly
16 suppressed band tails leading to gains in device performance, compared to all the previous SolEx-
17 based QD solar cells. With PCEs as high as 11.3%, this recipe, for the first time, also outperformed
18 solid-state LbL-deposited QD solar cells. Until this point, the absorber layers had to be limited to
19 <300 nm in thickness, owing to their moderate photocarrier diffusion lengths. This resulted in a
20 trade-off between optical absorption (short-circuit current, J_{SC}) and carrier extraction (FF). The
21 gain in J_{SC} for thicker absorbers was compromised by a decrease in FF. It was later found by Xu
22 *et al.* that re-dispersing these SolEx PbS QDs in an amine solvent mixture (BTA, amylamine and
23 hexylamine in a 7:2:1 volumetric ratio) led to the growth of a two-dimensional inorganic
24 passivating matrix around the QD surface leading to improved photocarrier diffusion length
25 (Figure 8e).¹⁰⁹ Formation of solvent- PbX_2 complexes was also found to increase solution viscosity,
26 resulting in thicker active layer deposition by spin-coating. This allowed for *ca.* 500 nm thick
27 absorbers with simultaneous boosts in J_{SC} and FF, and resulted in 12.5% PCE solar cells.
28
29
30
31
32
33
34
35
36
37
38
39
40
41
42
43
44
45
46
47
48
49
50
51
52
53
54
55
56
57
58
59
60

These latest solar cell advances suggest halide-ligands to be unique surface passivants. This choice makes sense in view of recent insights gleaned from inelastic neutron scattering and *ab initio* molecular dynamics simulations highlighting the role of QD surfaces in charge trapping.¹¹² Wood and co-workers have demonstrated that phonon modes on mechanically ‘soft’ QD surfaces couple strongly with electronic transitions leading to carrier trapping. This study highlights the necessity of employing surface ligands that exhibit low vibrational modes, such as halides. Halide surface passivation results in ‘rigid’ QD surfaces, suppressing the electron-phonon coupling and leading to reduced carrier recombination.¹¹³

One of the promises of SolEx QD inks is to enable long-range order in resulting solids by avoiding the disruptive SSE process and thus allow improved carrier mobilities and, potentially, band-like transport.^{74, 114-115} However, all of the reports on SolEx PbS QDs, to date, indicate presence of only the nearest-neighbor coherence peak in GISAXS similar to solid-state exchanged QDs, and a complete absence of long-range order. Long-range order has been associated with size dispersity of the initial OA-PbS QDs prior to exchange, and so further improvements in size dispersity can likely result in long-range order via SolEx. The biggest culprit by far, however, is likely to be the nonequilibrium solution-processing methods, whereby solidification of the solute has been shown, through extensive *in situ* characterization, to occur at the very last second(s) of the solution drying process.¹¹⁶ This is known to occur in spin-cast molecular,¹¹⁷⁻¹¹⁹ polymeric,^{116,}¹²⁰ and metal halide perovskite materials,¹²¹⁻¹²³ as well as in QD films.^{79, 109} In a rapidly drying solution, the solidification process involves complex phase transformation which is initiated by heterogeneous nucleation and growth at first, but quickly transition to bulk precipitation as the solution becomes highly supersaturated,¹²⁴ with the remaining solute becoming quenched into a disordered phase. The upside of rapid drying in solution processing is that it forms uniform films

which tend to be pinhole-free, a major requirement for solar cell devices to work. However, this compromise between mesoscopic order and macroscopic imperfections points to significant opportunities in leveraging innovations in ligand chemistry, self-assembly, formulation science and processing to make major improvements to photoactive layer and QD solid-state semiconductor engineering. Controlling the temporal and spatial onsets and mechanism of solidification should alter the quality of QD solids, analogous to how it has impacted other solution-processed semiconductors, such as conjugated organic materials and bulk metal halide perovskites, with direct impact on their solid-state semiconductor properties and PV device performance.

In this regard, the recent success of metal halide passivation is worth a closer look, because metallate-solvent complexes are known to form and can dominate the solution-processing of these materials via formation of a *sol* which can dramatically slow the effective drying kinetics by retaining the solvent in the as-cast film through a sol-gel process.^{121, 125} Our estimation of solvent retention varies from ca. 50% to 70% by volume in as-cast hybrid perovskite films.^{121, 123} We have also demonstrated that the metal halide formulation can extend the normal drying time of a solvent mixture from <20 seconds to >3 minutes without altering processing conditions.¹²³ The observation of enhanced solvent retention has been made in the latest generation of QDs co-solubilized with metal halides thanks to *in situ* measurements of the solution thinning kinetics during spin-coating,¹⁰⁹ which pointed to a sol-gel-like film formation mechanism in contrast to traditional QD solids, requiring thermal annealing to remove the trapped solvent. This constitutes among the first examples of a passivation strategy which can also alter the ink viscosity, solidification kinetics and mechanism of QD solid formation with direct implication on their optoelectronic properties.

1 2 3 **Atomic-ligand and Hybrid passivation** 4 5

6 A few other surface passivation schemes that were the state-of-the-art recently are worth
7 mentioning here. Most of these have now been outperformed by the novel, halide-based SolEx
8 schemes (discussed above). These schemes employed a combination of an initial solution-phase
9 and a solid-state exchange, and at the time, led to high performing solar cells. These attempts
10 (Figure 9) highlighted the importance of halide passivation and, therefore, guided the research
11 front toward the now-established halide-SolEx, and may offer lessons and inspiration for the lead
12 halide perovskite QD solar cells to adopt.
13
14

15 One of these schemes, the ‘atomic-ligand passivation’, employed an initial solution-phase step
16 where the OA-PbS QDs were first treated with a mixture of CdCl₂, tetradecylphosphonic
17 acid (TDPA), and oleylamine (OLA).¹²⁶ The resulting cadmium–tetradecylphosphonic acid (Cd–
18 TDPA) complex passivated the surface dangling bonds. The QD solid obtained from this ink was
19 then made to undergo an SSE with cetyltrimethylammonium bromide (CTAB) dissolved in
20 methanol (MeOH). This second step ensured that the final solid was left with purely inorganic
21 atomic passivants on the QD surfaces, resulting in LbL-deposited devices with PCEs of ~6%, a
22 QD PV record at the time.
23
24

25 Another similar scheme developed *n*-type PbS QDs by, first partially exchanging a few of the
26 surface OA ligands with iodide atomic ligands.¹¹¹ Tetrabutylammonium iodide (TBAI) precursor
27 was employed. This was then followed by an SSE with TBAI solution in MeOH. This ‘sol-hal’
28 approach resulted in an *n*-type QD solid which was exploited in a quantum-junction QD solar cell
29 (*n-p* homojunction architecture; to be discussed in detail later) with a PCE of 6.6%, besides the
30 demonstration of a record electron FET mobility at the time (for a QD solid with a bandgap > 1.2
31 eV) of 0.24 cm²V⁻¹s⁻¹.
32
33

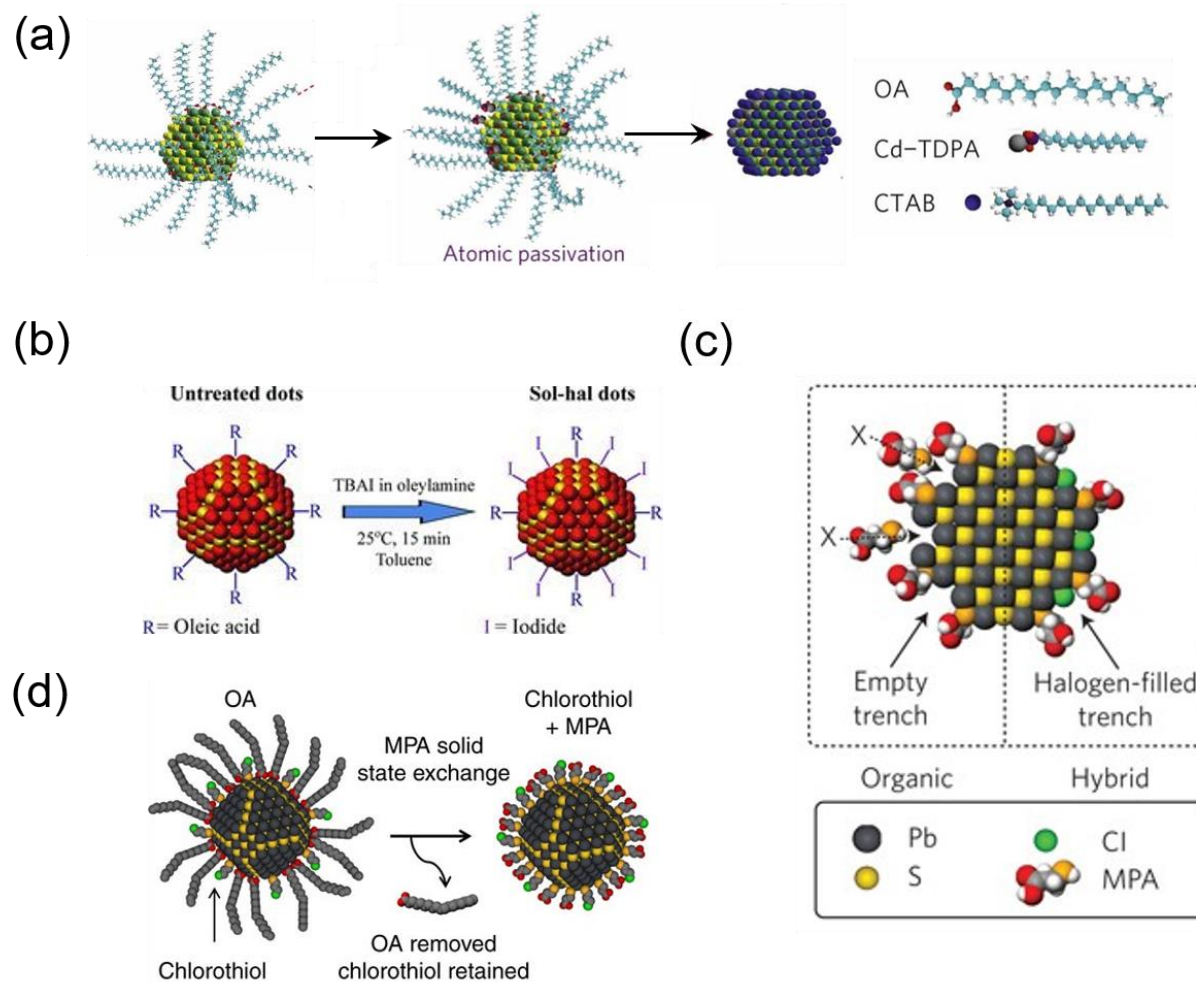


Figure 9. Schematics summarizing ligand exchange strategies that involved an initial solution-phase treatment followed by an SSE step. (a) Atomic ligand passivation scheme involving the removal of OA with Br atoms. Cetyltrimethylammonium bromide (CTAB) is used to carry the Br atoms to the surface. A solution-phase treatment of the OA-PbS QDs with a mixture of CdCl₂, TDPA, and OLA aimed at passivating the surface dangling bonds precedes the SSE. Reprinted with permission from ref. ¹²⁶, Copyright 2011 Springer Nature. (b) The sol-hal approach involves an initial solution-phase halide passivation that removes some of the weakly bound OA and replaces them with halogen atoms. Iodine is delivered via TBAI salt dissolved in MeOH. Reprinted with permission from ref. ¹¹¹, Copyright 2012 Wiley. This is followed by a TBAI-based SSE, resulting in an n-type QD solid (c) Schematic explaining the concept of hybrid passivation. SSE with organic ligands (MPA) leads to empty trenches on the QD surface owing to steric interaction between the organic molecules (left). These un-passivated trenches can behave as carrier traps. An initial solution-phase treatment employing atomic passivants (for example, halides) can avoid this scenario (right). Reprinted with permission from ref. ¹²⁷, Copyright 2012 Springer Nature. (d) This strategy involves a solution-phase ligand exchange step in which chlorothiols and CdCl₂ are introduced to the QD surface. This is followed by the usual SSE with MPA. Reprinted with permission from ref. ¹²⁸, Copyright 2014 Springer Nature.

In 2012, Ip and Thon showed that a ligand exchange strategy designed to deliver inorganic ligands in solution-phase followed by organic thiol molecules in solid-state can lead to improved trap passivation and closer packing of the QD solids.¹²⁷ This strategy, called the hybrid ligand exchange, translated into high performing solar cells with a certified record PCE of 7%. The strategy involved supplying cadmium chloride (CdCl_2) to the as-synthesized OA-PbS QDs in solution phase. Binding of the metal cations as well as the halide atoms to the surface atoms was confirmed spectroscopically. The halides and cations successfully tied to the surface sites that were otherwise not easily accessible due to steric hindrance of the bulky OA molecules. These pre-treated QDs were then subjected to an SSE with MPA, leading to efficiently coupled PV solids. The hybrid-passivated QD solids exhibited significantly suppressed trap states owing to enhanced surface passivation, as proved by ultra-violet and inverse photoemission spectroscopies (UPS and IPES) that allow direct measurements of the band tail states.¹²⁹ The concept of metal halide passivation can be used to tune a variety of the properties of PbX QD arrays through judicious choice of salts.¹³⁰

Nonetheless, it is highly likely that the harsh and rough nature of the SSE step might leach-off some of the surface passivation imparted to the QDs during the solution-exchange step, resulting in trap formation.⁸¹ To overcome this, a modification to the hybrid passivation scheme was developed with introduction of chlorothiols along with CdCl_2 in the solution-exchange step.¹²⁸ The strongly binding thiols remain attached to the QD surface during the harsh SSE step resulting in better-than-ever surface passivation. This resulted in enhanced carrier diffusion lengths driven by a suppression of recombination centers leading to PCEs of 8.5%.

1
2
3 While atomic and hybrid passivation approaches have been surpassed in the PbS QD literature,
4 we take the view that opportunities exist for such strategies in perovskite QDs, where ligand
5 passivation is comparatively rudimentary, but an active topic of research.⁹³
6
7
8
9
10

11 *QD doping*

12

13 Doping of the QD solid is crucial, just as doping of any other semiconductor, as it allows for
14 tailoring the transport properties by changing carrier concentration. This is the basis of
15 semiconductor heterojunctions, and is foundational for numerous applications, such as,
16 photodetectors, solar cells and transistors.^{19, 100, 131-140} Substantial effort has, consequently, focused
17 on realizing efficient doping of QDs. However, initial attempts which involved mixing of dopants
18 with the QD precursors in solution phase during synthesis were less successful.¹⁴¹
19
20
21
22
23
24
25
26

27 The striking observation by Guyot-Sionnest and co-workers that sodium biphenyl leads to $1S_e$ -
28 $1P_e$ intraband absorption in CdSe QDs via remote charge-transfer opened the door to realizing
29 successful doping schemes in QDs.¹⁴² Significant increase in film conductivity was observed for
30 CdSe QDs when potassium was used as the dopant.⁸³ Impressive enhancements in mobilities of
31 PbSe QD solids were found upon hydrazine treatment suggestive of charge transfer doping.¹⁹
32 Substitutional doping, which requires the dopant to replace an atom from the QD, forms the second
33 important category of doping in QDs.¹⁴³
34
35
36
37
38
39
40
41
42
43
44

45 *Ligands as remote dopants*

46

47 Besides enhancing electronic coupling between QDs, ligands can also be chemically and
48 electronically designed to alter and tune the QD carrier concentration, and can therefore act as
49 remote dopants.¹⁴² A charge-orbital balance picture has been suggested to predict the doping
50 phenomenon in QDs based on the overall stoichiometry.¹⁴⁴ Under this premise, (**Figure 10a**), the
51 nature of doping (*n*- or *p*-type) can be determined simply by calculating the total number of excess
52
53
54
55
56
57
58
59

electrons available to the QD. For the case of iodide ligands on PbS QDs, remote charge transfer results in an extra hole and, therefore, *p*-dopes the solid. Substitution of a sulfur atom with an iodide, on the other hand, results in an extra electron, *n*-doping the solid. Given the vast library of available ligands, the carrier concentration and doping of QDs can be tuned over a wide window (Figure 10b).

High carrier mobilities have been achieved for PbS QDs capped with iodide ligands.^{111, 144-147} Employing iodide ligands, *n*-type PbS QDs were realized leading to high efficiency quantum junction and inverted solar cells.¹⁴⁸⁻¹⁴⁹ Konstantatos group has demonstrated remote trap passivation by employing zinc oxide (ZnO) nanocrystals which were shown to remotely transfer electrons into the in-gap states of PbS QDs leading to suppression of trap-assisted carrier recombination.¹⁵⁰

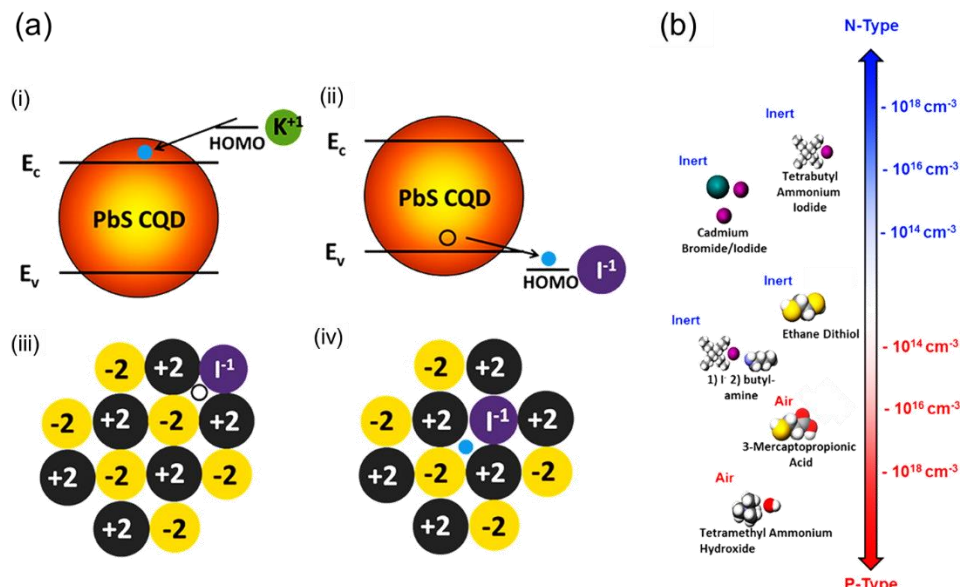


Figure 10. (a) Remote doping by the ligands can be explained from the alignment of energy levels at the interface of the QD and the ligand. A remote cation (potassium) with a shallow HOMO level (lying above the conduction band minima (CBM) of the QD) will behave as a donor, leading to *n*-doping (i). On the other hand, a remote anion (iodide) with HOMO deeper than the valence band maxima (VBM) of the QD will result in *p*-doping (ii). (iii) and (iv) represent remote and substitutional doping scenarios by iodide ligands, respectively. The type of doping can be

1
2
3 discerned simply by counting the total number of excess electrons in the system for each case.
4 Reprinted with permission from ref. ¹⁴⁴. Copyright 2012 American Chemical Society. (b) Effect
5 of various ligand treatments on the doping density of PbS QDs obtained from FET measurements.
6 Reprinted with permission from ref. ¹⁴⁴. Copyright 2012 American Chemical Society.
7

8 From the above discussion, it is clear that the secondary function of ligands as remote and
9 substitutional dopants has significantly helped QD PV. Employing ligands for doping, nonetheless,
10 involves modification of the QD surfaces. A key challenge of this approach is that ligands must
11 fulfill several important and occasionally competing tasks, such as effective trap state passivation,
12 reduction of interdot spacing, and *p*- or *n*-doping, simultaneously. To further enhance the doping
13 level and carrier concentration of the QD solids, a facile method is needed that is not limited by
14 the lack of binding sites (surface coverage) on the ligand-passivated QD surfaces. Electrochemical
15 doping is an interesting avenue; however, it is not compatible with practical applications since it
16 necessitates an externally applied bias.^{3, 83} There have been encouraging demonstrations of using
17 molecules of cobaltocene, decamethylferrocene and decamethylferrocenium as remote dopants for
18 EDT-PbSe and PbS QD solids;¹⁵¹⁻¹⁵² however, these reports lacked any demonstration of
19 molecular remote doping directly leading to solar cell applications.
20
21
22
23
24
25
26
27
28
29
30
31
32
33
34
35
36
37

Remote molecular doping

38 Although ligands can be used to affect doping in QDs, they chemically bind to the QD surfaces.
39 Any further control over doping for charge transport improvement and/or trap state passivation,
40 therefore, has to be performed via physisorption i.e. by a route independent of the docking sites
41 available on the surface. This can be achieved by using molecules that can penetrate the
42 nanoporous QD film and affect charge transfer without necessarily chemically binding to the QD
43 surface. Engel *et al.* demonstrated two orders of magnitude improvement in hole concentration
44 after *p*-doping EDT-PbSe QD films with decamethylferrocene and decamethylferrocenium via
45 reversible charge transfer from solution.¹⁵² Remarkably, Koh *et al.* efficiently converted the
46
47
48
49
50
51
52
53
54
55
56
57
58

1
2
3 insulating OA-PbS and OA-PbSe QD films into *n*-doped solids via electron transfer from
4 cobaltocene. This was realized via a post-fabrication single-step dipping.¹⁵¹ Similarly, benzyl
5 viologen has been used to induce heavy *n*-doping in exchanged PbS QD solids by a simple dipping
6 process, resulting in an electron mobility of $0.64 \text{ cm}^2 \text{V}^{-1} \text{s}^{-1}$ with SiO_2 gate dielectric.¹⁵³
7
8

9
10 Given these encouraging demonstrations, the authors of this review took the aim of enabling
11 molecular remote doping in the context of QD solar cells to controllably shift the position of the
12 Fermi level (E_F) inside the QD bandgap without having to alter the coating process of the QD solid
13 or its ligand chemistry.¹⁵⁴⁻¹⁵⁵ It was realized that the MPA-PbS QDs used as absorbers in *n-p*
14 heterojunction solar cells were marginally *n*-type, in accordance with earlier reports.¹⁵⁶⁻¹⁵⁷ This
15 means *p*-doping these absorbers will increase the quasi- E_F separation of ETL and the absorbers,
16 boosting V_{oc} . Excessive *p*-doping, however, is likely to considerably reduce depletion width in
17 the absorber resulting in reduced J_{sc} and FF. To this end, *p*-doping of the MPA-PbS QD solids
18 with an ACN solution of a metal-organic complex, molybdenum tris(1-(trifluoroacetyl)-2-
19 (trifluoromethyl)ethane-1,2-dithiolene), Mo(tfd-COCF₃)₃, was attempted. The choice of ACN was
20 done in accordance with our previous finding that it does not interact and modify the QD surface.⁸¹
21 The doping was carried out as a post-fabrication step by dipping the device in the dopant solution
22 for an optimized time (several mins), before electrode deposition. Band structure of the doped QD
23 solids was probed with UPS, which clearly showed migration of the E_F toward the middle of the
24 bandgap, suggesting *p*-doping. For higher dopant concentrations, significant shifts in the band
25 structure were observed. From this it was concluded that for these high dopant concentrations,
26 dopant molecules around the QDs formed dipoles, significantly shifting the VBM to large values.
27 As expected, device performances degraded in this dopant concentration regime. For the optimized
28
29
30
31
32
33
34
35
36
37
38
39
40
41
42
43
44
45
46
47
48
49
50
51
52
53
54
55
56
57
58
59
60

1
2
3 dopant concentration, device performance increased from PCE of 6.3% via concomitant
4 improvements in the J_{SC} , V_{OC} and FF leading a highest PCE of 7.8%.
5
6

7
8 The idea of molecular remote doping was next extended to *n-i-p* architecture solar cells that
9 utilized SolEx absorbers. Specifically, *p*-doping the EDT-PbS QD HTL for solar cells based on
10 MAPbI₃-PbS QD and PbX₂-PbS QD absorbers was targeted. The idea was inspired by the general
11 observation in silicon PV where a heavily *n*-doped Si layer is used to fully deplete the Si absorber
12 layer. EDT-PbS QD solids are known to be weakly *p*-doped,¹⁵⁸⁻¹⁵⁹ and further gains in hole
13 concentration are required in order to extend depletion in the absorber. Besides, both these absorber
14 layers are intrinsically *n*-doped, meaning that the ETL needs to be degenerately doped in order to
15 maintain band bending at the maximum power point (MPP) during device operation. This inherent
16 *n*-type nature of the absorbers and the difficulty in achieving degenerate *n*-type doping in the ETL
17 further necessitate efficient designs to enable *p*-doping in the HTL. Importantly, the *n-i-p*
18 architecture differs from the *n-p* architecture in that *p*-doping of the HTL can potentially increase
19 depletion width in the absorber benefiting charge collection while increasing V_{OC} .¹⁶⁰
20
21

22
23 With this target in mind, *p*-doping of the EDT-PbS QD solids was optimized, resorting to the
24 metal-organic complex, Mo(tfd-COCF₃)₃. Interestingly, the authors again found two distinct
25 dopant concentration regimes: the lower concentrations successfully tuned the E_F , while the higher
26 concentrations also led to surface dipoles and pushed down the entire band structure. A notable
27 challenge in doping the HTL in this architecture was to selectively dope the HTL (thickness ~30-
28 50 nm). This was achieved by briefly soaking the HTL upon device fabrication in the optimized
29 dopant concentration in a single step for ~30s. This led to improvement in the interfacial band
30 bending at the absorber:HTL interface and extended depletion in the absorber, resulting in
31 improvements in J_{SC} and FF and leading to overall increase in PCEs (best-performing device =
32
33

9.5% PCE). External quantum efficiency (EQE) measurements done at MPP confirmed that the optimally doped device was able to maintain better band bending at MPP, in accordance with extended depletion of the absorber.

Remote doping such as this is also very effective in perovskite QD systems such as CsPbI_3 QDs using 2,3,5,6-tetrafluoro-7,7,8,8-tetracyanoquinodimethane (F₄TCNQ) as the *p*-dopant or benzyl viologen as the *n*-dopant.¹⁶¹ Here, the modification of the QD array with remote dopants leads to a dramatic increase in the mobility of charges, and was used for efficient phototransistors.

From QD Solids to Solar Cell Devices

Thermalization of hot carriers to band edges accounts for 33% loss for a single-junction 1.1 eV bandgap solar cell. Besides this, the bandgap sets a lower limit on the wavelengths that can be absorbed by the PV device. Subtracting the losses incurred due to extraction of charges leaves 33% of the available solar power that can be harnessed by the solar cell, a number also called the SQ limit.¹² QD solar cells, however, are capable of breaching the SQ limit thanks to the possibility of harvesting hot carriers and MEG.¹⁰⁻¹¹ Besides, it is possible to absorb the below-gap IR photons that are otherwise wasted, by engineering intermediate bands in QDs.¹⁶² Although these features have not been explicitly exploited yet in QD PV, they make this technology one of the most promising thin film PV technologies in the long run to break the SQ limit, and has been among the guiding forces behind the intense research in this area over the past decade. Below, we chronicle the development of QD PV device architectures.

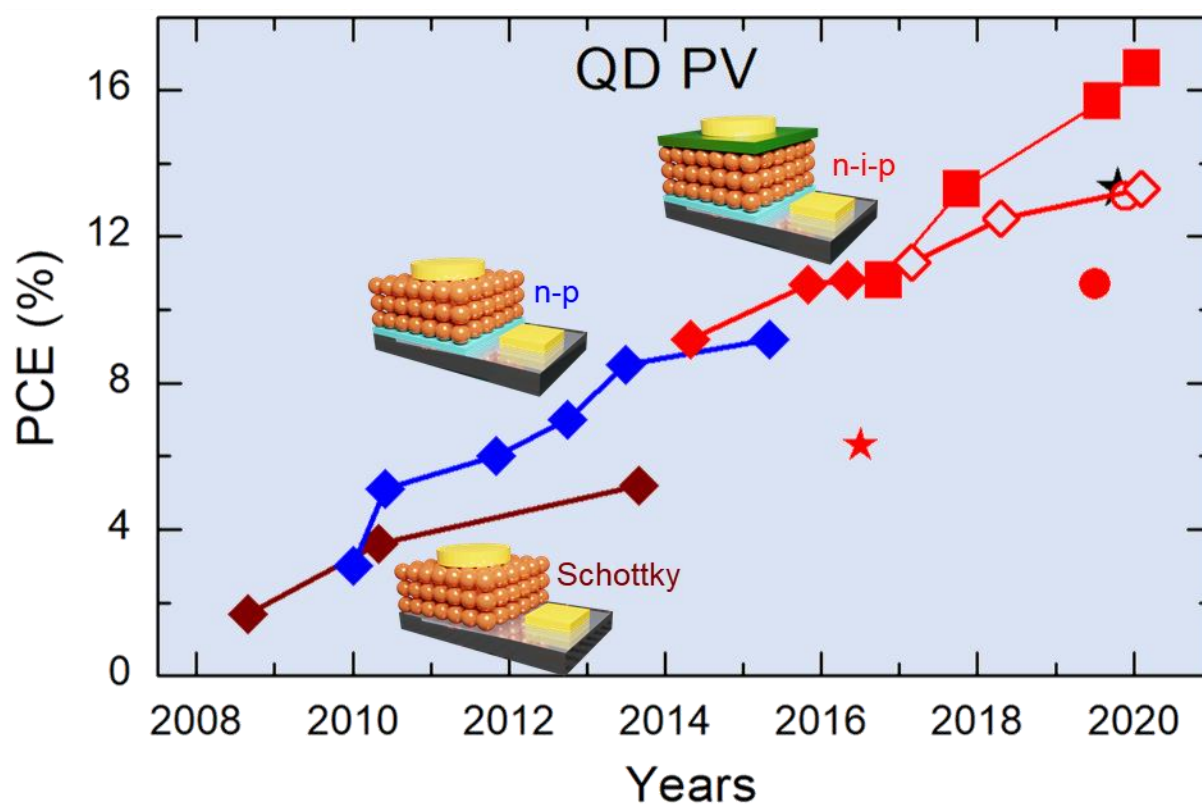


Figure 11. *PCEs for QD PV over the years.* The PCE growth can be ascribed, largely, to the introduction of three main QD solar cell architectures over time, Schottky (brown), DHJ (blue) and *n-i-p* (red). These device engineering breakthroughs have been further augmented along the way with robust surface passivation recipes and the deployment of SSE, and later, SPE. Datapoints shown in the graph are mentioned here in chronological order along with their references. All of the datapoints represented with solid symbols have employed SSE, while the open symbols represent SPE, with the exception of black-star that represents QD-sensitized solar cell.

◆ Schottky PbS QD PV: 1.7%,¹⁶³ 3.6%,¹⁶⁴ 5.2%,¹⁶⁵ ◆ *n-p* PbS QD PV: 3.0% (certified),¹⁶⁶ 5.1%,¹⁶⁷ 6.0%,¹²⁶ 7.0% (certified),¹²⁷ 8.5%,¹⁶⁸ 9.2%,¹⁶⁹ ◆ *n-i-p* PbS QD PV: 9.2%,¹⁷⁰ 10.7%,¹⁷¹ 10.8%,⁹⁵ ◇ *n-i-p* PbS QD PV (SPE): 11.3% (certified),⁹⁶ 12.5%,¹⁰⁹ 13.3%,²⁰ ■ *n-i-p* Perovskite QD PV: 10.8%,⁸⁶ 13.4% (certified),⁸⁵ 15.7% (certified),²⁴ 16.6% (certified),²⁵ ★ QD-sensitized PV: 13.3%,¹⁷² ★ *n-i-p* AgBiS₂ QD PV: 6.3% (certified),¹⁷³ ○ PbS QD/organic hybrid (SPE): 13.1%,²¹ ● *n-i-p* PbSe QD PV: 10.7%.¹⁷⁴

PbS QD PV efficiencies have risen dramatically over the last decade. The PCE growth is summarized in **Figure 11**, and can be categorized into three main eras: Schottky architecture era (brown), depleted heterojunction (DHJ) architecture era (blue) and *n-i-p* architecture era (red). In each of these eras, modifications to ligand exchange, control over doping type and amplitude, and

1
2
3 improvements in device architecture have combined to push the PCEs up. Major QD solar cell
4
5 architectures are briefly discussed below.
6
7

8 ***Schottky architecture***
9

10 Schottky solar cells employ a fairly simple architecture with a thin QD absorber layer
11 sandwiched between the top (a low-work function metal) and bottom Ohmic-contact transparent
12 (ITO) electrodes (**Figure 12a**). The QD absorber forms a Schottky contact with the metal electrode
13 which effectively separates excitons photo-generated in the absorber. The Schottky device
14 architecture primarily suffers from two major issues: i). since the junction is formed at the backside
15 (far-end) and transport in QDs is limited owing to small minority carrier diffusion lengths,
16 thickness of the absorber and hence absorption are limited, leading to ineffective collection of
17 charges generated at the back end of the cell. ii). A second disadvantage of this architecture is the
18 E_F -pinning limiting the open-circuit voltage (V_{oc}) which cannot exceed half the QD bandgap.
19 Schottky architecture was, in fact, the first to be studied in QD solar cells. The first demonstration
20 employed SSE with EDT ligands and led to PCEs of 1.8%.¹⁶³ Improvement was demonstrated
21 when a combination of SolEx and SSE was employed.¹⁶⁴ SSE with 1,4-benzenedithiol (BDT) has
22 recently taken these cells to 5.2%,¹⁶⁵ however, interest in Schottky architecture has waned since
23 the advent of the better-performing DHJ and *n-i-p* architectures. The growth of QD PV employing
24 the Schottky architecture is represented by the brown thread in Figure 11.
25
26

27 ***Depleted heterojunction (DHJ) architecture***
28

29 One of the first demonstrations of the DHJ architecture employed PbSe QDs in contact with a
30 ZnO layer and resulted in 1.6% PCE.¹⁷⁵ This architecture was adopted by the PbS QD
31 community,¹⁶⁶⁻¹⁶⁷ and was an immediate success resulting, simultaneously, in high J_{sc} and V_{oc}
32 and therefore high PCEs. These solar cells carry the obvious distinction of a *n-p* heterojunction
33 and therefore high PCEs. These solar cells carry the obvious distinction of a *n-p* heterojunction
34 and therefore high PCEs. These solar cells carry the obvious distinction of a *n-p* heterojunction
35 and therefore high PCEs. These solar cells carry the obvious distinction of a *n-p* heterojunction
36 and therefore high PCEs. These solar cells carry the obvious distinction of a *n-p* heterojunction
37 and therefore high PCEs. These solar cells carry the obvious distinction of a *n-p* heterojunction
38 and therefore high PCEs. These solar cells carry the obvious distinction of a *n-p* heterojunction
39 and therefore high PCEs. These solar cells carry the obvious distinction of a *n-p* heterojunction
40 and therefore high PCEs. These solar cells carry the obvious distinction of a *n-p* heterojunction
41 and therefore high PCEs. These solar cells carry the obvious distinction of a *n-p* heterojunction
42 and therefore high PCEs. These solar cells carry the obvious distinction of a *n-p* heterojunction
43 and therefore high PCEs. These solar cells carry the obvious distinction of a *n-p* heterojunction
44 and therefore high PCEs. These solar cells carry the obvious distinction of a *n-p* heterojunction
45 and therefore high PCEs. These solar cells carry the obvious distinction of a *n-p* heterojunction
46 and therefore high PCEs. These solar cells carry the obvious distinction of a *n-p* heterojunction
47 and therefore high PCEs. These solar cells carry the obvious distinction of a *n-p* heterojunction
48 and therefore high PCEs. These solar cells carry the obvious distinction of a *n-p* heterojunction
49 and therefore high PCEs. These solar cells carry the obvious distinction of a *n-p* heterojunction
50 and therefore high PCEs. These solar cells carry the obvious distinction of a *n-p* heterojunction
51 and therefore high PCEs. These solar cells carry the obvious distinction of a *n-p* heterojunction
52 and therefore high PCEs. These solar cells carry the obvious distinction of a *n-p* heterojunction
53 and therefore high PCEs. These solar cells carry the obvious distinction of a *n-p* heterojunction
54 and therefore high PCEs. These solar cells carry the obvious distinction of a *n-p* heterojunction
55 and therefore high PCEs. These solar cells carry the obvious distinction of a *n-p* heterojunction
56 and therefore high PCEs. These solar cells carry the obvious distinction of a *n-p* heterojunction
57 and therefore high PCEs. These solar cells carry the obvious distinction of a *n-p* heterojunction
58 and therefore high PCEs. These solar cells carry the obvious distinction of a *n-p* heterojunction
59 and therefore high PCEs. These solar cells carry the obvious distinction of a *n-p* heterojunction
60

1
2
3 between the *p*-type QD and the *n*-type wider bandgap metal oxide layers (Figure 12b). Importantly,
4 the depleted heterojunction is situated closer to the transparent front contact, overcoming the
5 charge extraction bottleneck associated with the Schottky architecture, leading to high FFs in
6 excess of 55%. Since the excitons generated at the back end had to rely on diffusion for extraction,
7 robust passivation schemes were developed to suppress traps and enhance diffusion lengths in the
8 solids. Atomic-ligand and hybrid passivation strategies made impacts and led to record PCEs at
9 the time.¹²⁶⁻¹²⁷ These strategies employed a pre-treatment of SolEx passivation of QDs, followed
10 by an SSE of the films, to ensure better overall surface passivation.
11
12

13 Since the DHJ architecture had to rely on diffusion-limited charge transport beyond the depleted
14 QD solid, it was argued that enhancing the depletion region would benefit charge extraction,
15 similar to the effect of increasing carrier diffusion lengths. This led to the concept of the ‘donor-
16 supply electrode’.^{168, 176} The electron accepting metal oxide was placed in contact with a shallow
17 work function front electrode. This effectively enhanced the electron density in the oxide layer via
18 charge-transfer doping. The *n*-type oxide with an increased free carrier density pushed forward the
19 depletion region in the QD solid, resulting in better charge collection. The concept led to 8.5%
20 PCE DHJ solar cells.¹⁶⁸ These devices employed hybrid passivated PbS QDs.
21
22

23 The hybrid passivation scheme, as mentioned earlier, involved a CdCl₂ surface treatment of the
24 QDs in the solution-phase, besides the usual solid-state treatment (with MPA) of the solid. It was
25 found that replacing CdCl₂ with amines in the SolEx induced partial fusion of the QDs leading to
26 self-passivation of the surfaces.¹⁶⁹ This modified hybrid passivation approach, effectively, reduced
27 the overall QD surface area leading to reduced surface traps.
28
29
30
31
32
33
34
35
36
37
38
39
40
41
42
43
44
45
46
47
48
49
50
51
52
53
54
55
56
57
58
59
60

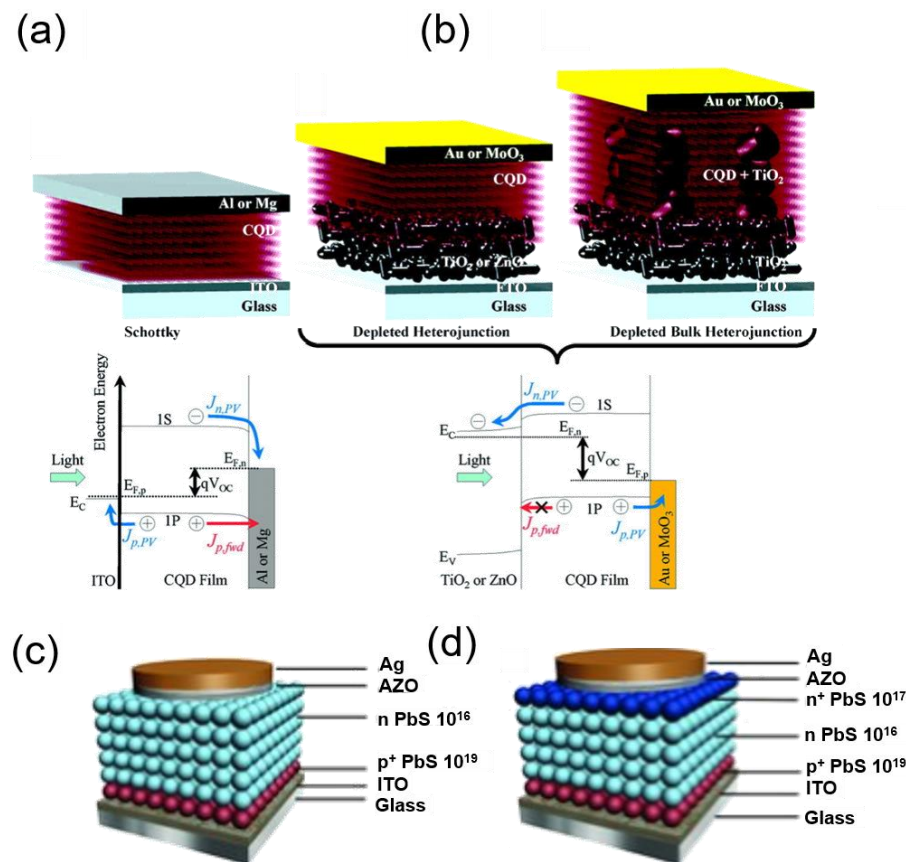


Figure 12. (a) Schottky device architecture, reprinted with permission from ref. ¹⁷⁷, Copyright 2011 American Chemical Society (b) DHJ (left) and DBJ (right) architectures, reprinted with permission from ref. ¹⁷⁷, Copyright 2011 American Chemical Society (c) quantum homojunction device architecture, reprinted with permission from ref. ¹⁷⁸, Copyright 2013 Wiley, and (d) graded doped device architecture, reprinted with permission from ref. ¹⁷⁸, Copyright 2013 Wiley.

These robust QDs featured record-high diffusion lengths in excess of 200 nm allowing fabrication of 600 nm thick absorber layers resulting in J_{SC} as high as 29.5 mA cm^{-2} . This strategy took the DHJ solar cells to 9.2%.

An interesting modification of the DHJ architecture targeted enhancement of charge extraction from the absorber by employing nanostructured electron acceptors. The idea is similar to the scheme well-known in organic PV where the electron-donating phase (donor) and electron-accepting phase (acceptor) are mixed together forming nanodomains improving charge extraction, circumventing the short carrier diffusion lengths in those materials.¹¹⁶ This architecture was called

1
2
3 the depleted bulk-heterojunction (DBJ) and aimed to break the photon absorption-carrier
4 extraction compromise in the DHJ solar cells (Figure 12b). Usually, nanopillars, nanowires or
5 larger nanoparticles of the electron acceptor were employed into which QDs were deposited.¹⁷⁹⁻¹⁸²
6
7 This allowed deposition of thicker PV solids and lent a three-dimensional spatial extent to the *n-p*
8 junction, compromising for the short diffusion lengths of minority carriers in these solids.¹⁸³⁻¹⁸⁴
9
10 PCEs with the bulk heterojunction architecture have very recently approached 10% by carefully
11 controlling the growth orientation of the ZnO nanowires, and enabling capillary attractive
12 interactions between the nanowires and PbS QDs that led to denser packing and increased
13 infiltration of the QDs.¹⁸⁵
14
15
16
17
18
19
20
21
22
23
24
25 ***Quantum homojunction***
26
27 The slight offset between the bands of the electron acceptor and the QD solid in the DHJs leads
28 to an unfavorable ‘spike’ at the interfacial band structure, which either hurts the V_{OC} or the J_{SC} ,
29 depending on its direction. This necessitates the concept of a homojunction which can guarantee a
30 smooth band bending at the interface. This requirement fueled the demonstration of the first
31 quantum homojunction QD solar cell.¹⁴⁹ It had an added advantage of photon absorption by both
32 the *n*- and *p*-sides of the junction, enhancing light harvesting. The architecture is shown in Figure
33 12c and employs a thick *n*-type QD solid atop a thin *p*-type QD layer. A highest performing device
34 of 5.4% PCE was achieved. Importantly, this was one of the first demonstrations of a PV device
35 employing *n*-type QDs.
36
37
38
39
40
41
42
43
44
45
46
47
48
49
50
51
52
53
54
55
56
57
58
59
60

The *n*-type solids employed in this architecture had low doping. Increasing the doping of these layers can lead to a higher V_{OC} , however, will decrease the depletion region width. To solve this, a graded doping approach was developed (Figure 12d).¹⁷⁸ A highly *n*-doped QD solid was placed

1
2
3 atop the *n*-type QD layer aiding carrier extraction and also the overall Voc. This adjustment led to
4
5 a 7.4% PCE quantum junction solar cell.
6
7
8

9 ***n-i-p architecture***

10
11 In 2014, Chuang *et al.* noticed that it was possible to affect energy level shifts in the QD band
12 structures by varying the surface ligands (**Figure 13a**).¹⁵⁶ Whereas halide ligands were found to
13 push the band structures deep (large electron affinities), thiols would render the QD band structures
14 shallow (small electron affinities). It was suggested that the overall changes to the band structures
15 were due to a combination of the QD-ligand interface dipole and the interface dipole moment of
16 the ligand.
17
18
19
20
21
22
23
24
25
26
27
28
29
30
31
32
33
34
35
36
37
38
39
40
41
42
43
44
45
46
47
48
49
50
51
52
53
54
55
56
57
58
59
60

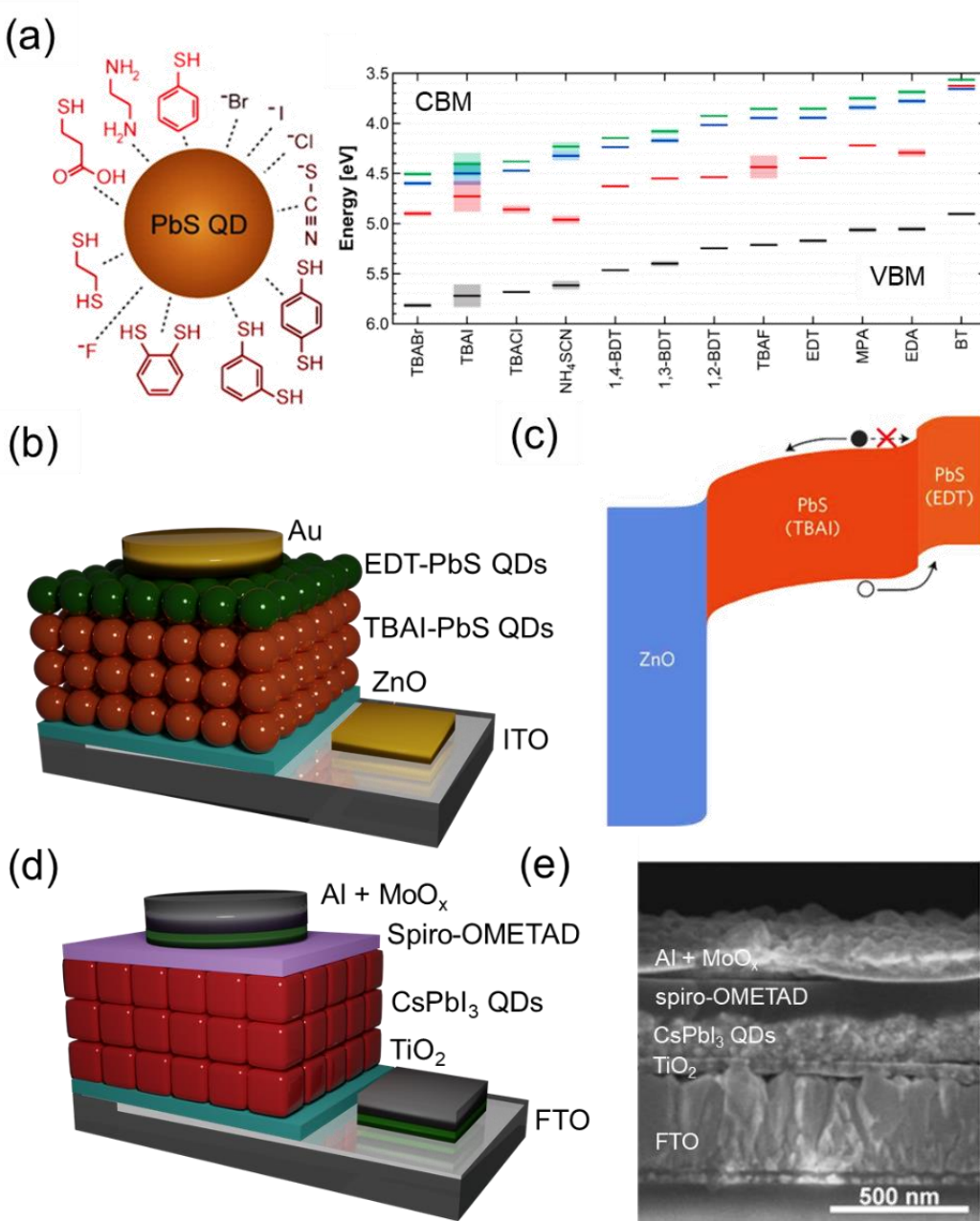


Figure 13. (a) The *n-i-p* architecture is based on the concept of ligand engineering of QD band structures. UPS was used to track the changes to the vacuum level for a variety of ligands. Reprinted with permission from ref. ¹⁵⁶, copyright 2014 American Chemical Society (b) With this information, suitably chosen ligands were employed to form the *n-i-p* device architecture where, (c) EDT-PbS QDs were used as the HTL reducing back-flow of photogenerated electrons. Reprinted with permission from ref. ¹⁷⁰, copyright 2014 Springer Nature. (d) CsPbI₃ QD solar cells also employ *n-i-p* architecture. (e) Cross-sectional SEM of a CsPbI₃ QD solar cell. Reprinted with permission from ref. ⁸⁶. Copyright 2016 AAAS.

This understanding led to the development of a novel device architecture wherein a thin film of EDT-PbS QDs with a shallow CBM was placed atop the absorber layer (Figure 13b, c).¹⁷⁰ This

1
2
3 additional layer prohibited backflow of photo-generated electrons into the hole-collecting
4 electrode while aiding hole-extraction and depleting the mildly *n*-type TBAI-PbS QD active layer.
5
6 It is important to mention that TBAI-PbS QD solids were earlier used as absorbers, however,
7 employing an EDT-PbS QD hole-transporting layer (HTL) helped increase the PCEs significantly,
8 besides enhancing air stability.¹⁷⁰ Recent findings suggest that it is this absorber:HTL junction in
9 these devices that is the dominant rectifying junction, as the TBAI-PbS QD absorber layer is *n*-
10 type.¹⁸⁶ The architecture is, therefore, essentially *n*⁺-*n*-*p*, and requires the HTL to be strongly *p*-
11 doped. TBAI ligands are known to leave organic residues that can likely hurt device performance.
12
13 Crisp *et al.* later demonstrated a path to organic-free exchanged PbS QD solids by developing an
14 SSE that involved post-treatment with PbI₂ with appreciable device performances.¹⁸⁷
15
16

17 This new device architecture has opened routes to further improvements and catalyzed the steep
18 growth in QD PV over the past couple of years, as Figure 11 (red thread) suggests. Soon after this
19 demonstration, a QD absorber exchanged with a combination of SolEx and SSE with halide ligands
20 (iodide) led to 10.2% PCEs, benefiting from enhanced passivation.¹⁸⁸ This was followed by a
21 vacuum level modulation of the electron-transporting layer (ETL) by self-assembled monolayers
22 resulting in a high Voc of 0.66 V with PCEs reaching 10.7%.⁹⁷ Modification of the electron
23 transporter with EDT has also been recently reported.¹⁸⁹
24
25

26 As discussed in the previous section, SolEx has been utilized to yield single-step deposited QD
27 absorbers, taking the QD PV technology a step closer to scalable fabrication. These solar cells
28 have also employed a top EDT-PbS QD HTL in an *n-i-p* configuration. Hybrid perovskites and
29 lead halide ligands have been used to cap the QD surfaces in solution-phase resulting in highly
30 efficient QD inks which have recently led to the realization of 12.5% PCE *n-i-p* solar cells.^{96-98, 109}
31
32
33
34
35
36
37
38
39
40
41
42
43
44
45
46
47
48
49
50
51
52
53
54
55
56
57
58
59
60

1
2
3 Although these solar cells did not require LbL build-up of the active layer, spin-coating was still
4 used to fabricate the absorber. The HTL, however, still requires SSE via LbL deposition (2 layers).
5
6

7
8 The *n-i-p* architecture has also been found to benefit tandem solar cells fabricated from QDs.¹⁹⁰
9 Two subcells of equally-sized QDs featuring TBAI-QDs as the absorber and EDT-QDs as the HTL
10 were connected via an ultrathin Au layer which acted as the inorganic recombination layer. The
11 overall device performance of the tandem device approached 9.0% which is almost twice the
12 previous best all-QD tandem solar cell.¹⁹¹
13
14

15
16 Nonetheless, there has been growing evidence that the *n-i-p* architecture suffers from inherent
17 doping issues with the HTL that directly hinder charge transport, ambient manufacturability and
18 stability of the *n-i-p* devices. It was found by Speirs *et al.* that the EDT-PbS QD HTL is
19 unoptimally *p*-doped, and a post-deposition treatment with sodium hydrosulfide (NaHS) was
20 found to effectively increase the hole concentration further depleting the TBAI-PbS QD active
21 layer, improving J_{SC} and FF in TBAI/EDT *n-i-p* architecture solar cells.¹⁵⁹ Further, the authors
22 found that the HTL needed to have an order of magnitude higher doping concentration compared
23 to the active layer, in order to fully deplete the active layer.¹⁵⁹ A similar observation was made by
24 us recently in the context of *n-i-p* solar cells that employed SolEx MAPbI₃-PbS QDs and PbX₂-
25 PbS QDs as the active layers and an EDT-PbS QD HTL. The large electron-affinity (EA) metal-
26 organic complex, Mo(tfd-COCF₃)₃, was used as the *p*-dopant to tune the E_F of the HTL, improving
27 J_{SC} and FF. This HTL doping strategy was also found to work for perovskite solar cells, as
28 demonstrated recently.¹⁹²
29
30
31
32
33
34
35
36
37
38
39
40
41
42
43
44
45
46
47
48
49
50
51
52
53
54
55
56
57
58
59
60

1
2
3 The suboptimal doping of the HTL has also been found to be a severe concern when PbS QD
4 solar cells are fabricated in high RH ambient conditions, proving to be a major bottleneck to
5 ambient manufacturability of these devices.^{22, 193}
6
7
8
9
10

11 It is important to note that this is currently the standard device architecture for CsPbI₃ QD solar
12 cells (Figure 13d, e). QD absorber layer is deposited using the SSE LbL process via spin-coating.
13 The as-cast QD film is soaked in methyl acetate (MeOAc) to enable ligand removal/exchange.⁸⁷
14 The architecture employs spiro-OMETAD as the HTL. Very recently, it was shown that forming
15 the absorber layer by layering CsPbI₃ QDs atop Cs_{0.25}FA_{0.75}PbI₃ QDs results in a charge separating
16 interface within the absorber.²⁴ This modified architecture resulted in certified ~16.6% PCE solar
17 cells.²⁴
18
19
20
21
22
23
24
25
26
27
28

QD-sensitized solar cells

29
30 QD-sensitized solar cells have been pursued since 1980s and competitive PCEs of >13% have
31 been recently reported.^{16-17, 172} An important distinction with the other QD device architectures is
32 that these solar cells are not based on QD solids, but use QDs to sensitize a mesoporous metal
33 oxide photoanode and are similar in design and operation to dye-sensitized solar cells. Electrons
34 photogenerated in the QDs upon light absorption are injected into the metal oxide, while an
35 electrolyte regenerates the oxidized QDs.¹⁹⁴
36
37
38
39
40
41
42
43
44

45 However, the appreciable carrier diffusion lengths in QDs enable planar device architectures to
46 perform equally efficiently in extracting photogenerated charge carriers. Further, QD-sensitized
47 solar cells require extra care in QD loading on the mesoporous photoanodes making the process
48 time-consuming. For higher PCEs, the architecture can also require liquid electrolytes that limit
49 device stability and can constrain handling and packaging presenting a scalability challenge.
50
51
52
53
54
55
56
57
58
59
60

Challenges, Opportunities, and Future Directions

Despite the significant inroads made over the last few years in improving surface passivation and charge extraction, considerable further progress is required to improve PCEs beyond 20% in a scalable fashion and/or possibly warrant their integration into hybrid tandem solar cells with other PV materials. Fundamental developments in materials science and device engineering, together with breakthroughs in precision synthesis, as well as the stability of QD solar cells and their scalable and ambient manufacturability have recently received attention and will help delineate the path forward for QD solar cells.

Improvements in charge extraction and collection

Optimum QD absorber layer thickness required to absorb all the incident light is *ca.* 1 μm , yet current device architectures employ significantly thinner absorbers (*ca.* 500 nm). Improved surface passivation schemes have helped increase carrier diffusion lengths which are, however, still generally limited to 100 nm,¹⁰⁹ holding back the achievable absorber thicknesses and therefore the J_{SC} . Improvements in QD passivation and mesoscale arrangement and ordering of closely packed QD solids via improved passivation and remote doping strategies, as well as precise solution processing of QD thin films, are expected to yield increases in the carrier diffusion length in QD solids. An alternative or complement to approaching this problem can be to search for highly *p*-doped HTLs, which can ensure full depletion of thick absorbers. This should potentially also increase the V_{OC} , another important parameter that needs attention, which is governed by the split in quasi- E_{F} of the *n*-type ETL and *p*-type HTL in *n-i-p* architecture devices. A third route can be development of highly efficient BHJs, which rely on nanostructured ETLs that penetrate into the absorber layer alleviating the problem of short diffusion lengths. Blending *p*- and *n*-type QDs into

nanodomains might also allow thicker absorbers without compromising charge collection, compared to the current layered device structures.¹⁹⁵

ETL plays a crucial role in the *n-i-p* architecture, in general, by depleting the absorber and extracting electrons while blocking hole backflow. This is still important in the context of the latest QD solar cells despite the fact that the absorber:ETL interface is not the dominant rectifying junction. ZnO nanoparticles have traditionally been used as the ETL in *n-i-p* QD solar cells. Although charge transport in ZnO ETLs is better compared to titania (TiO_x), exploring alternative ETLs with even higher electron mobilities and weaker optical absorption will be helpful. Besides, given the *n*-type nature of the generally used QD absorbers (TBAI-PbS, PbX₂-PbS), having strong *n*-doping in ETLs is desirable. Indium oxide (In₂O₃) has a wider bandgap (~3.8 eV) and a high electron density due to oxygen vacancies. In principle, it should allow better harvesting of the UV-photons which are otherwise absorbed by ZnO. Further *n*-doping of ETLs should increase absorber layer depletion. The higher energy UV-photons should help increase J_{SC} further, besides aiding MEG. Optical transparency to UV photons can also have implications on improving various stabilities of the CQD solar cells. In fact, we have recently found that replacing the standard, thick ZnO ETL in *n-i-p* CQD solar cells with an ultrathin bilayer In₂O₃/ZnO ETL leads to noticeably improved UV-stability, shelf-life and I-V hysteresis, while allowing 11% PCE.¹⁹⁶

Improvements in V_{oc}

In general, V_{oc} has been less than half the PbS QD bandgap. Even though PCEs have significantly improved from Schottky architectures to the current best-performing *n-i-p* PbS QD solar cells, V_{oc} has only increased from 0.50V to 0.65V, a comparatively less impressive ascent which needs attention. Band tails arising out of disorder in the PbS QD solid and sub-bandgap traps have been suggested to be the possible origin of the observed low V_{oc}.^{96, 160} An exciting

1
2
3 report on bulk nano-heterojunction device architecture employed a combination of MPA and zinc
4 iodide (ZnI_2) as ligands suppressing sub-bandgap traps, and led to a record high V_{OC} of $0.8V$.¹⁹⁷
5
6 This advanced device architecture involves incorporation of ZnO nanocrystals into the PbS QD
7 matrix which trap passivate the QD traps via remote charge transfer.^{150, 198} Although the overall
8 optical absorption is lowered hurting the J_{SC} , it is likely that with further optimization of this
9 architecture and systematic passivation of sub-gap and tail states, concomitant improvements in
10
11 V_{OC} and J_{SC} should be within reach. Size polydispersity is a well-known cause of V_{OC} deficit as it
12 creates inclusions inside the bandgap.¹⁹⁹ Controlling size polydispersity arising from QD fusion
13 during the exchange process can yield V_{OC} improvements, as Jo *et al.* have recently shown.²⁰⁰
14
15
16
17
18
19
20
21
22
23
24
25
26
27
28
29
30
31
32
33
34
35
36
37
38
39
40
41
42
43
44
45
46
47
48
49
50
51
52
53
54
55
56
57
58
59
60

Improvements in charge transport in QD solids, unfortunately, come at the cost of the long-range order that the long, insulating ligands impart. Bringing the QDs closer by ligand exchange increases the charge tunneling rate improving charge transport. However, the exchange process removes any signs of the initially existing mesoscale order creating a disordered arrangement of QDs within the solid and results in increased band tails, which are a source of the large V_{OC} -deficit QD PV currently suffers from.^{74, 96} We have reason to believe further gains in charge transport can be obtained if this disorder can be suppressed. There have been recent key advances where exchanged QD superlattices have been used to fabricate electronic devices with record carrier mobilities ($24\text{ cm}^2\text{V}^{-1}\text{s}^{-1}$).^{73, 146, 201} Promoting improved self-assembly via precision-controlled solidification processes should help improve the quality of QD solids and eliminate a source of energetic disorder. Suppressing size polydispersity, for instance, with the help of more fundamental and quantitative understanding of nucleation and growth mechanisms of colloidal nanomaterials, together with a transition to in-flow reaction synthesis together with process automation and machine-learning-guided experimentation, will enable improved QD quality,

1
2
3 defect mitigation, self-assembly as well as marked improvements in V_{OC} and charge extraction by
4 suppressing bandgap inclusions and enabling band-like transport.⁷⁴ Together, these steps will
5 accelerate the pathway to bringing >20% PCEs within reach in the coming few years.
6
7
8
9

10 Ligand exchange is also known to introduce non-radiative trap states in PbS QD solids leading
11 to a significant decrease in PLQY upon exchange.²⁰² It is known that every order-of-magnitude
12 reduction in PLQY corresponds to a 60 mV drop in V_{OC} .²⁰³ For 1.3 eV bandgap PbS QDs,
13 maximum achievable V_{OC} limited by SQ limit is 1.03 V, and implies that the latest solar cells with
14 a V_{OC} of 0.65 V possibly have PLQY in the range of 10⁻⁵%,²⁰² highlighting the need for further
15 improvements. There have been recent reports on using quasi-fermi level splitting (QFLS) to
16 understand V_{OC} -loss mechanisms in perovskite solar cells.²⁰⁴⁻²⁰⁵ Light intensity-dependent QFLS
17 measurements have helped decouple the impacts of perovskite absorber and charge extraction
18 layers on overall device performance.²⁰⁴ Such studies do not currently exist for PbS QD solar cells
19 and are urgently needed to understand carrier loss mechanisms for suppressing the significant V_{OC} -
20 losses and improve PCEs.
21
22
23
24
25
26
27
28
29
30
31
32
33
34
35
36
37

Tandem QD PV

38 Another key area which needs dedicated research focus is development of tandem and hybrid
39 tandem solar cells that integrate QD PV as the back cell to harvest the NIR component of solar
40 spectrum. There have been encouraging demonstrations of such device architectures over the last
41 few years where 1.3 eV solid-state exchanged PbS QDs have been employed.²⁰⁶⁻²⁰⁸
42
43
44
45
46
47
48

49 PCEs nearing 13% have lately been achieved for a hybrid QD:organic tandem solar cell design
50 that uses an organic bulk heterojunction as the back cell.²⁰⁹ Importantly, these solar cells
51 demonstrated appreciable long-term shelf-life. Similarly, a four-terminal tandem solar cell
52 utilizing dye-sensitized and QD subcells recently reached 12% PCE.²¹⁰ PbS QDs have also been
53
54
55
56
57
58
59
60

1
2
3 explored as rear subcells in tandem with CdTe QDs resulting in impressive voltages in excess of
4
5 1.1 V.²¹¹
6
7

8 A major advantage of QDs is their ability to absorb in the NIR spectral range. Fresh insights in
9 large-sized NIR QD PV solids have successfully pushed the >1100 nm wavelength EQEs to ~80%
10
11 seeing massive gains in J_{SC} and significantly improved harvest of NIR photons,^{7-8, 212-214} that
12 currently the most-efficient PV technologies including commercial Si, perovskites, and organic
13 tandem cells fail to harness.²¹⁵⁻²¹⁶ SolEx has enabled scalable fabrication of stable and high-
14 performing PbS QD solids, and integrating the larger-sized SolEx NIR PbS QDs as back cells with
15 the best single-junction organic solar cells (>18% PCE) should lead to further improvements
16 thanks to the spectral complementarity of the two semiconductor materials.²¹⁷⁻²¹⁸ This looks more
17 likely with the recent developments in CsPbI_3 QD PV where >16% PCE single-junction solar cells
18 have been reported. With non-fullerene acceptors (NFAs) now leading organic solar cells to >18%
19 PCEs, an organic-QD hybrid tandem solar cell can potentially be optimized to achieve PCE >20%
20 in the near term. For this to happen, efficient recombination layers and solvent compatibility
21 between the QD and organic sub-cells need to be realized, which requires development of new ink
22 formulations as well as robust recombination layers, as was recently demonstrated.²⁰⁶ In this
23 regard, SolEx can be helpful as a ready-to-coat QD ink minimizing solvent exposure, but ink
24 developments in general need to avoid damage to other solution-coated layers used in the
25 multilayer device stack.
26
27

48 *Long-term stability of QD PV*

49

50 Foremost attention to date has been focused at perfecting the QD surfaces and PV device
51 architectures, resulting in steady gains in charge transport and devices performances. However,
52 attention must now begin to focus on making QD solar cells an inherently stable technology. This
53
54

1
2
3 concern has recently been highlighted by Tan *et al.* who mentioned three types of stabilities as
4 crucial and timely requirements for further progress of QD PV: long-term device stability, QD ink
5 stability, and ambient manufacturability.²¹⁹
6
7

8 Solar cells with PCE >10% were shown to exhibit ambient shelf life of >1 year without
9 encapsulation (**Figure 14a**).²² More impressive still, they exhibited operational stability with 250
10 h of continuous operation under 100 mW.cm⁻² illumination in inert atmosphere. The devices
11 exhibited an initial burn-in which saturated after 3 h of operation, beyond which the PCEs were
12 remarkably stable.²² It is clear from Figure 14b that the QD solar cells undergo negligible
13 degradation after the burn-in, suggesting a lifetime significantly longer than 250 h. Similarly, UV-
14 resilience of the solar cells increased when the conventional thick ZnO ETL was replaced with
15 ultrathin In₂O₃/ZnO bilayers (Figure 14c), owing to enhanced optical transmittance and reduced
16 carrier recombination in these bilayer ETLs.¹⁹⁶ These results point toward the intrinsic stability
17 and promise of QD PV for long-term applications. Further efforts must target an understanding of
18 burn-in and ways of overcoming this initial performance degradation. It is important to translate
19 these early demonstrations to QD solar cell modules and subsequent field testing under various
20 environmental stressors, such as moisture, oxygen, heat and UV-light. Since the year-long ambient
21 stability discussed above was obtained for unencapsulated devices, encapsulated modules are
22 expected to show longer lifetimes given the extra layer of protection from moisture and oxygen
23 attack. Still, the stabilities discussed above for PbS QD PV are far lower than what are needed
24 under realistic conditions (>25 years), and further efforts are required to meet this goal. It is also
25 crucial to explore performance and stability of QD solar cells upon irradiation with high energy
26 radiation, such as alpha and beta particles, gamma ray photons, protons and neutrons. Such tests
27
28
29
30
31
32
33
34
35
36
37
38
39
40
41
42
43
44
45
46
47
48
49
50
51
52
53
54
55
56
57
58
59
60

1
2
3 will determine feasibility of QD PV for installation in low-earth orbit satellites with exposure to
4
5 ionizing radiation.
6
7

8 Dimensionality reduction has played a defining role in crystallographically and chemically
9 stabilizing all-inorganic perovskites at room temperature, and resulted in high-performing CsPbI_3
10
11 QD solar cells.^{24, 86} However, it is unclear at this time if these devices can demonstrate long-term
12 shelf life and operational stability. Given the ionic nature of CsPbI_3 , these QDs are expected to
13 suffer from degradation under moisture. Demonstration of effective passivation layers, such as 2D
14 perovskites in the context of bulk perovskite PV,²⁸ should therefore be a key step toward
15 establishing CsPbI_3 QD PV as a promising technology.
16
17
18
19
20
21
22
23
24
25
26
27
28
29
30
31
32
33
34
35
36
37
38
39
40
41
42
43
44
45
46
47
48
49
50
51
52
53
54
55
56
57
58
59
60

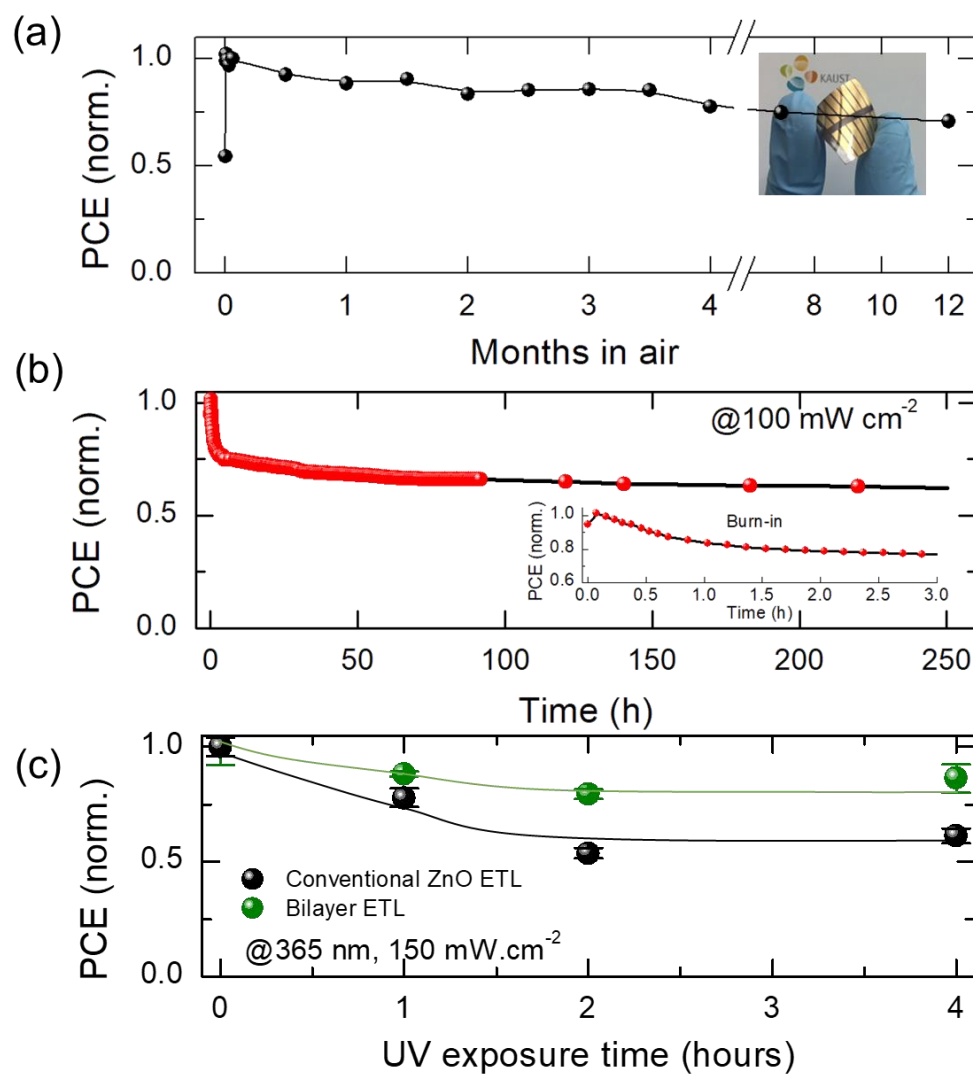


Figure 14. (a) Stability of unencapsulated devices over several months of storage in high-RH (50-60 %) ambient air. Inset shows a flexible device on plastic ITO substrate.²² (b) Photostability of unencapsulated devices over several hours of continuous light irradiation. Inset shows the initial burn-in, after which the PCE saturates. Reprinted with permission from ref. ²². Copyright 2018 Wiley. (c) Improved UV-resilience when ultrathin $\text{In}_2\text{O}_3/\text{ZnO}$ bilayer is used as ETL (green datapoints). Lines are drawn as a guide to the eye. Reprinted with permission from ref. ¹⁹⁶. Copyright 2020 American Chemical Society.

Scalable fabrication of QD PV

Solvent engineering

In the legacy LbL protocol for absorber layer fabrication via SSE, 10-12 repeats of the *coating-exchanging-rinsing* cycle are carried out. This makes the overall process highly time-taking and material consuming even if it is automated. It is important to understand the need behind such a

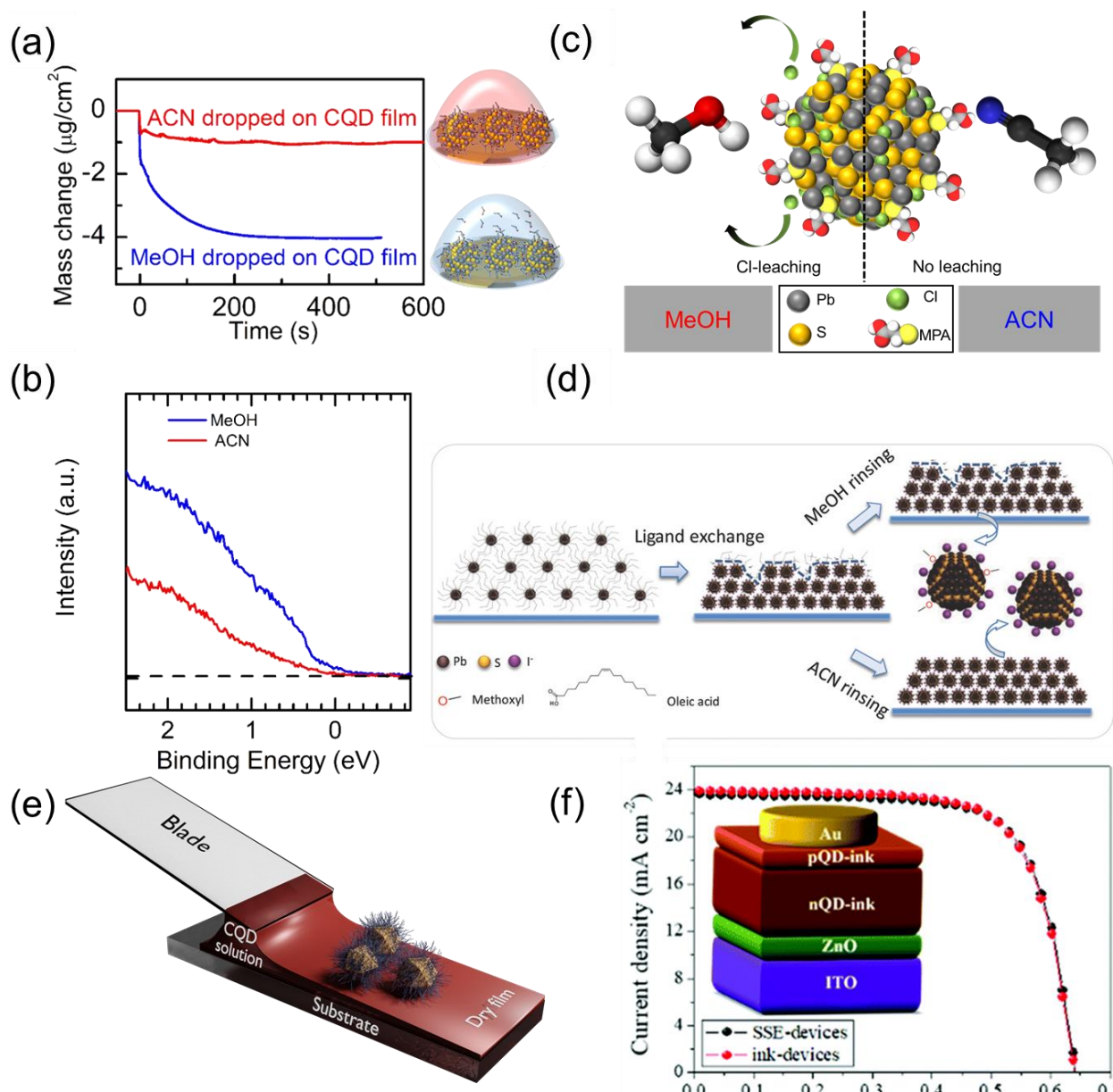
1
2
3 rigorous, time- and materials-wasting process. Limited carrier diffusion lengths in QDs constrain
4 the optimum absorber layer thickness, which is usually ~300 nm for MPA- and TBAI-PbS QDs.
5
6 In principle, a compact ~300 nm absorber can be achieved by: i) starting with a thick OA-PbS QD
7 film and soaking it with MPA or TBAI solutions for a long time (~several minutes), or ii) starting
8 with an initially thin OA-PbS QD film, soaking it with MPA or TBAI solutions for a shorter time
9 (~few sec), and repeating the process several times. In the nascent stages of QD PV, it was realized
10 that the choice i) would not be successful since the exchange resulted in a significant volume loss,
11 leading to observable cracks in the film which can act as barrier to charge flow during device
12 operation. Choice ii) was therefore accepted as the standard protocol. In this process, the as-cast
13 layer of OA-PbS QDs is usually ~80 nm thick, and requires a ~3s soaking in the MPA ligand
14 solution in MeOH (MPA/MeOH) to be fully exchanged without causing harm to the film. The
15 resulting cracks in the exchanged and rinsed film are filled by a subsequent OA-PbS QD layer
16 coated directly on top, which is then similarly exchanged and rinsed. Since the films require spin-
17 coating, the process entails significant materials wastage, is time-consuming and is definitely not
18 scalable.
19
20

21
22 With an aim of remedying this issue, a modified LbL scheme was sought which involved a far
23 fewer number of cycles.⁸¹ The strategy involved fabricating the ~300 nm absorber in 3 cycles of
24 100 nm per exchanged layer. Accordingly, each ~250 nm thick OA-PbS QD layer was exchanged
25 for ~60s in MPA/MeOH, resulting in ~100 nm exchanged MPA-PbS QD layer; however, the
26 overall device performance was significantly poorer compared to the 10-12 LbL solar cells. It has
27 been reported that protic solvents such as MeOH desorb carboxylate ligands from the surface of
28 QDs.²²⁰ An investigation into solvent-QD interactions in real time via a quartz crystal
29 microbalance (QCM) detected mass loss by the OA-PbS QD film in contact with MeOH (**Figure**
30
31
32
33
34
35
36
37
38
39
40
41
42
43
44
45
46
47
48
49
50
51
52
53
54
55
56
57
58
59
60

1
2
3 15a) suggesting that MeOH had a role in the observed performance loss. This solvent interaction
4 was found to leach-off the surface halide passivant (chloride) resulting in surface traps which were
5 directly measured using UPS (Figure 15b). Confirming the negative impact of a long exposure of
6 MeOH on device performance, a completely contrasting and aprotic solvent, acetonitrile (ACN)
7 was deployed as the processing solvent. ACN turned out to be a very benign solvent without any
8 halide leach-off. Modifying the ligand exchange process, QD absorbers were fabricated using
9 MPA/ACN solution in 3 LbL steps, resulting in solar cells that performed at par with the 10-12
10 LbL controls using the legacy MPA/MeOH. The demonstration highlighted that surface trap
11 mitigation, ligand chemistry, and process scalability are often indirectly coupled.
12
13
14
15
16
17
18
19
20
21
22
23
24
25
26
27
28
29
30
31
32
33
34
35
36
37
38
39
40
41
42
43
44
45
46
47
48
49
50
51
52
53
54
55
56
57
58
59
60

Lu *et al.* recently extended the idea of solvent engineering in the context of the *n-i-p* architecture QD solar cells (TBAI/EDT).²²¹ These solar cells, in general, require a TBAI/MeOH ligand exchange to build up the absorber layer via a 10-step LbL process, and an EDT/ACN ligand exchange to build up the HTL via a 2-step LbL process. Each step involves a few seconds of MeOH (absorber layer) or ACN (HTL) rinse to remove the unbound OA and excess TBAI or EDT ligands, respectively. The authors posited that replacing the MeOH rinses with ACN for the absorber layer build-up would reduce surface traps and morphological damage to the films (Figure 15d).²²² Doing so also allowed for reducing the number of steps in the LbL build-up with an impressive PCE of 10.6% achieved with as little as 2 LbL steps for the absorber layer, significantly curbing materials wastage. The strict requirement of a protic carrier solvent (MeOH) for enabling the TBAI-exchange with OA-PbS QDs has,¹⁴⁶ thus far, stymied any attempts at deploying an aprotic solvent (ACN) for this exchange, nonetheless, being able to do so successfully should, in principle, further reduce the surface trap density and boost the performance. This anticipation

1
2
3 stems from the fact that the TBAI/MeOH soak during the absorber layer build-up takes ~30s
4
5 allowing ample time for MeOH to interact and undesirably modify the QD surface.^{170, 221}
6
7



47
48 **Figure 15.** (a) Quantifying interaction of QD surface with MeOH and ACN using QCM in terms
49 of OA ligand removal. Reprinted with permission from ref. ⁸¹. Copyright 2014 Wiley (b) Near-
50 Fermi level density of states of the QD absorbers soaked for a long time in MeOH and ACN. Band
51 tails are observed for the MeOH treated absorber. Reprinted with permission from ref. ⁸¹.
52 Copyright 2014 Wiley (c) Schematic depicting the halide leaching effect of MeOH from the QD
53 surface. Reprinted with permission from ref. ⁸¹. Copyright 2014 Wiley (d) 'Solvent-curing' of the
54 n-i-p devices using ACN as the rinsing solvent. Reprinted with permission from ref. ²²¹. Copyright
55 2018 Wiley (e) Blade-coating of QD absorbers. (f) J-V curve (red) of a fully-bladed QD solar cell
56

1
2
3 that uses SolEx for both the absorber and the HTL. Also included is the *J-V* curve for the
4 corresponding device made by SSE (black). Reprinted with permission from ref.²²³ Copyright
5 2018 The Royal Society of Chemistry.
6

7 *Meniscus-guided scalable coating*
8
9

10 Despite highlighting the underlying link between surface trap mitigation and process scalability,
11 the above studies have relied on spin-coating. In 2018, scalable fabrication of PbS QD solar cells
12 with >10% PCEs was reported using blade-coating, a meniscus-guided coating technique. Blade-
13 coating is a low-cost, roll-to-roll compatible solution printing technique and is an established
14 prototyping technique for the industrially-compatible slot-die coating (Figure 15e). SolEx PbX₂-
15 PbS QD absorber and EDT-PbS QD HTL were blade-coated in a single step at industrially
16 compatible coating speeds of ~18 m.min⁻¹ in high-RH ambient conditions.²² Importantly, these
17 devices required ~25 times less QD material compared to the best spin-coated QD solar cell to
18 date.¹⁰⁹ This report also included demonstration of a 1.1 cm² active area device with >9% PCE,
19 highlighting the large-area compatibility of QD PV. These high coating speeds enabled by blade-
20 coating are directly compatible with industrial requirements of roll-to-roll fabrication.²²⁴ Around
21 the same time, Aqoma *et al.* reported a blade-coated QD solar cell with 10% PCE where both the
22 absorber and HTL employed SolEx.²²³ This design had the advantage of completely avoiding SSE
23 that the EDT-PbS QD HTL requires (Figure 15f).
24
25

26 Scalable fabrication of PbS QD solids and devices needs to be next demonstrated using slot-die
27 coating, which is an industrially compatible coating technique with large-area, high-throughput
28 and continuous manufacturing capabilities. A recent *in situ* X-ray scattering study exploring
29 fundamental aspects of OA-PbS QD self-assembly during slot-die coating are therefore a welcome
30 advance.²²⁵ It is also crucial to realize that ready-to-coat SolEx HTLs merit focused research
31 attention, as do other device layers, including the ETL and conducting electrodes. However, the
32
33
34
35
36
37
38
39
40
41
42
43
44
45
46
47
48
49
50
51
52
53
54
55
56
57
58
59
60

latter two are less specific to QD PV and benefit from material and technology transfer from other areas of thin film PV. An alternate HTL can be the utilization of polymeric HTLs that do not rely on a post-treatment. In this regard, the demonstration of ~12% PCE PbS QD solar cells using organic π -conjugated polymer based HTLs deposited in a single-step atop the SolEx PbS QD absorber is a promising step.^{223, 226-228}

Majority of the reports on CsPbX_3 QD solar cells have relied on spin-coating. This is expected since these QDs employ SSE which is moreso compatible with spin-coating or dip-coating, and no SolEx recipe is yet available. Attention should therefore be given to enabling exchange in solution-phase, which should allow for single-step deposition of the QD inks via sheet-to-sheet and roll-to-roll compatible coating techniques.

Ambient air coating of QD solids

Majority of the high-performing QD solar cells reported so far have been fabricated in low-RH controlled environments using spin-coating.²²⁹ Although efficient at the laboratory-scale for demonstration of proof-of-concepts, this fabrication route is unscalable due to the involved materials wastage and large costs involved due to moisture control. There have been encouraging developments with demonstration of ambient-fabricated devices using blade-coating, although PCEs have remained low.^{164, 230-231} There have also been demonstrations of spray-coated QD solar cells, though, LbL spray-coating consumed ~3 times more QD material ($\text{g} \cdot \text{m}^{-2}$) compared to LbL spin-coating, as discussed above.^{94, 232} In general, ambient processing and fabrication of QD solids are expected to face hurdles given the possibility of QD surface interaction with ambient moisture and oxygen. To test this proposition, SolEx and subsequent *n-i-p* solar cell fabrication were recently carried out in a highly humid ambient environment ($\text{RH} > 60\%$).²² The as-prepared devices performed poorly, with an average of 4.5% PCE.²² These devices were also highly unstable in

1
2
3 ambient and lost ~85% of the initial PCEs after 1-month of storage. A detailed atomic analysis of
4 the various layers in the stack gave us evidence that the EDT-PbS QD HTL was, in fact, the
5 manufacturability bottleneck. EDT-PbS QDs have an affinity to partially oxidize forming $(SO_4)^{2-}$
6 and $(SO_3)^{2-}$ surface species, which scales with QD size.^{80, 233} In the process, some of the bound
7 EDT ligands are lost. This oxidation results in a slight shift of the E_F closer to the VBM (*p*-
8 doping).²² In a high-RH ambient, however, moisture attacks the surface of these QDs, blocking
9 ingress of oxygen and leading to an unoptimally *p*-doped HTL. As-prepared devices, therefore,
10 behave poorly due to charge extraction issues arising from an unfavorable ‘spike’ at the
11 absorber:HTL interfacial band structure. It was found that storing these devices in an oxygen-rich
12 dry-air environment for a few hours led to a significant PCE boost, largely stemming from
13 increases in V_{OC} and FF. These efforts helped realize QD solar cells with >10% PCE (best-
14 performing device = 11.0% PCE) processed and fabricated under high-RH ambient environment,
15 on relatively twice the active areas (0.1 cm^2) compared to what are usually reported. In fact, a
16 slight improvement in PCEs has been observed earlier upon ambient air storage of the fully-
17 prepared devices.^{170, 182}

38 ***Non-toxic QDs through green chemistry***

39
40 A green approach to QD PV would ideally involve green QDs, chemistry and solvents –
41 components that are non-toxic, require small amounts of energy to manufacture, and have limited
42 carbon footprint.

43
44 There is growing epidemiological evidence that Pb can possibly cause cancer and other health-
45 related issues by inducing DNA and genetic damage both in humans and animals.²³⁴ International
46 Agency on Research on Cancer (IARC) *Monographs on the Evaluation of Carcinogenic Risks to*
47 *Humans* (Vol 87, 2006) classified inorganic Pb compounds under Group 2B ('probably

1
2
3 carcinogenic to humans'). Impact of organic Pb compounds on health is inconclusive. This
4 necessitates search for Pb-free QD systems that can be transformed into an efficient and health-
5 friendly PV technology. It is important to note that PbS is not deliquescent due to the strong Pb-S
6 bond. Inorganic perovskite QDs, however, currently rely on Pb as the B-site metal cation,
7 highlighting the need for a non-toxic alternative. The demonstration of a 6.3% PCE solar cell based
8 on AgBiS₂ QDs as the absorber is an important step in the right direction.¹⁷³ This impressive
9 performance was achieved with only a 35 nm thick absorber layer, which highlights the room for
10 improvement of these materials as light harvesting QDs for PV applications.
11
12

13 A recent demonstration of on-device Pb-sequestration in high-performing bulk perovskite solar
14 cells holds significant promise with regard to Pb toxicity.⁷⁶ The solar cell was coated with an
15 optically transparent, Pb-absorbing, organic film that effectively sequestered ~96% Pb when the
16 damaged (intentionally shattered) device was soaked in water, remarkably containing Pb leakage
17 to the environment. Similar studies are required to demonstrate robustness and safety with PbS
18 and CsPbI₃ QD solar cells.
19
20

21 Similarly, it is crucial to explore alternatives to the currently-used toxic precursors and solvents
22 for the synthesis of QDs and device fabrication. Synthesis of PbS QDs requires bis(trimethylsilyl)
23 sulfide as a precursor which is considered toxic. To the best of our knowledge, all of the reports
24 on SolEx PbS QDs have used DMF as the polar solvent during the exchange step. DMF is readily
25 absorbed through the skin and can potentially cause damage to the liver. BTA, a toxic and highly
26 flammable solvent, is commonly used to solubilize SolEx PbS QDs. QD solids spin- and blade-
27 coated out of BTA result in highly-quality, smooth and shiny films and high-performing solar
28 cells, given the low boiling point of the solvent and its adequate viscosity.^{22, 96, 109} In fact, prior
29 attempts at using DMSO as the solvent for SolEx PbS QDs were less successful due to its high
30
31

boiling point hurting film quality and device performance.¹⁰⁶ Further studies should therefore be targeted toward exploring the considerable green solvent space which other semiconductors, such as organic polymers and bulk hybrid perovskites,²³⁵⁻²³⁷ have started exploiting.

Compared to the case of SolEx, PbS QD solar cells fabricated using SSE currently present a greener route as the exchange process requires the relatively greener solvent, MeOH.²³⁸⁻²³⁹ Although ACN, a toxic solvent, has also been used in *n-p* architecture devices and is the standard solvent for delivering EDT ligands for HTL fabrication in *n-i-p* solar cells,^{81, 109} the overall amount of the solvent needed is significantly low, alleviating the risk to an extent.

In terms of green solvents, CsPbI₃ QDs appear to have a significant advantage over PbS QDs. Most of the solvents required for synthesis of these QDs and fabrication of solar cells are considerably less toxic (methyl acetate, octadecene, hexane).

With the chemistry and physics of Pb-based QDs understood at a fundamental level, PCE soon to surpass 20%, and industry-compatible manufacturing being demonstrated, it will soon be time to look for and translate this rich understanding to efficient non-toxic, Earth-abundant, greener alternatives so that low-cost QD optoelectronics becomes a reality to meet the projected spiraling energy demand of society this century.

Perspectives on next-generation advanced manufacturing of QD PV

Next-generation QD PV manufacturing would require advances on both accelerated R&D as well as integration of upstream QD ink synthesis and downstream roll-to-roll module fabrication. The recent advancements in autonomous i) QD development and surface engineering and ii) thin-film coating, shown in **Figure 16** can revolutionize the current paradigm of QD PV development. We briefly discuss below the state-of-the-art on these fronts and suggest future guidelines.

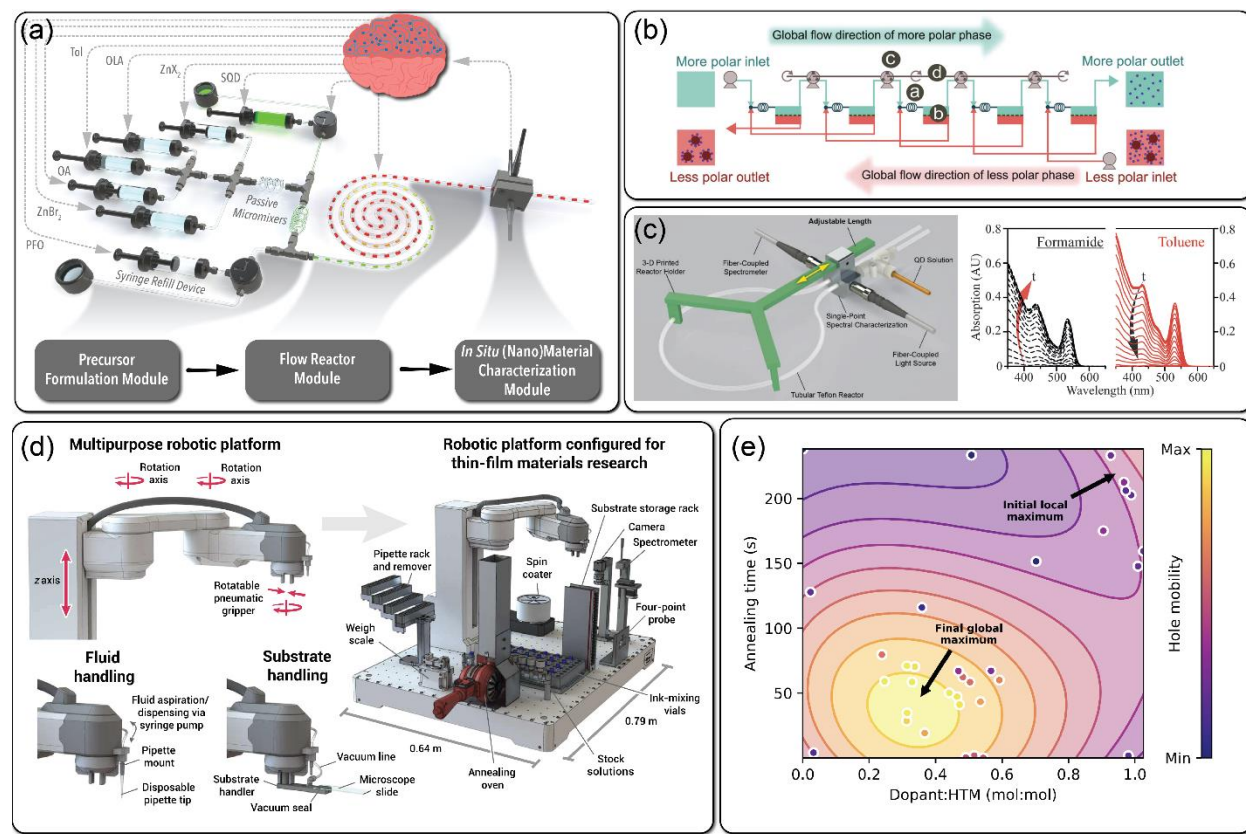


Figure 16. (a) Schematic of the recently developed ‘artificial chemist’ platform for autonomous synthesis of colloidal QDs. Reprinted with permission from ref. ⁶¹, copyright 2020 Wiley (b) Microfluidic purification, reprinted with permission from ref. ²⁴⁰, copyright 2017 The Royal Society of Chemistry, and (c) surface engineering of QDs, reprinted with permission from ref. ²⁴¹, copyright 2017 Wiley (d) Schematic of a self-driving robotic platform for accelerated studies of thin film coating. Reprinted with permission from ref. ²⁴² (e) Rapid identification of the desired processing conditions using the self-driving robotic platform shown in panel (d). Datapoints correspond to the experimental conditions (annealing time and dopant ratio) sampled by the algorithm during the experimental run for optimizing hole mobility of an organic semiconductor. The algorithm-driven robot makes a fast transition from the local to the global maximum in hole mobility, without the need to study the full parameter space cutting down the time and materials required. Reprinted with permission from ref. ²⁴²

Continuous manufacturing of QD inks

As discussed previously in section 2.2, microfluidic synthesis of QDs integrated with *in situ* diagnostic probes can enable low-cost, highly efficient manufacturing of QDs with desired optoelectronic properties for downstream applications in PV devices. To achieve a true end-to-end continuous manufacturing scheme of QDs utilizing modular process units, new technological

advancements beyond continuous precursor formulation and flow synthesis modules (Figure 16a) are needed. Specifically, robust continuous purification and surface engineering of QDs will be a crucial requirement within an end-to-end QD manufacturing platform to achieve high-quality purification of as-synthesized QDs as well as application-guided surface engineering of the purified QDs. Automated QD purification strategies utilizing liquid-liquid extraction (Figure 16b) or column-based separation approaches have been demonstrated to be promising techniques for facile integration with flow synthesis.^{240, 243} In addition to the formulation, synthesis, purification, and surface engineering modules (Figure 16c), advanced process controllers connected to live-streamed *in situ* diagnostic probes are needed to ensure high-quality manufacturing of QDs with the desired figure of merits for the downstream processing.

Data-driven optimization of QD synthesis

In a recent study, Li *et al.* developed an automated microfluidic platform for rapid screening of the effect of surface ligand structure on the optical properties of CsPbBr₃ QDs utilizing *in situ* PL monitoring.²⁴⁴ Expedited parameter screening using automation can be beneficial to the industry for rapid, data-driven optimization of the final product without the need for laborious experimentation, driving down labor and materials costs.⁴⁶ Bezinge *et al.* demonstrated targeted synthesis of multinary perovskite nanocrystals using a droplet-based microfluidic reactor informed by a self-optimizing algorithm.²⁴⁵ It was demonstrated that utilizing the self-optimizing microfluidic platform, multinary perovskite nanocrystals could be synthesized on-demand for a pre-defined peak emission wavelength. The system was further demonstrated to make intelligent predictions about certain spectral properties of the nanocrystals.²⁴⁵ Recently, Epps *et al.* developed a self-driving modular flow reactor, called *Artificial Chemist*, for simultaneous hands-free optimization of PLQY and FWHM of metal halide perovskite QDs at any desired peak emission

1
2
3 energy (Figure 16a).⁶¹ Utilizing an artificial intelligence-based decision-making strategy combined
4 with prior information from in-house generated QD synthesis data, the artificial chemist was able
5 to synthesize optimal (*i.e.*, maximum PLQY with minimum FWHM) metal halide perovskite QDs
6 for any emission color in less than 15 min. Furthermore, the authors demonstrated an autonomous
7 reconfigurability of the artificial chemist from the accelerated R&D mode to continuous QD
8 manufacturing mode for scaled-up production of the in-flow optimized QDs. There has also been
9 recent progress on improving size dispersity in PbS QDs guided by machine learning algorithms.
10
11 Voznyy *et al.* developed a model using Bayesian neural networks to optimize PbS QD synthesis.²⁴⁶
12 The model led to key insights into the role of OLA in controlling size dispersity enabling synthesis
13 of wide bandgap (~2 eV) PbS QDs with a half-width at half-maximum (HWHM) of 145 meV, and
14 smaller bandgaps (~0.83 eV) with HWHM of only 24 meV.²⁴⁶ Several higher energy transitions
15 were readily observed in the absorption spectra, an indication of improved size dispersity. Wide
16 bandgap QDs are exciting for hybrid tandem PV applications to reduce spectral overlap between
17 subcells, however, Voc-losses typically increase for larger bandgaps likely due to increased
18 polydispersity.²⁰⁹ Therefore, demonstration of ~2 eV PbS QDs with low FWHM is an encouraging
19 development.
20
21
22
23
24
25
26
27
28
29
30
31
32
33
34
35
36
37
38
39
40
41
42
43
44
45
46
47
48
49
50
51
52
53
54
55
56
57
58
59
60

Manufacturing throughput is another important factor that needs to be considered when developing end-to-end QD manufacturing platforms. The key factors controlling manufacturing throughput are the QD formation kinetics, reaction yield, microfluidic reactor geometry, and maximum initial precursor concentrations without causing fouling and reactor clogging. For example, the fast formation kinetics of fully inorganic lead halide perovskite QDs⁵⁶ can be leveraged to achieve manufacturing throughputs up to 0.1 kg/day QD solids in a single-channel microfluidic reactor. The manufacturing throughput can be further increased by utilizing parallel

1
2
3 microfluidic reactors (*i.e.*, scaling-out) connected to the same source of precursors and operated
4 through a fluidic distribution module.⁴⁴⁻⁴⁵
5
6

7
8 *End-to-end manufacturing of QD PV*
9

10 Finally, we believe that automation has a substantial role to play in industrial adoption of QD
11 PV. Smart fabrication of QD PV appears increasingly likely in the near term given the focused
12 attention on using machine-learning-guided automation to optimize QD synthesis by several
13 research groups, as discussed above, as well as renewed focus on downstream processing such as
14 machine-learning-guided coating of thin films.²⁴²
15
16

17 Considering the above-mentioned developments in continuous manufacturing and processing of
18 colloidal QDs, a fully automated manufacturing scheme can be envisioned for end-to-end
19 manufacturing of QD PV modules with high-quality QDs and minimum batch-to-batch variation.
20 In this proposed design based on recent advancements noted in Figure 16, a modular flow reactor
21 integrated with *in situ* diagnostic probe will continuously manufacture QDs with bespoke
22 properties (composition, size, ligands, concentration, throughput) at an industrially-relevant
23 throughput (10-50 kg/day). The modular microfluidic QD manufacturing platform will include
24 continuous in-series precursor formulation, flow reactor, purification, and surface engineering
25 modules. The continuously manufactured optimized colloidal QD ink will then be automatically
26 transferred to the downstream roll-to-roll device fabrication module for large-scale fabrication of
27 QD PV cells.
28
29

30 Assuming that (i) the coating speed of 1080 m.hr⁻¹ we recently demonstrated for small-area PbS
31 QD solar cells are scalable to a 1 m-wide continuous roll-to-roll manufacturing line, and (ii) under
32 optimized absorber thickness conditions 1 g of QDs is required to coat 1 m² of the roll, we estimate
33 a daily QD requirement of ~26 kg. As discussed above, this requirement can be met using scaled-
34
35

1
2
3 out microfluidic reactors. These coating speeds correspond to a total annual coated area of 9.5
4 million m². Considering a stabilized module PCE of 15%, we project >1.4 GW of annual electrical
5 power production capacity for each of these distributed QD PV manufacturing sites.
6
7
8
9
10

11 It has been recently suggested that synthesis costs dictate the overall \$/W for QD PV and the
12 current standards for QD ink synthesis have been projected to fail in enabling feasible production
13 costs of 0.20 \$/W, making this technology currently less viable for industrial scale-up.⁴⁶ The QD
14 synthesis throughput considered in the study in question, after surveying the available synthesis
15 protocols, are in the range of 12 g for CsPbI₃ QDs and 250 g for PbS QDs. The results suggest that
16 improving the synthesis throughput can potentially drive down \$/W by reducing materials required
17 and labor costs.⁴⁶ Solvent recycling can also likely reduce the production costs. We believe the
18 future directions we have pointed out above are key to improving economic feasibility of this
19 promising technology. The currently achievable manufacturing throughput for perovskite QDs
20 with a low-cost single-channel microfluidic reactor is ~ 100 g/day, which is clearly aligned with
21 industrial adoption and can be easily scaled-up to 1-10 kg/day using a numbered-up strategy.^{44, 56-}
22
23
24
25
26
27
28
29
30
31
32
33
34
35
36
37
38
39
40
41
42
43
44
45
46
47
48
49
50
51
52
53
54
55
56
57
58
59
59
60

Conclusions and Outlook

QD PV is one of the fastest growing fields in thin-film optoelectronics and offers benefits beyond
the reach of contemporary PV technologies. PCEs have risen sharply to >16% in 2020 after recent
breakthroughs in perovskite QDs. We have chronicled the development of this PV technology over
the recent years with detailed discussion on the various chemical passivation schemes and device
designs that have combinedly played a central role in its rapid ascent. Solution-phase ligand

1
2
3 exchange and the *n-i-p* device architecture have been the major milestones in the young history of
4 this nascent field. Scalable fabrication and ambient manufacturability of efficient QD solar cells,
5 along with demonstrations of machine learning-guided automated flow reactor synthesis of QDs
6 with high throughput are important recent demonstrations that highlight their potential for market
7 entry in the short term.
8
9

10
11 We have suggested a few key areas that should be focus of research going forward to push the
12 PCEs above 20%. This includes improving extraction of photogenerated charge carriers (FF), and
13 suppressing size polydispersity that can potentially enhance V_{OC} and charge transport in PbS QDs.
14 Hybrid tandem solar cell designs are suggested as the fastest route to >20% PCE, although single
15 junction devices should be considerably simpler and cheaper to produce. Focus on efficient
16 recombination layers and solvent compatibility between organic and QD subcells should lead to
17 major advances. To this end, both wide bandgap and NIR QDs appear promising, as front and rear
18 subcells, respectively. Most of the chemical approaches so far have been developed for visible-to-
19 NIR QDs with 1.3 eV bandgap. Future research should explore developing efficient ligand
20 exchange, improving charge transport and extraction, and suppressing size dispersity in wide
21 bandgap (~ 1.5 – 2 eV) and NIR (~ 0.6 – 0.8 eV) PbS QDs to meet the demand and promise of
22 hybrid tandem PV.
23
24

25 There has been considerably less attention on non-toxic alternatives to QD PV. With growing
26 evidence of health-related issues associated with inorganic Pb salts, this topic should see increased
27 research activity. In this regard, AgBiS₂ QD solar cells have been a promising development.
28 Similarly, it is important to screen the various precursors and solvents used for QD synthesis for
29 toxicity and cost. Greener and sustainable alternatives will help in scale-up of this technology and
30 drive down the materials cost involved. Of great importance is the search for an on-device Pb
31
32

1
2
3 sequestration technology that suppresses Pb leach-off upon damage to QD PV module without
4
5 compromising device performance. A similar demonstration for bulk perovskite solar cells is a
6
7 highly encouraging step in this direction, and suggests that the present unavailability of a robust
8
9 Pb-free QD PV should not be an impediment to industrial scale-up provided this demonstration of
10
11 Pb-sequestration is transferable to QD solar cells.
12
13

14
15 Overall, these demonstrations of ambient manufacturability and scalable fabrication of QD
16
17 PV,^{22, 223} along with recent interest in automated and autonomous flow-synthesis of QDs on
18
19 demand,⁵⁸ are promising signs for this nascent field.²⁴⁷ Combinedly, these latest developments can
20
21 bring down the materials and labor costs involved which have been projected as the main
22
23 contributors to the total manufacturing cost for QD PV modules,⁴⁶ smoothing their journey to the
24
25 manufacturing line and enabling annual gigawatt power production.
26
27

28
29
30
31
32
33 ASSOCIATED CONTENT
34
35

36
37 **Supporting Information**
38
39

40 AUTHOR INFORMATION
41
42

43 **Corresponding Authors**
44

45 ahmad.kirmani@nrel.gov, @AhmadRKirmani
46

47 aamassi@ncsu.edu
48

49 **Notes**
50
51

52 The authors declare no competing financial interest.
53
54
55
56
57

1
2
3
4
5 AUTHOR BIOGRAPHIES
6
7
8
9
10
11
12
13
14
15
16
17

Ahmad R. Kirmani: Ahmad R. Kirmani is a postdoctoral researcher at the Chemical & Nanoscience Center, National Renewable Energy Laboratory (NREL). He has a PhD degree in materials science from the King Abdullah University of Science & Technology (KAUST), and was a guest researcher at the National Institute of Standards and Technology (NIST) prior to joining NREL. His research interests include roll-to-roll compatible coating and characterization of inorganic semiconductor inks, such as, colloidal quantum dots, hybrid perovskites and metal oxides.

Joey M. Luther: Joseph Luther has been a senior research scientist at the National Renewable Energy Laboratory since 2009. His group's research focuses on developing optoelectronic technologies utilizing solution processed nanomaterials such as colloidal semiconducting quantum dots and halide perovskite materials.

Milad Abolhasani: Milad Abolhasani is an Assistant Professor in the Department of Chemical and Biomolecular Engineering at North Carolina State University. He received his Ph.D. degree (2014) from the Department of Mechanical and Industrial Engineering in collaboration with the Department of Chemistry at the University of Toronto. Prior to joining NC State University in 2016, he was an NSERC postdoctoral fellow in the Department of Chemical Engineering at Massachusetts Institute of Technology. Dr. Abolhasani leads a diverse research group that studies flow chemistry strategies tailored towards accelerated development and manufacturing of solution-processed materials using autonomous robotic experimentation in flow.

Aram Amassian: Aram Amassian is an Associate Professor of Materials Science and Engineering and a member of the Carbon Electronics Cluster. He received his Ph.D. degree (2006) in Engineering Physics from Ecole Polytechnique in Montreal, Canada. Prior to joining NC State University (2018), he was an NSERC postdoctoral fellow in Materials Science and Engineering at Cornell University (2006-2009) and was subsequently founding faculty at the King Abdullah University of Science and Technology (KAUST), 2009-2018, where he held the Career Development SABIC Chair (2013-2016). Dr. Amassian's research is focused on solution-processed hybrid semiconductors, particularly for (opto)electronic and photovoltaic applications, where he has developed *in situ* characterization strategies for thin film deposition in lab-scale and fab-scale processes.

ACKNOWLEDGMENT

This work was authored in part by the Alliance for Sustainable Energy, Limited Liability Company, the manager and operator of the National Renewable Energy Laboratory under contract no. DE-AC36-08GO28308. The views expressed in the article do not necessarily represent the views of the Department of Energy or the U.S. Government. NREL authors were funded through a technical service agreement with Equinor. AA and MA acknowledge financial support from the UNC Research Opportunities Initiative (UNC-ROI) grant and the North Carolina State University.

References

1. Aldakov, D.; Reiss, P., Safer-by-Design Fluorescent Nanocrystals: Metal Halide Perovskites vs Semiconductor Quantum Dots. *The Journal of Physical Chemistry C* **2019**, *123* (20), 12527-12541.
2. Wang, C.; Shim, M.; Guyot-Sionnest, P., Electrochromic nanocrystal quantum dots. *Science* **2001**, *291* (5512), 2390-2.
3. Liu, H.; Keuleyan, S.; Guyot-Sionnest, P., n- and p-Type HgTe Quantum Dot Films. *The Journal of Physical Chemistry C* **2011**, *116* (1), 1344-1349.
4. Deng, Z.; Guyot-Sionnest, P., Intraband Luminescence from HgSe/CdS Core/Shell Quantum Dots. *ACS Nano* **2016**, *10* (2), 2121-7.
5. Shen, G.; Guyot-Sionnest, P., HgS and HgS/CdS Colloidal Quantum Dots with Infrared Intraband Transitions and Emergence of a Surface Plasmon. *The Journal of Physical Chemistry C* **2016**, *120* (21), 11744-11753.
6. Kiani, A.; Sutherland, B. R.; Kim, Y.; Ouellette, O.; Levina, L.; Walters, G.; Dinh, C.-T.; Liu, M.; Voznyy, O.; Lan, X.; Labelle, A. J.; Ip, A. H.; Proppe, A.; Ahmed, G. H.; Mohammed, O. F.; Hoogland, S.; Sargent, E. H., Single-step colloidal quantum dot films for infrared solar harvesting. *Appl. Phys. Lett.* **2016**, *109* (18), 183105.
7. Bi, Y.; Bertran, A.; Gupta, S.; Ramiro, I.; Pradhan, S.; Christodoulou, S.; Majji, S.-N.; Akgul, M. Z.; Konstantatos, G., Solution processed infrared- and thermo-photovoltaics based on 0.7 eV bandgap PbS colloidal quantum dots. *Nanoscale* **2019**, *11* (3), 838-843.
8. Bi, Y.; Pradhan, S.; Gupta, S.; Akgul, M. Z.; Stavrinidis, A.; Konstantatos, G., Infrared Solution-Processed Quantum Dot Solar Cells Reaching External Quantum Efficiency of 80% at 1.35 μ m and J_{sc} in Excess of 34 mA cm $^{-2}$. *Adv. Mater.* **2018**, *30* (7), 1704928.
9. Nozik, A. J., Quantum dot solar cells. *Physica E: Low-dimensional Systems and Nanostructures* **2002**, *14* (1), 115-120.
10. Semonin, O. E.; Luther, J. M.; Choi, S.; Chen, H. Y.; Gao, J.; Nozik, A. J.; Beard, M. C., Peak external photocurrent quantum efficiency exceeding 100% via MEG in a quantum dot solar cell. *Science* **2011**, *334* (6062), 1530-3.

- 1
2
3
4
5
6
7
8
9
10
11
12
13
14
15
16
17
18
19
20
21
22
23
24
25
26
27
28
29
30
31
32
33
34
35
36
37
38
39
40
41
42
43
44
45
46
47
48
49
50
51
52
53
54
55
56
57
58
59
60
11. Schaller, R. D.; Klimov, V. I., High Efficiency Carrier Multiplication in PbSe Nanocrystals: Implications for Solar Energy Conversion. *Phys. Rev. Lett.* **2004**, 92 (18), 186601.
 12. Shockley, W.; Queisser, H. J., Detailed Balance Limit of Efficiency of p-n Junction Solar Cells. *J. Appl. Phys.* **1961**, 32 (3), 510-519.
 13. Nozik, A. J., Spectroscopy and hot electron relaxation dynamics in semiconductor quantum wells and quantum dots. *Annu. Rev. Phys. Chem.* **2001**, 52 (1), 193-231.
 14. Huynh, W. U.; Dittmer, J. J.; Alivisatos, A. P., Hybrid Nanorod-Polymer Solar Cells. *Science* **2002**, 295 (5564), 2425-2427.
 15. Vogel, R.; Pohl, K.; Weller, H., Sensitization of highly porous, polycrystalline TiO₂ electrodes by quantum sized CdS. *Chem. Phys. Lett.* **1990**, 174 (3), 241-246.
 16. Zaban, A.; Mićić, O. I.; Gregg, B. A.; Nozik, A. J., Photosensitization of Nanoporous TiO₂ Electrodes with InP Quantum Dots. *Langmuir* **1998**, 14 (12), 3153-3156.
 17. Plass, R.; Pelet, S.; Krueger, J.; Grätzel, M.; Bach, U., Quantum Dot Sensitization of Organic-Inorganic Hybrid Solar Cells. *The Journal of Physical Chemistry B* **2002**, 106 (31), 7578-7580.
 18. McDonald, S. A.; Konstantatos, G.; Zhang, S.; Cyr, P. W.; Klem, E. J. D.; Levina, L.; Sargent, E. H., Solution-processed PbS quantum dot infrared photodetectors and photovoltaics. *Nat Mater* **2005**, 4 (2), 138-142.
 19. Talapin, D. V.; Murray, C. B., PbSe nanocrystal solids for n- and p-channel thin film field-effect transistors. *Science* **2005**, 310 (5745), 86-9.
 20. Choi, M.-J.; García de Arquer, F. P.; Proppe, A. H.; Seifitokaldani, A.; Choi, J.; Kim, J.; Baek, S.-W.; Liu, M.; Sun, B.; Biondi, M.; Scheffel, B.; Walters, G.; Nam, D.-H.; Jo, J. W.; Ouellette, O.; Voznyy, O.; Hoogland, S.; Kelley, S. O.; Jung, Y. S.; Sargent, E. H., Cascade surface modification of colloidal quantum dot inks enables efficient bulk homojunction photovoltaics. *Nature Communications* **2020**, 11 (1), 103.
 21. Baek, S.-W.; Jun, S.; Kim, B.; Proppe, A. H.; Ouellette, O.; Voznyy, O.; Kim, C.; Kim, J.; Walters, G.; Song, J. H.; Jeong, S.; Byun, H. R.; Jeong, M. S.; Hoogland, S.; García de Arquer, F. P.; Kelley, S. O.; Lee, J.-Y.; Sargent, E. H., Efficient hybrid colloidal quantum dot/organic solar cells mediated by near-infrared sensitizing small molecules. *Nature Energy* **2019**, 4 (11), 969-976.
 22. Kirmani, A. R.; Sheikh, A. D.; Niazi, M. R.; Haque, M. A.; Liu, M.; de Arquer, F. P. G.; Xu, J.; Sun, B.; Voznyy, O.; Gasparini, N.; Baran, D.; Wu, T.; Sargent, E. H.; Amassian, A., Overcoming the Ambient Manufacturability-Scalability-Performance Bottleneck in Colloidal Quantum Dot Photovoltaics. *Adv. Mater.* **2018**, 30 (35), e1801661.
 23. Sun, B.; Johnston, A.; Xu, C.; Wei, M.; Huang, Z.; Jiang, Z.; Zhou, H.; Gao, Y.; Dong, Y.; Ouellette, O.; Zheng, X.; Liu, J.; Choi, M.-J.; Gao, Y.; Baek, S.-W.; Laquai, F.; Bakr, O. M.; Ban, D.; Voznyy, O.; García de Arquer, F. P.; Sargent, E. H., Monolayer Perovskite Bridges Enable Strong Quantum Dot Coupling for Efficient Solar Cells. *Joule* **2020**, 4 (7), 1542-1556.
 24. Zhao, Q.; Hazarika, A.; Chen, X.; Harvey, S. P.; Larson, B. W.; Teeter, G. R.; Liu, J.; Song, T.; Xiao, C.; Shaw, L.; Zhang, M.; Li, G.; Beard, M. C.; Luther, J. M., High efficiency perovskite quantum dot solar cells with charge separating heterostructure. *Nat Commun* **2019**, 10 (1), 2842.
 25. Hao, M.; Bai, Y.; Zeiske, S.; Ren, L.; Liu, J.; Yuan, Y.; Zarrabi, N.; Cheng, N.; Ghasemi, M.; Chen, P.; Lyu, M.; He, D.; Yun, J.-H.; Du, Y.; Wang, Y.; Ding, S.; Armin, A.; Meredith, P.; Liu, G.; Cheng, H.-M.; Wang, L., Ligand-assisted cation-exchange engineering for high-

- 1
2
3 efficiency colloidal $\text{Cs}_1\text{-xFAxPbI}_3$ quantum dot solar cells with reduced phase segregation.
4 *Nature Energy* **2020**, *5* (1), 79-88.
- 5 26. Akin, S.; Altintas, Y.; Mutlugun, E.; Sonmezoglu, S., Cesium lead based inorganic
6 perovskite quantum-dots as interfacial layer for highly stable perovskite solar cells with
7 exceeding 21% efficiency. *Nano Energy* **2019**, *60*, 557-566.
- 8 27. Cen, Y.-l.; Shi, J.-j.; Zhang, M.; Wu, M.; Du, J.; Guo, W.-h.; Liu, S.-m.; Han, S.-p.; Zhu,
9 Y.-h., Design of Lead-Free and Stable Two-Dimensional Dion–Jacobson-Type
10 Chalcogenide Perovskite $\text{A}'\text{La}_2\text{B}_3\text{S}_{10}$ ($\text{A}' = \text{Ba/Sr/Ca}$; $\text{B} = \text{Hf/Zr}$) with Optimal Band Gap,
11 Strong Optical Absorption, and High Efficiency for Photovoltaics. *Chem. Mater.* **2020**, *32*
12 (6), 2450-2460.
- 13 28. Grancini, G.; Roldán-Carmona, C.; Zimmermann, I.; Mosconi, E.; Lee, X.; Martineau, D.;
14 Narbey, S.; Oswald, F.; De Angelis, F.; Graetzel, M.; Nazeeruddin, M. K., One-Year stable
15 perovskite solar cells by 2D/3D interface engineering. *Nature Communications* **2017**, *8* (1),
16 15684.
- 17 29. Yusoff, A. R. b. M.; Nazeeruddin, M. K., Low-Dimensional Perovskites: From Synthesis
18 to Stability in Perovskite Solar Cells. *Advanced Energy Materials* **2018**, *8* (26), 1702073.
- 19 30. Huang, P.; Kazim, S.; Wang, M.; Ahmad, S., Toward Phase Stability: Dion–Jacobson
20 Layered Perovskite for Solar Cells. *ACS Energy Letters* **2019**, *4* (12), 2960-2974.
- 21 31. Eadington, P.; Prosser, A. P., Oxidation of Lead Sulfide in Aqueous Suspensions. *Trans.
22 Inst. Min. Metall.* **1969**, *78*, 74-82.
- 23 32. Choi, H.; Ko, J.-H.; Kim, Y.-H.; Jeong, S., Steric-Hindrance-Driven Shape Transition in
24 PbS Quantum Dots: Understanding Size-Dependent Stability. *J. Am. Chem. Soc.* **2013**, *135*
25 (14), 5278-5281.
- 26 33. Murray, C. B.; Norris, D. J.; Bawendi, M. G., Synthesis and characterization of nearly
27 monodisperse CdE (E = sulfur, selenium, tellurium) semiconductor nanocrystallites. *J. Am.
28 Chem. Soc.* **1993**, *115* (19), 8706-8715.
- 29 34. Peng, X.; Wickham, J.; Alivisatos, A. P., Kinetics of II-VI and III-V Colloidal
30 Semiconductor Nanocrystal Growth: “Focusing” of Size Distributions. *J. Am. Chem. Soc.*
31 **1998**, *120* (21), 5343-5344.
- 32 35. Murray, C. B.; Kagan, C. R.; Bawendi, M. G., Synthesis and Characterization of
33 Monodisperse Nanocrystals and Close-Packed Nanocrystal Assemblies. *Annu. Rev. Mater.
34 Sci.* **2000**, *30* (1), 545-610.
- 35 36. Kim, J. Y.; Voznyy, O.; Zhitomirsky, D.; Sargent, E. H., 25th Anniversary Article: Colloidal
36 Quantum Dot Materials and Devices: A Quarter-Century of Advances. *Adv. Mater.* **2013**,
37 *25* (36), 4986-5010.
- 38 37. Hines, M. A.; Scholes, G. D., Colloidal PbS Nanocrystals with Size-Tunable Near-Infrared
39 Emission: Observation of Post-Synthesis Self-Narrowing of the Particle Size Distribution.
40 *Adv. Mater.* **2003**, *15* (21), 1844-1849.
- 41 38. Park, J.; Joo, J.; Kwon, S. G.; Jang, Y.; Hyeon, T., Synthesis of Monodisperse Spherical
42 Nanocrystals. *Angew. Chem. Int. Ed.* **2007**, *46* (25), 4630-4660.
- 43 39. Hou, B.; Cho, Y.; Kim, B. S.; Hong, J.; Park, J. B.; Ahn, S. J.; Sohn, J. I.; Cha, S.; Kim, J.
44 M., Highly Monodispersed PbS Quantum Dots for Outstanding Cascaded-Junction Solar
45 Cells. *ACS Energy Letters* **2016**, *1* (4), 834-839.
- 46 40. Čapek, R. K.; Yanover, D.; Lifshitz, E., Size control by rate control in colloidal PbSe
47 quantum dot synthesis. *Nanoscale* **2015**, *7* (12), 5299-5310.

- 1
2
3
4
5
6
7
8
9
10
11
12
13
14
15
16
17
18
19
20
21
22
23
24
25
26
27
28
29
30
31
32
33
34
35
36
37
38
39
40
41
42
43
44
45
46
47
48
49
50
51
52
53
54
55
56
57
58
59
60
41. Peng, Z. A.; Peng, X., Formation of High-Quality CdTe, CdSe, and CdS Nanocrystals Using CdO as Precursor. *J. Am. Chem. Soc.* **2001**, *123* (1), 183-184.
 42. Qu, L.; Peng, Z. A.; Peng, X., Alternative Routes toward High Quality CdSe Nanocrystals. *Nano Lett.* **2001**, *1* (6), 333-337.
 43. Pradhan, N.; Reifsnyder, D.; Xie, R.; Aldana, J.; Peng, X., Surface Ligand Dynamics in Growth of Nanocrystals. *J. Am. Chem. Soc.* **2007**, *129* (30), 9500-9509.
 44. Nightingale, A. M.; Bannock, J. H.; Krishnadasan, S. H.; O'Mahony, F. T. F.; Haque, S. A.; Sloan, J.; Drury, C.; McIntyre, R.; deMello, J. C., Large-scale synthesis of nanocrystals in a multichannel droplet reactor. *Journal of Materials Chemistry A* **2013**, *1* (12), 4067.
 45. Wang, L.; Karadaghi, L. R.; Brutney, R. L.; Malmstadt, N., Self-optimizing parallel millifluidic reactor for scaling nanoparticle synthesis. *Chem. Commun.* **2020**, *56* (26), 3745-3748.
 46. Jean, J.; Xiao, J.; Nick, R.; Moody, N.; Nasilowski, M.; Bawendi, M.; Bulović, V., Synthesis cost dictates the commercial viability of lead sulfide and perovskite quantum dot photovoltaics. *Energy & Environmental Science* **2018**, *11* (9), 2295-2305.
 47. Chan, E. M.; Mathies, R. A.; Alivisatos, A. P., Size-Controlled Growth of CdSe Nanocrystals in Microfluidic Reactors. *Nano Lett.* **2003**, *3* (2), 199-201.
 48. Chan, E. M.; Alivisatos, A. P.; Mathies, R. A., High-Temperature Microfluidic Synthesis of CdSe Nanocrystals in Nanoliter Droplets. *J. Am. Chem. Soc.* **2005**, *127* (40), 13854-13861.
 49. Yen, B. K. H.; Stott, N. E.; Jensen, K. F.; Bawendi, M. G., A Continuous-Flow Microcapillary Reactor for the Preparation of a Size Series of CdSe Nanocrystals. *Adv. Mater.* **2003**, *15* (21), 1858-1862.
 50. Yen, B. K. H.; Günther, A.; Schmidt, M. A.; Jensen, K. F.; Bawendi, M. G., A Microfabricated Gas-Liquid Segmented Flow Reactor for High-Temperature Synthesis: The Case of CdSe Quantum Dots. *Angew. Chem. Int. Ed.* **2005**, *44* (34), 5447-5451.
 51. Krishnadasan, S.; Brown, R. J.; deMello, A. J.; deMello, J. C., Intelligent routes to the controlled synthesis of nanoparticles. *Lab Chip* **2007**, *7* (11), 1434-41.
 52. Lignos, I.; Protesescu, L.; Stavrakis, S.; Piveteau, L.; Speirs, M. J.; Loi, M. A.; Kovalenko, M. V.; deMello, A. J., Facile Droplet-based Microfluidic Synthesis of Monodisperse IV–VI Semiconductor Nanocrystals with Coupled In-Line NIR Fluorescence Detection. *Chem. Mater.* **2014**, *26* (9), 2975-2982.
 53. Kubendhiran, S.; Bao, Z.; Dave, K.; Liu, R.-S., Microfluidic Synthesis of Semiconducting Colloidal Quantum Dots and Their Applications. *ACS Applied Nano Materials* **2019**, *2* (4), 1773-1790.
 54. Li, S. L. H., Jeff C.; Howes, Philip D.; deMello, Andrew J. , Microfluidic Tools for the Synthesis of Bespoke Quantum Dots. In *Nanotechnology and Microfluidics*, 2019; pp 109-148.
 55. Abolhasani, M.; Coley, C. W.; Xie, L.; Chen, O.; Bawendi, M. G.; Jensen, K. F., Oscillatory Microprocessor for Growth and in Situ Characterization of Semiconductor Nanocrystals. *Chem. Mater.* **2015**, *27* (17), 6131-6138.
 56. Lignos, I.; Stavrakis, S.; Nedelcu, G.; Protesescu, L.; deMello, A. J.; Kovalenko, M. V., Synthesis of Cesium Lead Halide Perovskite Nanocrystals in a Droplet-Based Microfluidic Platform: Fast Parametric Space Mapping. *Nano Lett.* **2016**, *16* (3), 1869-77.

- 1
2
3 57. Epps, R. W.; Felton, K. C.; Coley, C. W.; Abolhasani, M., Automated microfluidic platform
4 for systematic studies of colloidal perovskite nanocrystals: towards continuous nano-
5 manufacturing. *Lab Chip* **2017**, *17* (23), 4040-4047.
6 58. Abdel-Latif, K.; Epps, R. W.; Kerr, C. B.; Papa, C. M.; Castellano, F. N.; Abolhasani, M.,
7 Facile Room-Temperature Anion Exchange Reactions of Inorganic Perovskite Quantum
8 Dots Enabled by a Modular Microfluidic Platform. *Adv. Funct. Mater.* **2019**, *29* (23),
9 1900712.
10 59. Lignos, I.; Morad, V.; Shynkarenko, Y.; Bernasconi, C.; Maceiczyk, R. M.; Protesescu, L.;
11 Bertolotti, F.; Kumar, S.; Ochsenbein, S. T.; Masciocchi, N.; Guagliardi, A.; Shih, C. J.;
12 Bodnarchuk, M. I.; deMello, A. J.; Kovalenko, M. V., Exploration of Near-Infrared-
13 Emissive Colloidal Multinary Lead Halide Perovskite Nanocrystals Using an Automated
14 Microfluidic Platform. *ACS Nano* **2018**, *12* (6), 5504-5517.
15 60. Kerr, C. B.; Epps, R. W.; Abolhasani, M., A low-cost, non-invasive phase velocity and
16 length meter and controller for multiphase lab-in-a-tube devices. *Lab Chip* **2019**, *19* (12),
17 2107-2113.
18 61. Epps, R. W.; Bowen, M. S.; Volk, A. A.; Abdel-Latif, K.; Han, S.; Reyes, K. G.; Amassian,
19 A.; Abolhasani, M., Artificial Chemist: An Autonomous Quantum Dot Synthesis Bot. *Adv.*
20 *Mater.* **2020**, *32* (30), e2001626.
21 62. Stolle, C. J.; Harvey, T. B.; Korgel, B. A., Nanocrystal photovoltaics: a review of recent
22 progress. *Current Opinion in Chemical Engineering* **2013**, *2* (2), 160-167.
23 63. Fu, H.; Tsang, S.-W., Infrared colloidal lead chalcogenide nanocrystals: Synthesis,
24 properties, and photovoltaic applications. *Nanoscale* **2012**, *4* (7), 2187-2201.
25 64. Hillhouse, H. W.; Beard, M. C., Solar cells from colloidal nanocrystals: Fundamentals,
26 materials, devices, and economics. *Current Opinion in Colloid & Interface Science* **2009**,
27 *14* (4), 245-259.
28 65. Semonin, O. E.; Luther, J. M.; Beard, M. C., Quantum dots for next-generation
29 photovoltaics. *Mater. Today* **2012**, *15* (11), 508-515.
30 66. Moreels, I.; Justo, Y.; De Geyter, B.; Haustraete, K.; Martins, J. C.; Hens, Z., Size-Tunable,
31 Bright, and Stable PbS Quantum Dots: A Surface Chemistry Study. *ACS Nano* **2011**, *5* (3),
32 2004-2012.
33 67. Vanmaekelbergh, D.; Liljeroth, P., Electron-conducting quantum dot solids: novel materials
34 based on colloidal semiconductor nanocrystals. *Chem. Soc. Rev.* **2005**, *34* (4), 299-312.
35 68. Weidman, M. C.; Smilgies, D.-M.; Tisdale, W. A., Kinetics of the self-assembly of
36 nanocrystal superlattices measured by real-time in situ X-ray scattering. *Nature Materials*
37 **2016**, *15*, 775.
38 69. Maiti, S.; André, A.; Banerjee, R.; Hagenlocher, J.; Konovalov, O.; Schreiber, F.; Scheele,
39 M., Monitoring Self-Assembly and Ligand Exchange of PbS Nanocrystal Superlattices at
40 the Liquid/Air Interface in Real Time. *The Journal of Physical Chemistry Letters* **2018**, *9*
41 (4), 739-744.
42 70. Choi, J. J.; Bealing, C. R.; Bian, K.; Hughes, K. J.; Zhang, W.; Smilgies, D.-M.; Hennig, R.
43 G.; Engstrom, J. R.; Hanrath, T., Controlling Nanocrystal Superlattice Symmetry and
44 Shape-Anisotropic Interactions through Variable Ligand Surface Coverage. *J. Am. Chem.*
45 *Soc.* **2011**, *133* (9), 3131-3138.
46 71. Hanrath, T.; Choi, J. J.; Smilgies, D.-M., Structure/Processing Relationships of Highly
47 Ordered Lead Salt Nanocrystal Superlattices. *ACS Nano* **2009**, *3* (10), 2975-2988.
48
49
50
51
52
53
54
55
56
57
58
59
60

- 1
2
3
4
5
6
7
8
9
10
11
12
13
14
15
16
17
18
19
20
21
22
23
24
25
26
27
28
29
30
31
32
33
34
35
36
37
38
39
40
41
42
43
44
45
46
47
48
49
50
51
52
53
54
55
56
57
58
59
60
72. Bian, K.; Choi, J. J.; Kaushik, A.; Clancy, P.; Smilgies, D.-M.; Hanrath, T., Shape-Anisotropy Driven Symmetry Transformations in Nanocrystal Superlattice Polymorphs. *ACS Nano* **2011**, *5* (4), 2815-2823.
73. Balazs, D. M.; Matysiak, B. M.; Momand, J.; Shulga, A. G.; Ibanez, M.; Kovalenko, M. V.; Kooi, B. J.; Loi, M. A., Electron Mobility of 24 cm(2) V(-1) s(-1) in PbSe Colloidal-Quantum-Dot Superlattices. *Adv. Mater.* **2018**, *30* (38), e1802265.
74. Guyot-Sionnest, P., Electrical Transport in Colloidal Quantum Dot Films. *J Phys Chem Lett* **2012**, *3* (9), 1169-75.
75. Kagan, C. R.; Murray, C. B., Charge transport in strongly coupled quantum dot solids. *Nat Nanotechnol* **2015**, *10* (12), 1013-26.
76. Septianto, R. D.; Liu, L.; Iskandar, F.; Matsushita, N.; Iwasa, Y.; Bisri, S. Z., On-demand tuning of charge accumulation and carrier mobility in quantum dot solids for electron transport and energy storage devices. *NPG Asia Materials* **2020**, *12* (1), 33.
77. Kirmanni, A. R.; Walters, G.; Kim, T.; Sargent, E. H.; Amassian, A., Optimizing Solid-State Ligand Exchange for Colloidal Quantum Dot Optoelectronics: How Much Is Enough? *ACS Applied Energy Materials* **2020**, *3* (6), 5385-5392.
78. Carey, G. H.; Abdelhady, A. L.; Ning, Z.; Thon, S. M.; Bakr, O. M.; Sargent, E. H., Colloidal Quantum Dot Solar Cells. *Chem. Rev.* **2015**, *115* (23), 12732-12763.
79. Carey, G. H.; Chou, K. W.; Yan, B.; Kirmanni, A. R.; Amassian, A.; Sargent, E. H., Materials processing strategies for colloidal quantum dot solar cells: advances, present-day limitations, and pathways to improvement. *MRS Communications* **2013**, *3* (2), 83-90.
80. Luther, J. M.; Law, M.; Song, Q.; Perkins, C. L.; Beard, M. C.; Nozik, A. J., Structural, optical, and electrical properties of self-assembled films of PbSe nanocrystals treated with 1,2-ethanedithiol. *ACS Nano* **2008**, *2* (2), 271-80.
81. Kirmanni, A. R.; Carey, G. H.; Abdelsamie, M.; Yan, B.; Cha, D.; Rollny, L. R.; Cui, X.; Sargent, E. H.; Amassian, A., Effect of solvent environment on colloidal-quantum-dot solar-cell manufacturability and performance. *Adv. Mater.* **2014**, *26* (27), 4717-23.
82. Guyot-Sionnest, P.; Wang, C., Fast Voltammetric and Electrochromic Response of Semiconductor Nanocrystal Thin Films†. *The Journal of Physical Chemistry B* **2003**, *107* (30), 7355-7359.
83. Yu, D.; Wang, C.; Guyot-Sionnest, P., n-Type conducting CdSe nanocrystal solids. *Science* **2003**, *300* (5623), 1277-80.
84. Murphy, J. E.; Beard, M. C.; Nozik, A. J., Time-Resolved Photoconductivity of PbSe Nanocrystal Arrays. *The Journal of Physical Chemistry B* **2006**, *110* (50), 25455-25461.
85. Sanehira, E. M.; Marshall, A. R.; Christians, J. A.; Harvey, S. P.; Ciesielski, P. N.; Wheeler, L. M.; Schulz, P.; Lin, L. Y.; Beard, M. C.; Luther, J. M., Enhanced mobility CsPbI₃ quantum dot arrays for record-efficiency, high-voltage photovoltaic cells. *Sci Adv* **2017**, *3* (10), eaao4204.
86. Swarnkar, A.; Marshall, A. R.; Sanehira, E. M.; Chernomordik, B. D.; Moore, D. T.; Christians, J. A.; Chakrabarti, T.; Luther, J. M., Quantum dot-induced phase stabilization of alpha-CsPbI₃ perovskite for high-efficiency photovoltaics. *Science* **2016**, *354* (6308), 92-95.
87. Wheeler, L. M.; Sanehira, E. M.; Marshall, A. R.; Schulz, P.; Suri, M.; Anderson, N. C.; Christians, J. A.; Nordlund, D.; Sokaras, D.; Kroll, T.; Harvey, S. P.; Berry, J. J.; Lin, L. Y.; Luther, J. M., Targeted Ligand-Exchange Chemistry on Cesium Lead Halide Perovskite

- 1
- 2
- 3 Quantum Dots for High-Efficiency Photovoltaics. *J. Am. Chem. Soc.* **2018**, *140* (33), 10504-10513.
- 4
- 5 88. Grisorio, R.; Di Clemente, M. E.; Fanizza, E.; Allegretta, I.; Altamura, D.; Striccoli, M.;
- 6 Terzano, R.; Giannini, C.; Irimia-Vladu, M.; Suranna, G. P., Exploring the surface
- 7 chemistry of cesium lead halide perovskite nanocrystals. *Nanoscale* **2019**, *11* (3), 986-999.
- 8
- 9 89. Park, J. H.; Lee, A.-y.; Yu, J. C.; Nam, Y. S.; Choi, Y.; Park, J.; Song, M. H., Surface Ligand
- 10 Engineering for Efficient Perovskite Nanocrystal-Based Light-Emitting Diodes. *ACS*
- 11 *Applied Materials & Interfaces* **2019**, *11* (8), 8428-8435.
- 12
- 13 90. Wu, H.; Zhang, Y.; Lu, M.; Zhang, X.; Sun, C.; Zhang, T.; Colvin, V. L.; Yu, W. W.,
- 14 Surface ligand modification of cesium lead bromide nanocrystals for improved light-
- 15 emitting performance. *Nanoscale* **2018**, *10* (9), 4173-4178.
- 16
- 17 91. Zheng, W.; Li, Z.; Zhang, C.; Wang, B.; Zhang, Q.; Wan, Q.; Kong, L.; Li, L., Stabilizing
- 18 perovskite nanocrystals by controlling protective surface ligands density. *Nano Research*
- 19 **2019**, *12* (6), 1461-1465.
- 20
- 21 92. Imran, M.; Ijaz, P.; Goldoni, L.; Maggioni, D.; Petralanda, U.; Prato, M.; Almeida, G.;
- 22 Infante, I.; Manna, L., Simultaneous Cationic and Anionic Ligand Exchange For Colloidally
- 23 Stable CsPbBr₃ Nanocrystals. *ACS Energy Letters* **2019**, *4* (4), 819-824.
- 24
- 25 93. Lu, H.; Zhu, X.; Miller, C.; Martin, J. S.; Chen, X.; Miller, E. M.; Yan, Y.; Beard, M. C.,
- 26 Enhanced photoredox activity of CsPbBr₃ nanocrystals by quantitative colloidal ligand
- 27 exchange. *The Journal of Chemical Physics* **2019**, *151* (20), 204305.
- 28
- 29 94. Kramer, I. J.; Minor, J. C.; Moreno-Bautista, G.; Rollny, L.; Kanjanaboops, P.; Kopilovic,
- 30 D.; Thon, S. M.; Carey, G. H.; Chou, K. W.; Zhitomirsky, D.; Amassian, A.; Sargent, E. H.,
- 31 Efficient Spray-Coated Colloidal Quantum Dot Solar Cells. *Adv. Mater.* **2015**, *27* (1), 116-121.
- 32
- 33 95. Liu, M.; de Arquer, F. P.; Li, Y.; Lan, X.; Kim, G. H.; Voznyy, O.; Jagadamma, L. K.;
- 34 Abbas, A. S.; Hoogland, S.; Lu, Z.; Kim, J. Y.; Amassian, A.; Sargent, E. H., Double-Sided
- 35 Junctions Enable High-Performance Colloidal-Quantum-Dot Photovoltaics. *Adv. Mater.*
- 36 **2016**, *28* (21), 4142-8.
- 37
- 38 96. Liu, M.; Voznyy, O.; Sabatini, R.; Garcia de Arquer, F. P.; Munir, R.; Balawi, A. H.; Lan,
- 39 X.; Fan, F.; Walters, G.; Kirmani, A. R.; Hoogland, S.; Laquai, F.; Amassian, A.; Sargent,
- 40 E. H., Hybrid organic-inorganic inks flatten the energy landscape in colloidal quantum dot
- 41 solids. *Nat Mater* **2017**, *16* (2), 258-263.
- 42
- 43 97. Yang, Z.; Janmohamed, A.; Lan, X.; García de Arquer, F. P.; Voznyy, O.; Yassitepe, E.;
- 44 Kim, G.-H.; Ning, Z.; Gong, X.; Comin, R.; Sargent, E. H., Colloidal Quantum Dot
- 45 Photovoltaics Enhanced by Perovskite Shelling. *Nano Lett.* **2015**, *15* (11), 7539-7543.
- 46
- 47 98. Aqoma, H.; Al Mubarok, M.; Hadmojo, W. T.; Lee, E.-H.; Kim, T.-W.; Ahn, T. K.; Oh, S.-
- 48 H.; Jang, S.-Y., High-Efficiency Photovoltaic Devices using Trap-Controlled Quantum-Dot
- 49 Ink prepared via Phase-Transfer Exchange. *Adv. Mater.* **2017**, *29* (19), 1605756-n/a.
- 50
- 51 99. Choi, H.; Lee, J.-G.; Mai, X. D.; Beard, M. C.; Yoon, S. S.; Jeong, S., Supersonically Spray-
- 52 Coated Colloidal Quantum Dot Ink Solar Cells. *Scientific Reports* **2017**, *7* (1), 622.
- 53
- 54 100. Kovalenko, M. V.; Scheele, M.; Talapin, D. V., Colloidal Nanocrystals with Molecular
- 55 Metal Chalcogenide Surface Ligands. *Science* **2009**, *324* (5933), 1417-1420.
- 56
- 57 101. Chung, D. S.; Lee, J.-S.; Huang, J.; Nag, A.; Ithurria, S.; Talapin, D. V., Low Voltage,
- 58 Hysteresis Free, and High Mobility Transistors from All-Inorganic Colloidal Nanocrystals.
- 59 *Nano Lett.* **2012**, *12* (4), 1813-1820.
- 60

- 1
2
3
4
5
6
7
8
9
10
11
12
13
14
15
16
17
18
19
20
21
22
23
24
25
26
27
28
29
30
31
32
33
34
35
36
37
38
39
40
41
42
43
44
45
46
47
48
49
50
51
52
53
54
55
56
57
58
59
60
102. Lee, J.-S.; Kovalenko, M. V.; Huang, J.; Chung, D. S.; Talapin, D. V., Band-like transport, high electron mobility and high photoconductivity in all-inorganic nanocrystal arrays. *Nat Nano* **2011**, *6* (6), 348-352.
103. Crisp, R. W.; Schrauben, J. N.; Beard, M. C.; Luther, J. M.; Johnson, J. C., Coherent exciton delocalization in strongly coupled quantum dot arrays. *Nano Lett.* **2013**, *13* (10), 4862-9.
104. Gur, I.; Fromer, N. A.; Geier, M. L.; Alivisatos, A. P., Air-Stable All-Inorganic Nanocrystal Solar Cells Processed from Solution. *Science* **2005**, *310* (5747), 462-465.
105. Johnston, K. W.; Pattantyus-Abraham, A. G.; Clifford, J. P.; Myrskog, S. H.; MacNeil, D. D.; Levina, L.; Sargent, E. H., Schottky-quantum dot photovoltaics for efficient infrared power conversion. *Appl. Phys. Lett.* **2008**, *92* (15), 151115.
106. Fischer, A.; Rollny, L.; Pan, J.; Carey, G. H.; Thon, S. M.; Hoogland, S.; Voznyy, O.; Zhitomirsky, D.; Kim, J. Y.; Bakr, O. M.; Sargent, E. H., Directly Deposited Quantum Dot Solids Using a Colloidally Stable Nanoparticle Ink. *Adv. Mater.* **2013**, *25* (40), 5742-5749.
107. Zhang, H.; Jang, J.; Liu, W.; Talapin, D. V., Colloidal Nanocrystals with Inorganic Halide, Pseudohalide, and Halometallate Ligands. *ACS Nano* **2014**, *8* (7), 7359-7369.
108. Ning, Z.; Dong, H.; Zhang, Q.; Voznyy, O.; Sargent, E. H., Solar Cells Based on Inks of n-Type Colloidal Quantum Dots. *ACS Nano* **2014**, *8* (10), 10321-10327.
109. Xu, J.; Voznyy, O.; Liu, M.; Kirmani, A. R.; Walters, G.; Munir, R.; Abdelsamie, M.; Proppe, A. H.; Sarkar, A.; Garcia de Arquer, F. P.; Wei, M.; Sun, B.; Liu, M.; Ouellette, O.; Quintero-Bermudez, R.; Li, J.; Fan, J.; Quan, L.; Todorovic, P.; Tan, H.; Hoogland, S.; Kelley, S. O.; Stefik, M.; Amassian, A.; Sargent, E. H., 2D matrix engineering for homogeneous quantum dot coupling in photovoltaic solids. *Nat Nanotechnol* **2018**, *13* (6), 456-462.
110. Dirin, D. N.; Dreyfuss, S.; Bodnarchuk, M. I.; Nedelcu, G.; Papagiorgis, P.; Itskos, G.; Kovalenko, M. V., Lead Halide Perovskites and Other Metal Halide Complexes As Inorganic Capping Ligands for Colloidal Nanocrystals. *J. Am. Chem. Soc.* **2014**, *136* (18), 6550-6553.
111. Ning, Z.; Ren, Y.; Hoogland, S.; Voznyy, O.; Levina, L.; Stadler, P.; Lan, X.; Zhitomirsky, D.; Sargent, E. H., All-Inorganic Colloidal Quantum Dot Photovoltaics Employing Solution-Phase Halide Passivation. *Adv. Mater.* **2012**, *24* (47), 6295-6299.
112. Bozyigit, D.; Yazdani, N.; Yarema, M.; Yarema, O.; Lin, W. M. M.; Volk, S.; Vuttivorakulchai, K.; Luisier, M.; Juranyi, F.; Wood, V., Soft surfaces of nanomaterials enable strong phonon interactions. *Nature* **2016**, *531* (7596), 618-622.
113. Yazdani, N.; Bozyigit, D.; Vuttivorakulchai, J.; Luisier, M.; Wood, V., Influence of the Surface of a Nanocrystal on its Electronic and Phononic Properties. *arXiv:1611.09930* **2016**.
114. Talapin, D. V.; Lee, J.-S.; Kovalenko, M. V.; Shevchenko, E. V., Prospects of Colloidal Nanocrystals for Electronic and Optoelectronic Applications. *Chem. Rev.* **2010**, *110* (1), 389-458.
115. Boles, M. A.; Engel, M.; Talapin, D. V., Self-Assembly of Colloidal Nanocrystals: From Intricate Structures to Functional Materials. *Chem. Rev.* **2016**, *116* (18), 11220-11289.
116. Richter, L. J.; DeLongchamp, D. M.; Amassian, A., Morphology Development in Solution-Processed Functional Organic Blend Films: An In Situ Viewpoint. *Chem. Rev.* **2017**, *117* (9), 6332-6366.
117. Wei Chou, K.; Ullah Khan, H.; Niazi, M. R.; Yan, B.; Li, R.; Payne, M. M.; Anthony, J. E.; Smilgies, D.-M.; Amassian, A., Late stage crystallization and healing during spin-coating

- 1
2
3
4
5
6
7
8
9
10
11
12
13
14
15
16
17
18
19
20
21
22
23
24
25
26
27
28
29
30
31
32
33
34
35
36
37
38
39
40
41
42
43
44
45
46
47
48
49
50
51
52
53
54
55
56
57
58
59
60
- enhance carrier transport in small-molecule organic semiconductors. *Journal of Materials Chemistry C* **2014**, 2 (28), 5681-5689.
118. Smilgies, D.-M.; Li, R.; Giri, G.; Chou, K. W.; Diao, Y.; Bao, Z.; Amassian, A., Look fast: Crystallization of conjugated molecules during solution shearing probed in-situ and in real time by X-ray scattering. *physica status solidi (RRL) – Rapid Research Letters* **2013**, 7 (3), 177-179.
119. Giri, G.; Li, R.; Smilgies, D.-M.; Li, E. Q.; Diao, Y.; Lenn, K. M.; Chiu, M.; Lin, D. W.; Allen, R.; Reinspach, J.; Mannsfeld, S. C. B.; Thoroddsen, S. T.; Clancy, P.; Bao, Z.; Amassian, A., One-dimensional self-confinement promotes polymorph selection in large-area organic semiconductor thin films. *Nature Communications* **2014**, 5 (1), 3573.
120. Chou, K. W.; Yan, B.; Li, R.; Li, E. Q.; Zhao, K.; Anjum, D. H.; Alvarez, S.; Gassaway, R.; Biocca, A.; Thoroddsen, S. T.; Hexemer, A.; Amassian, A., Spin-Cast Bulk Heterojunction Solar Cells: A Dynamical Investigation. *Adv. Mater.* **2013**, 25 (13), 1923-1929.
121. Munir, R.; Sheikh, A. D.; Abdelsamie, M.; Hu, H.; Yu, L.; Zhao, K.; Kim, T.; Tall, O. E.; Li, R.; Smilgies, D.-M.; Amassian, A., Hybrid Perovskite Thin-Film Photovoltaics: In Situ Diagnostics and Importance of the Precursor Solvate Phases. *Adv. Mater.* **2017**, 29 (2), 1604113-n/a.
122. Tang, M.-C.; Barrit, D.; Munir, R.; Li, R.; Barbé, J. M.; Smilgies, D.-M.; Del Gobbo, S.; Anthopoulos, T. D.; Amassian, A., Bismuth-Based Perovskite-Inspired Solar Cells: In Situ Diagnostics Reveal Similarities and Differences in the Film Formation of Bismuth- and Lead-Based Films. *Solar RRL* **2019**, 3 (7), 1800305.
123. Wang, K.; Tang, M.-C.; Dang, H. X.; Munir, R.; Barrit, D.; De Bastiani, M.; Aydin, E.; Smilgies, D.-M.; De Wolf, S.; Amassian, A., Kinetic Stabilization of the Sol–Gel State in Perovskites Enables Facile Processing of High-Efficiency Solar Cells. *Adv. Mater.* **2019**, 31 (32), 1808357.
124. Li, R.; Khan, H. U.; Payne, M. M.; Smilgies, D.-M.; Anthony, J. E.; Amassian, A., Heterogeneous Nucleation Promotes Carrier Transport in Solution-Processed Organic Field-Effect Transistors. *Adv. Funct. Mater.* **2013**, 23 (3), 291-297.
125. Barrit, D.; Cheng, P.; Tang, M.-C.; Wang, K.; Dang, H.; Smilgies, D.-M.; Liu, S.; Anthopoulos, T. D.; Zhao, K.; Amassian, A., Impact of the Solvation State of Lead Iodide on Its Two-Step Conversion to MAPbI₃: An In Situ Investigation. *Adv. Funct. Mater.* **2019**, 29 (47), 1807544.
126. Tang, J.; Kemp, K. W.; Hoogland, S.; Jeong, K. S.; Liu, H.; Levina, L.; Furukawa, M.; Wang, X.; Debnath, R.; Cha, D.; Chou, K. W.; Fischer, A.; Amassian, A.; Asbury, J. B.; Sargent, E. H., Colloidal-quantum-dot photovoltaics using atomic-ligand passivation. *Nat Mater* **2011**, 10 (10), 765-771.
127. Ip, A. H.; Thon, S. M.; Hoogland, S.; Voznyy, O.; Zhitomirsky, D.; Debnath, R.; Levina, L.; Rollny, L. R.; Carey, G. H.; Fischer, A.; Kemp, K. W.; Kramer, I. J.; Ning, Z.; Labelle, A. J.; Chou, K. W.; Amassian, A.; Sargent, E. H., Hybrid passivated colloidal quantum dot solids. *Nat Nano* **2012**, 7 (9), 577-582.
128. Zhitomirsky, D.; Voznyy, O.; Levina, L.; Hoogland, S.; Kemp, K. W.; Ip, A. H.; Thon, S. M.; Sargent, E. H., Engineering colloidal quantum dot solids within and beyond the mobility-invariant regime. *Nat Commun* **2014**, 5, 3803.
129. Katsiev, K.; Ip, A. H.; Fischer, A.; Tanabe, I.; Zhang, X.; Kirmani, A. R.; Voznyy, O.; Rollny, L. R.; Chou, K. W.; Thon, S. M.; Carey, G. H.; Cui, X.; Amassian, A.; Dowben, P.; Sargent, E. H.; Bakr, O. M., The Complete In-Gap Electronic Structure of Colloidal

- 1
- 2
- 3 Quantum Dot Solids and Its Correlation with Electronic Transport and Photovoltaic
- 4 Performance. *Adv. Mater.* **2014**, *26* (6), 937-942.
- 5
- 6 130. Marshall, A. R.; Young, M. R.; Nozik, A. J.; Beard, M. C.; Luther, J. M., Exploration of
- 7 Metal Chloride Uptake for Improved Performance Characteristics of PbSe Quantum Dot
- 8 Solar Cells. *J Phys Chem Lett* **2015**, *6* (15), 2892-9.
- 9 131. Deng, Z.; Jeong, K. S.; Guyot-Sionnest, P., Colloidal quantum dots intraband
- 10 photodetectors. *ACS Nano* **2014**, *8* (11), 11707-14.
- 11 132. Jeong, K. S.; Deng, Z.; Keuleyan, S.; Liu, H.; Guyot-Sionnest, P., Air-Stable n-Doped
- 12 Colloidal HgS Quantum Dots. *J Phys Chem Lett* **2014**, *5* (7), 1139-43.
- 13 133. Norris, D. J.; Efros, A. L.; Erwin, S. C., Doped nanocrystals. *Science* **2008**, *319* (5871),
- 14 1776-9.
- 15 134. Mocatta, D.; Cohen, G.; Schattner, J.; Millo, O.; Rabani, E.; Banin, U., Heavily doped
- 16 semiconductor nanocrystal quantum dots. *Science* **2011**, *332* (6025), 77-81.
- 17
- 18 135. Gresback, R.; Kramer, N. J.; Ding, Y.; Chen, T.; Kortshagen, U. R.; Nozaki, T., Controlled
- 19 doping of silicon nanocrystals investigated by solution-processed field effect transistors.
- 20 *ACS Nano* **2014**, *8* (6), 5650-6.
- 21
- 22 136. Cagnello, M.; Johnston-Peck, A. C.; Diroll, B. T.; Wong, E.; Datta, B.; Damodhar, D.;
- 23 Doan-Nguyen, V. V.; Herzing, A. A.; Kagan, C. R.; Murray, C. B., Substitutional doping
- 24 in nanocrystal superlattices. *Nature* **2015**, *524* (7566), 450-3.
- 25
- 26 137. Garcia de Arquer, F. P.; Lasanta, T.; Bernechea, M.; Konstantatos, G., Tailoring the
- 27 Electronic Properties of Colloidal Quantum Dots in Metal-Semiconductor Nanocomposites
- 28 for High Performance Photodetectors. *Small* **2015**, *11* (22), 2636-41.
- 29
- 30 138. Stavrinidis, A.; Rath, A. K.; de Arquer, F. P.; Diedenhofen, S. L.; Magen, C.; Martinez, L.;
- 31 So, D.; Konstantatos, G., Heterovalent cation substitutional doping for quantum dot
- 32 homojunction solar cells. *Nat Commun* **2013**, *4*, 2981.
- 33
- 34 139. Vlaskin, V. A.; Barrows, C. J.; Erickson, C. S.; Gamelin, D. R., Nanocrystal diffusion
- 35 doping. *J. Am. Chem. Soc.* **2013**, *135* (38), 14380-9.
- 36
- 37 140. Buonsanti, R.; Milliron, D. J., Chemistry of Doped Colloidal Nanocrystals. *Chem. Mater.*
- 38 **2013**, *25* (8), 1305-1317.
- 39
- 40 141. Mikulec, F. V.; Kuno, M.; Bennati, M.; Hall, D. A.; Griffin, R. G.; Bawendi, M. G.,
- 41 Organometallic Synthesis and Spectroscopic Characterization of Manganese-Doped CdSe
- 42 Nanocrystals. *J. Am. Chem. Soc.* **2000**, *122* (11), 2532-2540.
- 43
- 44 142. Shim, M.; Guyot-Sionnest, P., n-type colloidal semiconductor nanocrystals. *Nature* **2000**,
- 45 *407* (6807), 981-3.
- 46
- 47 143. Zhitomirsky, D.; Furukawa, M.; Tang, J.; Stadler, P.; Hoogland, S.; Voznyy, O.; Liu, H.;
- 48 Sargent, E. H., N-Type Colloidal-Quantum-Dot Solids for Photovoltaics. *Adv. Mater.* **2012**,
- 49 *24* (46), 6181-6185.
- 50
- 51 144. Voznyy, O.; Zhitomirsky, D.; Stadler, P.; Ning, Z.; Hoogland, S.; Sargent, E. H., A Charge-
- 52 Orbital Balance Picture of Doping in Colloidal Quantum Dot Solids. *ACS Nano* **2012**, *6* (9),
- 53 8448-8455.
- 54
- 55 145. Adinolfi, V.; Kramer, I. J.; Labelle, A. J.; Sutherland, B. R.; Hoogland, S.; Sargent, E. H.,
- 56 Photojunction Field-Effect Transistor Based on a Colloidal Quantum Dot Absorber Channel
- 57 Layer. *ACS Nano* **2015**, *9* (1), 356-362.
- 58
- 59 146. Balazs, A. A.; Dirin, D. N.; Fang, H. H.; Protesescu, L.; ten Brink, G. H.; Kooi, B. J.;
- 60 Kovalenko, M. V.; Loi, M. A., Counterion-Mediated Ligand Exchange for PbS Colloidal
- 61 Quantum Dot Superlattices. *ACS Nano* **2015**, *9* (12), 11951-9.

- 1
2
3
4
5
6
7
8
9
10
11
12
13
14
15
16
17
18
19
20
21
22
23
24
25
26
27
28
29
30
31
32
33
34
35
36
37
38
39
40
41
42
43
44
45
46
47
48
49
50
51
52
53
54
55
56
57
58
59
60
147. Bederak, D.; Balazs, D. M.; Sukharevska, N. V.; Shulga, A. G.; Abdu-Aguye, M.; Dirin, D. N.; Kovalenko, M. V.; Loi, M. A., Comparing Halide Ligands in PbS Colloidal Quantum Dots for Field-Effect Transistors and Solar Cells. *ACS Appl Nano Mater* **2018**, *1* (12), 6882-6889.
148. Ning, Z.; Voznyy, O.; Pan, J.; Hoogland, S.; Adinolfi, V.; Xu, J.; Li, M.; Kirmani, A. R.; Sun, J. P.; Minor, J.; Kemp, K. W.; Dong, H.; Rollny, L.; Labelle, A.; Carey, G.; Sutherland, B.; Hill, I.; Amassian, A.; Liu, H.; Tang, J.; Bakr, O. M.; Sargent, E. H., Air-stable n-type colloidal quantum dot solids. *Nat Mater* **2014**, *13* (8), 822-8.
149. Tang, J.; Liu, H.; Zhitomirsky, D.; Hoogland, S.; Wang, X.; Furukawa, M.; Levina, L.; Sargent, E. H., Quantum Junction Solar Cells. *Nano Lett.* **2012**, *12* (9), 4889-4894.
150. Rath, A. K.; Pelayo Garcia de Arquer, F.; Stavrinadis, A.; Lasanta, T.; Bernechea, M.; Diedenhofen, S. L.; Konstantatos, G., Remote Trap Passivation in Colloidal Quantum Dot Bulk Nano-heterojunctions and Its Effect in Solution-Processed Solar Cells. *Adv. Mater.* **2014**, *26* (27), 4741-4747.
151. Koh, W.-k.; Koposov, A. Y.; Stewart, J. T.; Pal, B. N.; Robel, I.; Pietryga, J. M.; Klimov, V. I., Heavily doped n-type PbSe and PbS nanocrystals using ground-state charge transfer from cobaltocene. **2013**, *3*, 2004.
152. Engel, J. H.; Surendranath, Y.; Alivisatos, A. P., Controlled Chemical Doping of Semiconductor Nanocrystals Using Redox Buffers. *J. Am. Chem. Soc.* **2012**, *134* (32), 13200-13203.
153. Nugraha, M. I.; Kumagai, S.; Watanabe, S.; Sytnyk, M.; Heiss, W.; Loi, M. A.; Takeya, J., Enabling Ambipolar to Heavy n-Type Transport in PbS Quantum Dot Solids through Doping with Organic Molecules. *ACS Applied Materials & Interfaces* **2017**, *9* (21), 18039-18045.
154. Kirmani, A. R.; García de Arquer, F. P.; Fan, J. Z.; Khan, J. I.; Walters, G.; Hoogland, S.; Wehbe, N.; Said, M. M.; Barlow, S.; Laquai, F.; Marder, S. R.; Sargent, E. H.; Amassian, A., Molecular Doping of the Hole-Transporting Layer for Efficient, Single-Step-Deposited Colloidal Quantum Dot Photovoltaics. *ACS Energy Letters* **2017**, *2* (9), 1952-1959.
155. Kirmani, A. R.; Kiani, A.; Said, M. M.; Voznyy, O.; Wehbe, N.; Walters, G.; Barlow, S.; Sargent, E. H.; Marder, S. R.; Amassian, A., Remote Molecular Doping of Colloidal Quantum Dot Photovoltaics. *ACS Energy Letters* **2016**, *1* (5), 922-930.
156. Brown, P. R.; Kim, D.; Lunt, R. R.; Zhao, N.; Bawendi, M. G.; Grossman, J. C.; Bulović, V., Energy Level Modification in Lead Sulfide Quantum Dot Thin Films through Ligand Exchange. *ACS Nano* **2014**, *8* (6), 5863-5872.
157. Balazs, D. M.; Nugraha, M. I.; Bisri, S. Z.; Sytnyk, M.; Heiss, W.; Loi, M. A., Reducing charge trapping in PbS colloidal quantum dot solids. *Appl. Phys. Lett.* **2014**, *104* (11), 112104.
158. Speirs, M. J.; Balazs, D. M.; Fang, H. H.; Lai, L. H.; Protesescu, L.; Kovalenko, M. V.; Loi, M. A., Origin of the increased open circuit voltage in PbS–CdS core–shell quantum dot solar cells. *Journal of Materials Chemistry A* **2015**, *3* (4), 1450-1457.
159. Speirs, M. J.; Dirin, D. N.; Abdu-Aguye, M.; Balazs, D. M.; Kovalenko, M. V.; Loi, M. A., Temperature dependent behaviour of lead sulfide quantum dot solar cells and films. *Energy & Environmental Science* **2016**, *9* (9), 2916-2924.
160. Chuang, C.-H. M.; Maurano, A.; Brandt, R. E.; Hwang, G. W.; Jean, J.; Buonassisi, T.; Bulović, V.; Bawendi, M. G., Open-Circuit Voltage Deficit, Radiative Sub-Bandgap States, and Prospects in Quantum Dot Solar Cells. *Nano Lett.* **2015**, *15* (5), 3286-3294.

- 1
2
3
4
5
6
7
8
9
10
11
12
13
14
15
16
17
18
19
20
21
22
23
24
25
26
27
28
29
30
31
32
33
34
35
36
37
38
39
40
41
42
43
44
45
46
47
48
49
50
51
52
53
54
55
56
57
58
59
60
161. Gaulding, E. A.; Hao, J.; Kang, H. S.; Miller, E. M.; Habisreutinger, S. N.; Zhao, Q.; Hazarika, A.; Sercel, P. C.; Luther, J. M.; Blackburn, J. L., Conductivity Tuning via Doping with Electron Donating and Withdrawing Molecules in Perovskite CsPbI_3 Nanocrystal Films. *Adv. Mater.* **2019**, *31* (27), e1902250.
 162. Luque, A.; Martí, A., Increasing the Efficiency of Ideal Solar Cells by Photon Induced Transitions at Intermediate Levels. *Phys. Rev. Lett.* **1997**, *78* (26), 5014-5017.
 163. Luther, J. M.; Law, M.; Beard, M. C.; Song, Q.; Reese, M. O.; Ellingson, R. J.; Nozik, A. J., Schottky solar cells based on colloidal nanocrystal films. *Nano Lett.* **2008**, *8* (10), 3488-92.
 164. Debnath, R.; Tang, J.; Barkhouse, D. A.; Wang, X.; Pattantyus-Abraham, A. G.; Brzozowski, L.; Levina, L.; Sargent, E. H., Ambient-Processed Colloidal Quantum Dot Solar Cells via Individual Pre-Encapsulation of Nanoparticles. *J. Am. Chem. Soc.* **2010**, *132* (17), 5952-5953.
 165. Piliego, C.; Protesescu, L.; Bisri, S. Z.; Kovalenko, M. V.; Loi, M. A., 5.2% efficient PbS nanocrystal Schottky solar cells. *Energy & Environmental Science* **2013**, *6* (10), 3054-3059.
 166. Luther, J. M.; Gao, J.; Lloyd, M. T.; Semonin, O. E.; Beard, M. C.; Nozik, A. J., Stability assessment on a 3% bilayer PbS/ZnO quantum dot heterojunction solar cell. *Adv. Mater.* **2010**, *22* (33), 3704-7.
 167. Pattantyus-Abraham, A. G.; Kramer, I. J.; Barkhouse, A. R.; Wang, X.; Konstantatos, G.; Debnath, R.; Levina, L.; Raabe, I.; Nazeeruddin, M. K.; Grätzel, M.; Sargent, E. H., Depleted-Heterojunction Colloidal Quantum Dot Solar Cells. *ACS Nano* **2010**, *4* (6), 3374-3380.
 168. Maraghechi, P.; Labelle, A. J.; Kirmani, A. R.; Lan, X.; Adachi, M. M.; Thon, S. M.; Hoogland, S.; Lee, A.; Ning, Z.; Fischer, A.; Amassian, A.; Sargent, E. H., The Donor-Supply Electrode Enhances Performance in Colloidal Quantum Dot Solar Cells. *ACS Nano* **2013**, *7* (7), 6111-6116.
 169. Carey, G. H.; Levina, L.; Comin, R.; Voznyy, O.; Sargent, E. H., Record Charge Carrier Diffusion Length in Colloidal Quantum Dot Solids via Mutual Dot-To-Dot Surface Passivation. *Adv. Mater.* **2015**, *27* (21), 3325-3330.
 170. Chuang, C.-H. M.; Brown, P. R.; Bulović, V.; Bawendi, M. G., Improved performance and stability in quantum dot solar cells through band alignment engineering. *Nature Materials* **2014**, *13*, 796.
 171. Kim, G.-H.; García de Arquer, F. P.; Yoon, Y. J.; Lan, X.; Liu, M.; Voznyy, O.; Yang, Z.; Fan, F.; Ip, A. H.; Kanjanaboons, P.; Hoogland, S.; Kim, J. Y.; Sargent, E. H., High-Efficiency Colloidal Quantum Dot Photovoltaics via Robust Self-Assembled Monolayers. *Nano Lett.* **2015**, *15* (11), 7691-7696.
 172. Zhang, L.; Rao, H.; Pan, Z.; Zhong, X., ZnSxSe_{1-x} Alloy Passivation Layer for High-Efficiency Quantum-Dot-Sensitized Solar Cells. *ACS Applied Materials & Interfaces* **2019**, *11* (44), 41415-41423.
 173. Bernechea, M.; Miller, N. C.; Xercavins, G.; So, D.; Stavrinidis, A.; Konstantatos, G., Solution-processed solar cells based on environmentally friendly AgBiS_2 nanocrystals. *Nature Photonics* **2016**, *10*, 521.
 174. Ahmad, W.; He, J.; Liu, Z.; Xu, K.; Chen, Z.; Yang, X.; Li, D.; Xia, Y.; Zhang, J.; Chen, C., Lead Selenide (PbSe) Colloidal Quantum Dot Solar Cells with >10% Efficiency. *Adv. Mater.* **2019**, *31* (33), 1900593.

- 1
2
3 175. Leschkies, K. S.; Beatty, T. J.; Kang, M. S.; Norris, D. J.; Aydil, E. S., Solar Cells Based
4 on Junctions between Colloidal PbSe Nanocrystals and Thin ZnO Films. *ACS Nano* **2009**,
5 3 (11), 3638-3648.
6 176. Koleilat, G. I.; Wang, X.; Labelle, A. J.; Ip, A. H.; Carey, G. H.; Fischer, A.; Levina, L.;
7 Brzozowski, L.; Sargent, E. H., A Donor-Supply Electrode (DSE) for Colloidal Quantum
8 Dot Photovoltaics. *Nano Lett.* **2011**, 11 (12), 5173-5178.
9 177. Kramer, I. J.; Sargent, E. H., Colloidal Quantum Dot Photovoltaics: A Path Forward. *ACS
10 Nano* **2011**, 5 (11), 8506-8514.
11 178. Ning, Z.; Zhitomirsky, D.; Adinolfi, V.; Sutherland, B.; Xu, J.; Voznyy, O.; Maraghechi,
12 P.; Lan, X.; Hoogland, S.; Ren, Y.; Sargent, E. H., Graded Doping for Enhanced Colloidal
13 Quantum Dot Photovoltaics. *Adv. Mater.* **2013**, 25 (12), 1719-1723.
14 179. Barkhouse, D. A. R.; Debnath, R.; Kramer, I. J.; Zhitomirsky, D.; Pattantyus-Abraham, A.
15 G.; Levina, L.; Etgar, L.; Grätzel, M.; Sargent, E. H., Depleted Bulk Heterojunction
16 Colloidal Quantum Dot Photovoltaics. *Adv. Mater.* **2011**, 23 (28), 3134-3138.
17 180. Kramer, I. J.; Zhitomirsky, D.; Bass, J. D.; Rice, P. M.; Topuria, T.; Krupp, L.; Thon, S. M.;
18 Ip, A. H.; Debnath, R.; Kim, H.-C.; Sargent, E. H., Ordered Nanopillar Structured
19 Electrodes for Depleted Bulk Heterojunction Colloidal Quantum Dot Solar Cells. *Adv.
20 Mater.* **2012**, 24 (17), 2315-2319.
21 181. Jean, J.; Chang, S.; Brown, P. R.; Cheng, J. J.; Rekemeyer, P. H.; Bawendi, M. G.;
22 Gradečak, S.; Bulović, V., ZnO Nanowire Arrays for Enhanced Photocurrent in PbS
23 Quantum Dot Solar Cells. *Adv. Mater.* **2013**, 25 (20), 2790-2796.
24 182. Rekemeyer, P. H.; Chang, S.; Chuang, C.-H. M.; Hwang, G. W.; Bawendi, M. G.; Gradečak,
25 S., Enhanced Photocurrent in PbS Quantum Dot Photovoltaics via ZnO Nanowires and
26 Band Alignment Engineering. *Advanced Energy Materials* **2016**, 6 (24), 1600848-n/a.
27 183. Wang, H.; Gonzalez-Pedro, V.; Kubo, T.; Fabregat-Santiago, F.; Bisquert, J.; Sanehira, Y.;
28 Nakazaki, J.; Segawa, H., Enhanced Carrier Transport Distance in Colloidal PbS Quantum-
29 Dot-Based Solar Cells Using ZnO Nanowires. *The Journal of Physical Chemistry C* **2015**,
30 119 (49), 27265-27274.
31 184. Cheng, J. J.; Chuang, C.-H. M.; Hentz, O.; Rekemeyer, P. H.; Bawendi, M. G.; Gradečak,
32 S., Dimension- and Surface-Tailored ZnO Nanowires Enhance Charge Collection in
33 Quantum Dot Photovoltaic Devices. *ACS Applied Energy Materials* **2018**, 1 (5), 1815-1822.
34 185. Shi, G.; Kaewprajak, A.; Ling, X.; Hayakawa, A.; Zhou, S.; Song, B.; Kang, Y.; Hayashi,
35 T.; Altun, M. E.; Nakaya, M.; Liu, Z.; Wang, H.; Sagawa, T.; Ma, W., Finely
36 Interpenetrating Bulk Heterojunction Structure for Lead Sulfide Colloidal Quantum Dot
37 Solar Cells by Convective Assembly. *ACS Energy Letters* **2019**, 4 (4), 960-967.
38 186. Rekemeyer, P. H.; Chuang, C.-H. M.; Bawendi, M. G.; Gradečak, S., Minority Carrier
39 Transport in Lead Sulfide Quantum Dot Photovoltaics. *Nano Lett.* **2017**, 17 (10), 6221-
40 6227.
41 187. Crisp, R. W.; Kroupa, D. M.; Marshall, A. R.; Miller, E. M.; Zhang, J.; Beard, M. C.; Luther,
42 J. M., Metal halide solid-state surface treatment for high efficiency PbS and PbSe QD solar
43 cells. *Sci Rep* **2015**, 5, 9945.
44 188. Lan, X.; Voznyy, O.; Kiani, A.; García de Arquer, F. P.; Abbas, A. S.; Kim, G.-H.; Liu, M.;
45 Yang, Z.; Walters, G.; Xu, J.; Yuan, M.; Ning, Z.; Fan, F.; Kanjanaboons, P.; Kramer, I.;
46 Zhitomirsky, D.; Lee, P.; Perelgut, A.; Hoogland, S.; Sargent, E. H., Passivation Using
47 Molecular Halides Increases Quantum Dot Solar Cell Performance. *Adv. Mater.* **2016**, 28
48 (2), 299-304.
49
50
51
52
53
54
55
56
57
58
59
60

- 1
2
3
4
5
6
7
8
9
10
11
12
13
14
15
16
17
18
19
20
21
22
23
24
25
26
27
28
29
30
31
32
33
34
35
36
37
38
39
40
41
42
43
44
45
46
47
48
49
50
51
52
53
54
55
56
57
58
59
60
189. Azmi, R.; Oh, S.-H.; Jang, S.-Y., High-Efficiency Colloidal Quantum Dot Photovoltaic Devices Using Chemically Modified Heterojunctions. *ACS Energy Letters* **2016**, *1* (1), 100-106.
190. Shi, G.; Wang, Y.; Liu, Z.; Han, L.; Liu, J.; Wang, Y.; Lu, K.; Chen, S.; Ling, X.; Li, Y.; Cheng, S.; Ma, W., Stable and Highly Efficient PbS Quantum Dot Tandem Solar Cells Employing a Rationally Designed Recombination Layer. *Advanced Energy Materials* **2017**, *1602667*-n/a.
191. Wang, X.; Koleilat, G. I.; Tang, J.; Liu, H.; Kramer, I. J.; Debnath, R.; Brzozowski, L.; Barkhouse, D. A. R.; Levina, L.; Hoogland, S.; Sargent, E. H., Tandem colloidal quantum dot solar cells employing a graded recombination layer. *Nat Photon* **2011**, *5* (8), 480-484.
192. Pellarque, A.; Noel, N. K.; Habisreutinger, S. N.; Zhang, Y.; Barlow, S.; Marder, S. R.; Snaith, H. J., Efficient and Stable Perovskite Solar Cells Using Molybdenum Tris(dithiolene)s as p-Dopants for Spiro-OMeTAD. *ACS Energy Letters* **2017**, *2* (9), 2044-2050.
193. Tavakoli Dastjerdi, H.; Tavakoli, R.; Yadav, P.; Prochowicz, D.; Saliba, M.; Tavakoli, M. M., Oxygen Plasma-Induced p-Type Doping Improves Performance and Stability of PbS Quantum Dot Solar Cells. *ACS Appl Mater Interfaces* **2019**, *11* (29), 26047-26052.
194. Pan, Z.; Rao, H.; Mora-Seró, I.; Bisquert, J.; Zhong, X., Quantum dot-sensitized solar cells. *Chem. Soc. Rev.* **2018**, *47* (20), 7659-7702.
195. Yang, Z.; Fan, J. Z.; Proppe, A. H.; Arquer, F. P. G. d.; Rossouw, D.; Voznyy, O.; Lan, X.; Liu, M.; Walters, G.; Quintero-Bermudez, R.; Sun, B.; Hoogland, S.; Botton, G. A.; Kelley, S. O.; Sargent, E. H., Mixed-quantum-dot solar cells. *Nature Communications* **2017**, *8* (1), 1325.
196. Kirmani, A. R.; Eisner, F.; Mansour, A. E.; Firdaus, Y.; Chaturvedi, N.; Seitkhan, A.; Nugraha, M. I.; Yarali, E.; García de Arquer, F. P.; Sargent, E. H.; Anthopoulos, T. D.; Amassian, A., Colloidal Quantum Dot Photovoltaics Using Ultrathin, Solution-Processed Bilayer In₂O₃/ZnO Electron Transport Layers with Improved Stability. *ACS Applied Energy Materials* **2020**, *3* (6), 5135-5141.
197. Pradhan, S.; Stavrinidis, A.; Gupta, S.; Christodoulou, S.; Konstantatos, G., Breaking the Open-Circuit Voltage Deficit Floor in PbS Quantum Dot Solar Cells through Synergistic Ligand and Architecture Engineering. *ACS Energy Letters* **2017**, *2* (6), 1444-1449.
198. Rath, A. K.; Bernechea, M.; Martinez, L.; de Arquer, F. P. G.; Osmond, J.; Konstantatos, G., Solution-processed inorganic bulk nano-heterojunctions and their application to solar cells. *Nat Photon* **2012**, *6* (8), 529-534.
199. Zhitomirsky, D.; Kramer, I. J.; Labelle, A. J.; Fischer, A.; Debnath, R.; Pan, J.; Bakr, O. M.; Sargent, E. H., Colloidal Quantum Dot Photovoltaics: The Effect of Polydispersity. *Nano Lett.* **2012**, *12* (2), 1007-1012.
200. Jo, J. W.; Kim, Y.; Choi, J.; de Arquer, F. P. G.; Walters, G.; Sun, B.; Ouellette, O.; Kim, J.; Proppe, A. H.; Quintero-Bermudez, R.; Fan, J.; Xu, J.; Tan, C. S.; Voznyy, O.; Sargent, E. H., Enhanced Open-Circuit Voltage in Colloidal Quantum Dot Photovoltaics via Reactivity-Controlled Solution-Phase Ligand Exchange. *Adv. Mater.* **2017**, *29* (43), 1703627.
201. Alimoradi Jazi, M.; Janssen, V. A. E. C.; Evers, W. H.; Tadjine, A.; Delerue, C.; Siebbeles, L. D. A.; van der Zant, H. S. J.; Houtepen, A. J.; Vanmaekelbergh, D., Transport Properties of a Two-Dimensional PbSe Square Superstructure in an Electrolyte-Gated Transistor. *Nano Lett.* **2017**, *17* (9), 5238-5243.

- 1
2
3 202. Shulga, A. G.; Kahmann, S.; Dirin, D. N.; Graf, A.; Zaumseil, J.; Kovalenko, M. V.; Loi,
4 M. A., Electroluminescence Generation in PbS Quantum Dot Light-Emitting Field-Effect
5 Transistors with Solid-State Gating. *ACS Nano* **2018**, *12* (12), 12805-12813.
6
7 203. Luo, D.; Su, R.; Zhang, W.; Gong, Q.; Zhu, R., Minimizing non-radiative recombination
8 losses in perovskite solar cells. *Nature Reviews Materials* **2020**, *5* (1), 44-60.
9
10 204. Stolterfoht, M.; Grischek, M.; Caprioglio, P.; Wolff, C. M.; Gutierrez-Partida, E.; Peña-
11 Camargo, F.; Rothhardt, D.; Zhang, S.; Raoufi, M.; Wolansky, J.; Abdi-Jalebi, M.; Stranks,
12 S. D.; Albrecht, S.; Kirchartz, T.; Neher, D., How To Quantify the Efficiency Potential of
13 Neat Perovskite Films: Perovskite Semiconductors with an Implied Efficiency Exceeding
14 28%. *Adv. Mater.* **2020**, *32* (17), 2000080.
15
16 205. Stolterfoht, M.; Wolff, C. M.; Márquez, J. A.; Zhang, S.; Hages, C. J.; Rothhardt, D.;
17 Albrecht, S.; Burn, P. L.; Meredith, P.; Unold, T.; Neher, D., Visualization and suppression
18 of interfacial recombination for high-efficiency large-area pin perovskite solar cells. *Nature
Energy* **2018**, *3* (10), 847-854.
19
20 206. Kim, T.; Firdaus, Y.; Kirmani, A. R.; Liang, R.-Z.; Hu, H.; Liu, M.; El Labban, A.;
21 Hoogland, S.; Beaujuge, P. M.; Sargent, E. H.; Amassian, A., Hybrid Tandem Quantum
22 Dot/Organic Solar Cells with Enhanced Photocurrent and Efficiency via Ink and Interlayer
23 Engineering. *ACS Energy Letters* **2018**, *3* (6), 1307-1314.
24
25 207. Kim, T.; Gao, Y.; Hu, H.; Yan, B.; Ning, Z.; Jagadamma, L. K.; Zhao, K.; Kirmani, A. R.;
26 Eid, J.; Adachi, M. M.; Sargent, E. H.; Beaujuge, P. M.; Amassian, A., Hybrid tandem solar
27 cells with depleted-heterojunction quantum dot and polymer bulk heterojunction subcells.
Nano Energy **2015**, *17*, 196-205.
28
29 208. Kim, T.; Palmiano, E.; Liang, R. Z.; Hu, H.; Murali, B.; Kirmani, A. R.; Firdaus, Y.; Gao,
30 Y.; Sheikh, A.; Yuan, M.; Mohammed, O. F.; Hoogland, S.; Beaujuge, P. M.; Sargent, E.
31 H.; Amassian, A., Hybrid tandem quantum dot/organic photovoltaic cells with
32 complementary near infrared absorption. *Appl. Phys. Lett.* **2017**, *110* (22), 223903.
33
34 209. Aqoma, H.; Imran, I. F.; Mubarok, M. A.; Hadmojo, W. T.; Do, Y. R.; Jang, S.-Y., Efficient
35 Hybrid Tandem Solar Cells Based on Optical Reinforcement of Colloidal Quantum Dots
36 with Organic Bulk Heterojunctions. *Advanced Energy Materials* **2020**, *10* (7), 1903294.
37
38 210. Yuan, L.; Michaels, H.; Roy, R.; Johansson, M.; Öberg, V.; Andruszkiewicz, A.; Zhang,
39 X.; Freitag, M.; Johansson, E. M. J., Four-Terminal Tandem Solar Cell with Dye-Sensitized
40 and PbS Colloidal Quantum-Dot-Based Subcells. *ACS Applied Energy Materials* **2020**, *3*
(4), 3157-3161.
41
42 211. Crisp, R. W.; Pach, G. F.; Kurley, J. M.; France, R. M.; Reese, M. O.; Nanayakkara, S. U.;
43 MacLeod, B. A.; Talapin, D. V.; Beard, M. C.; Luther, J. M., Tandem Solar Cells from
44 Solution-Processed CdTe and PbS Quantum Dots Using a ZnTe-ZnO Tunnel Junction.
Nano Lett. **2017**, *17* (2), 1020-1027.
45
46 212. Kim, J.; Ouellette, O.; Voznyy, O.; Wei, M.; Choi, J.; Choi, M.-J.; Jo, J. W.; Baek, S.-W.;
47 Fan, J.; Saidaminov, M. I.; Sun, B.; Li, P.; Nam, D.-H.; Hoogland, S.; Lu, Z.-H.; García de
48 Arquer, F. P.; Sargent, E. H., Butylamine-Catalyzed Synthesis of Nanocrystal Inks Enables
49 Efficient Infrared CQD Solar Cells. *Adv. Mater.* **2018**, *30* (45), 1803830.
50
51 213. Kim, Y.; Che, F.; Jo, J. W.; Choi, J.; García de Arquer, F. P.; Voznyy, O.; Sun, B.; Kim, J.;
52 Choi, M.-J.; Quintero-Bermudez, R.; Fan, F.; Tan, C. S.; Bladt, E.; Walters, G.; Proppe, A.
53 H.; Zou, C.; Yuan, H.; Bals, S.; Hofkens, J.; Roeffaers, M. B. J.; Hoogland, S.; Sargent, E.
54 H., A Facet-Specific Quantum Dot Passivation Strategy for Colloid Management and
55 Efficient Infrared Photovoltaics. *Adv. Mater.* **2019**, *0* (0), 1805580.

- 1
2
3
4
5
6
7
8
9
10
11
12
13
14
15
16
17
18
19
20
21
22
23
24
25
26
27
28
29
30
31
32
33
34
35
36
37
38
39
40
41
42
43
44
45
46
47
48
49
50
51
52
53
54
55
56
57
58
59
60
214. Sun, B.; Ouellette, O.; García de Arquer, F. P.; Voznyy, O.; Kim, Y.; Wei, M.; Proppe, A. H.; Saidaminov, M. I.; Xu, J.; Liu, M.; Li, P.; Fan, J. Z.; Jo, J. W.; Tan, H.; Tan, F.; Hoogland, S.; Lu, Z. H.; Kelley, S. O.; Sargent, E. H., Multibandgap quantum dot ensembles for solar-matched infrared energy harvesting. *Nature Communications* **2018**, 9 (1), 4003.
215. Che, X.; Li, Y.; Qu, Y.; Forrest, S. R., High fabrication yield organic tandem photovoltaics combining vacuum- and solution-processed subcells with 15% efficiency. *Nature Energy* **2018**, 3 (5), 422-427.
216. Meng, L.; Zhang, Y.; Wan, X.; Li, C.; Zhang, X.; Wang, Y.; Ke, X.; Xiao, Z.; Ding, L.; Xia, R.; Yip, H.-L.; Cao, Y.; Chen, Y., Organic and solution-processed tandem solar cells with 17.3% efficiency. *Science* **2018**, 361 (6407), 1094-1098.
217. Fan, B.; Zhang, D.; Li, M.; Zhong, W.; Zeng, Z.; Ying, L.; Huang, F.; Cao, Y., Achieving over 16% efficiency for single-junction organic solar cells. *Science China Chemistry* **2019**, 62 (6), 746-752.
218. An, Q.; Ma, X.; Gao, J.; Zhang, F., Solvent additive-free ternary polymer solar cells with 16.27% efficiency. *Science Bulletin* **2019**, 64 (8), 504-506.
219. Tan, L.; Li, P.; Sun, B.; Chaker, M.; Ma, D., Stabilities Related to Near-Infrared Quantum Dot-Based Solar Cells: The Role of Surface Engineering. *ACS Energy Letters* **2017**, 2 (7), 1573-1585.
220. Hassinen, A.; Moreels, I.; De Nolf, K.; Smet, P. F.; Martins, J. C.; Hens, Z., Short-Chain Alcohols Strip X-Type Ligands and Quench the Luminescence of PbSe and CdSe Quantum Dots, Acetonitrile Does Not. *J. Am. Chem. Soc.* **2012**, 134 (51), 20705-20712.
221. Lu, K.; Wang, Y.; Liu, Z.; Han, L.; Shi, G.; Fang, H.; Chen, J.; Ye, X.; Chen, S.; Yang, F.; Shulga, A. G.; Wu, T.; Gu, M.; Zhou, S.; Fan, J.; Loi, M. A.; Ma, W., High-Efficiency PbS Quantum-Dot Solar Cells with Greatly Simplified Fabrication Processing via “Solvent-Curing”. *Adv. Mater.* **2018**, 30 (25), 1707572.
222. Song, J. H.; Choi, H.; Kim, Y.-H.; Jeong, S., High Performance Colloidal Quantum Dot Photovoltaics by Controlling Protic Solvents in Ligand Exchange. *Advanced Energy Materials* **2017**, 7 (15), 1700301.
223. Aqoma, H.; Jang, S.-Y., Solid-state-ligand-exchange free quantum dot ink-based solar cells with an efficiency of 10.9%. *Energy & Environmental Science* **2018**, 11 (6), 1603-1609.
224. Deng, Y.; Zheng, X.; Bai, Y.; Wang, Q.; Zhao, J.; Huang, J., Surfactant-controlled ink drying enables high-speed deposition of perovskite films for efficient photovoltaic modules. *Nature Energy* **2018**, 3 (7), 560-566.
225. Chen, W.; Tang, H.; Li, N.; Scheel, M. A.; Xie, Y.; Li, D.; Körstgens, V.; Schwartzkopf, M.; Roth, S. V.; Wang, K.; Sun, X. W.; Müller-Buschbaum, P., Colloidal PbS quantum dot stacking kinetics during deposition via printing. *Nanoscale Horizons* **2020**, 5 (5), 880-885.
226. Aqoma, H.; Mubarok, M. A.; Lee, W.; Hadmojo, W. T.; Park, C.; Ahn, T. K.; Ryu, D. Y.; Jang, S.-Y., Improved Processability and Efficiency of Colloidal Quantum Dot Solar Cells Based on Organic Hole Transport Layers. *Advanced Energy Materials* **2018**, 8 (23), 1800572.
227. Mubarok, M. A.; Aqoma, H.; Wibowo, F. T. A.; Lee, W.; Kim, H. M.; Ryu, D. Y.; Jeon, J.-W.; Jang, S.-Y., Molecular Engineering in Hole Transport π -Conjugated Polymers to Enable High Efficiency Colloidal Quantum Dot Solar Cells. *Advanced Energy Materials* **2020**, 10 (8), 1902933.
228. Zhang, Y.; Kan, Y.; Gao, K.; Gu, M.; Shi, Y.; Zhang, X.; Xue, Y.; Zhang, X.; Liu, Z.; Zhang, Y.; Yuan, J.; Ma, W.; Jen, A. K. Y., Hybrid Quantum Dot/Organic Heterojunction:

- 1
- 2
- 3 A Route to Improve Open-Circuit Voltage in PbS Colloidal Quantum Dot Solar Cells. *ACS Energy Letters* **2020**, 2335-2342.
- 4
- 5 229. Chernomordik, B. D.; Marshall, A. R.; Pach, G. F.; Luther, J. M.; Beard, M. C., Quantum
- 6 Dot Solar Cell Fabrication Protocols. *Chem. Mater.* **2016**, 29 (1), 189-198.
- 7
- 8 230. Abbas, M. A.; Basit, M. A.; Yoon, S. J.; Lee, G. J.; Lee, M. D.; Park, T. J.; Kamat, P. V.;
- 9 Bang, J. H., Revival of Solar Paint Concept: Air-Processable Solar Paints for the Fabrication
- 10 of Quantum Dot-Sensitized Solar Cells. *The Journal of Physical Chemistry C* **2017**, 121
- 11 (33), 17658-17670.
- 12
- 13 231. Genovese, M. P.; Lightcap, I. V.; Kamat, P. V., Sun-Believable Solar Paint. A
- 14 Transformative One-Step Approach for Designing Nanocrystalline Solar Cells. *ACS Nano*
- 15 **2012**, 6 (1), 865-872.
- 16
- 17 232. Kramer, I. J.; Moreno-Bautista, G.; Minor, J. C.; Kopilovic, D.; Sargent, E. H., Colloidal
- 18 quantum dot solar cells on curved and flexible substrates. *Appl. Phys. Lett.* **2014**, 105 (16),
- 19 163902.
- 20
- 21 233. Tang, J.; Brzozowski, L.; Barkhouse, D. A. R.; Wang, X.; Debnath, R.; Wolowiec, R.;
- 22 Palmiano, E.; Levina, L.; Pattantyus-Abraham, A. G.; Jamakosmanovic, D.; Sargent, E. H.,
- 23 Quantum Dot Photovoltaics in the Extreme Quantum Confinement Regime: The Surface-
- 24 Chemical Origins of Exceptional Air- and Light-Stability. *ACS Nano* **2010**, 4 (2), 869-878.
- 25
- 26 234. Silbergeld, E. K.; Waalkes, M.; Rice, J. M., Lead as a carcinogen: Experimental evidence
- 27 and mechanisms of action. *American Journal of Industrial Medicine* **2000**, 38 (3), 316-323.
- 28
- 29 235. Zhang, S.; Ye, L.; Zhang, H.; Hou, J., Green-solvent-processable organic solar cells. *Mater.*
- 30 *Today* **2016**, 19 (9), 533-543.
- 31
- 32 236. Ma, Z.; Zhao, B.; Gong, Y.; Deng, J.; Tan, Z. a., Green-solvent-processable strategies for
- 33 achieving large-scale manufacture of organic photovoltaics. *Journal of Materials Chemistry A* **2019**, 7 (40), 22826-22847.
- 34
- 35 237. Tian, S.; Li, J.; Li, S.; Bu, T.; Mo, Y.; Wang, S.; Li, W.; Huang, F., A facile green solvent
- 36 engineering for up-scaling perovskite solar cell modules. *Solar Energy* **2019**, 183, 386-391.
- 37
- 38 238. Jessop, P. G., Searching for green solvents. *Green Chemistry* **2011**, 13 (6), 1391-1398.
- 39
- 40 239. Byrne, F. P.; Jin, S.; Paggiola, G.; Petchey, T. H. M.; Clark, J. H.; Farmer, T. J.; Hunt, A.
- 41 J.; Robert McElroy, C.; Sherwood, J., Tools and techniques for solvent selection: green
- 42 solvent selection guides. *Sustainable Chemical Processes* **2016**, 4 (1), 7.
- 43
- 44 240. Shen, Y.; Weeranoppanant, N.; Xie, L.; Chen, Y.; Lusardi, M. R.; Imbrogno, J.; Bawendi,
- 45 M. G.; Jensen, K. F., Multistage extraction platform for highly efficient and fully continuous
- 46 purification of nanoparticles. *Nanoscale* **2017**, 9 (23), 7703-7707.
- 47
- 48 241. Shen, Y.; Abolhasani, M.; Chen, Y.; Xie, L.; Yang, L.; Coley, C. W.; Bawendi, M. G.;
- 49 Jensen, K. F., In-Situ Microfluidic Study of Biphase Nanocrystal Ligand-Exchange
- 50 Reactions Using an Oscillatory Flow Reactor. *Angew. Chem. Int. Ed. Engl.* **2017**, 56 (51),
- 51 16333-16337.
- 52
- 53 242. MacLeod, B. P.; Parlane, F. G. L.; Morrissey, T. D.; Häse, F.; Roch, L. M.; Dettelbach, K.
- 54 E.; Moreira, R.; Yunker, L. P. E.; Rooney, M. B.; Deeth, J. R.; Lai, V.; Ng, G. J.; Situ, H.;
- 55 Zhang, R. H.; Elliott, M. S.; Haley, T. H.; Dvorak, D. J.; Aspuru-Guzik, A.; Hein, J. E.;
- 56 Berlinguette, C. P., Self-driving laboratory for accelerated discovery of thin-film materials.
- 57 *Science Advances* **2020**, 6 (20), eaaz8867.
- 58
- 59 243. Niu, G.; Zhang, L.; Ruditskiy, A.; Wang, L.; Xia, Y., A Droplet-Reactor System Capable
- 60 of Automation for the Continuous and Scalable Production of Noble-Metal Nanocrystals.
- Nano Lett.* **2018**, 18 (6), 3879-3884.

- 1
2
3 244. Li, S.; Baker, R. W.; Lignos, I.; Yang, Z.; Stavrakis, S.; Howes, P. D.; deMello, A. J.,
4 Automated microfluidic screening of ligand interactions during the synthesis of cesium lead
5 bromide nanocrystals. *Molecular Systems Design & Engineering* **2020**, 5 (6), 1118-1130.
6
7 245. Bezinge, L.; Maceiczyk, R. M.; Lignos, I.; Kovalenko, M. V.; deMello, A. J., Pick a Color
8 MARIA: Adaptive Sampling Enables the Rapid Identification of Complex Perovskite
9 Nanocrystal Compositions with Defined Emission Characteristics. *ACS Appl Mater
10 Interfaces* **2018**, 10 (22), 18869-18878.
11
12 246. Voznyy, O.; Levina, L.; Fan, J. Z.; Askerka, M.; Jain, A.; Choi, M.-J.; Ouellette, O.;
13 Todorović, P.; Sagar, L. K.; Sargent, E. H., Machine Learning Accelerates Discovery of
14 Optimal Colloidal Quantum Dot Synthesis. *ACS Nano* **2019**, 13 (10), 11122-11128.
15
16 247. Kirmani, A. R., Commercializing colloidal quantum dot photovoltaics. *MRS Bull.* **2019**, 44
17 (7), 524-525.
18
19
20
21
22
23
24
25
26
27
28
29
30
31
32
33
34
35
36
37
38
39
40
41
42 QUOTES
43
44 1). “*The solution-phase ligand exchange or SolEx yields an exchanged, ready-to-coat QD ink that
45 helps realize single-step deposited active layers, moving away from the time- and materials-
46 wasting LbL process.*”
47
48
49
50
51
52 2). “*Considering a stabilized module PCE of 15%, we project >1.4 GW of annual electrical power
53 production capacity for each of these distributed QD PV manufacturing sites.*”
54
55
56
57
58
59
60

1
2
3) *“The currently achievable manufacturing throughput for perovskite QDs with a low-cost*
4 *single-channel microfluidic reactor is ~ 100 g/day, which is clearly aligned with industrial*
5 *adoption and can be easily scaled-up to 1-10 kg/day using a numbered-up strategy.”*

6
7
8
9
10) *“Future research should explore developing efficient ligand exchange, improving charge*
11 *transport and extraction, and suppressing size dispersity in wide bandgap (~ 1.5 – 2 eV) and*
12 *NIR (~ 0.6 – 0.8 eV) PbS QDs to meet the demand and promise of hybrid tandem PV.”*

13
14
15
16
17
18) *“Overall, these demonstrations of ambient manufacturability and scalable fabrication of QD*
19 *PV along with recent interest in automated and autonomous flow-synthesis of QDs on demand,*
20 *are promising signs for this nascent field.”*